AD_____

Award Number: W81XWH-04-1-0411

TITLE: Simultaneous Monitoring of Vascular Oxygenation and Tissue Oxygen Tension of Breast Tumors Under Hyperbaric Oxygen Exposure

PRINCIPAL INVESTIGATOR: Mengna Xia
Hanli Liu

CONTRACTING ORGANIZATION: The University of Texas at Arlington
Arlington, TX 76019

REPORT DATE: April 2008

TYPE OF REPORT: Annual Summary

PREPARED FOR: U.S. Army Medical Research and Materiel Command
Fort Detrick, Maryland 21702-5012

REPORT DOCUMENTATION PAGE

Form Approved
OMB No. 0704-0188

1. REPORT DATE *(DD-MM-YYYY)*	2. REPORT TYPE	3. DATES COVERED *(From - To)*
08-APR-2008	annual summary	9 MAR 2004 - 8 MAR 2008

4. TITLE AND SUBTITLE
Simultaneous Monitoring of Vascular Oxygenation and Tissue Oxygen Tension of Breast Tumors under Hyperbaric Oxygen Exposure

5a. CONTRACT NUMBER
W81XWH-04-1-0411

5b. GRANT NUMBER

5c. PROGRAM ELEMENT NUMBER

6. AUTHOR(S)

Mengna Xia and Hanli Liu

Email: mengnaxia@yahoo.com

5d. PROJECT NUMBER

5e. TASK NUMBER

5f. WORK UNIT NUMBER

7. PERFORMING ORGANIZATION NAME(S) AND ADDRESS(ES)

The University of Texas at Arlington and
The Univ. of Texas Southwestern
Medical Center at Dallas
Arlington, TX 76019

*
P.O. Box 19138
The Univ. of Texas at Arlington
Arlington, TX 76019

8. PERFORMING ORGANIZATION REPORT NUMBER

9. SPONSORING / MONITORING AGENCY NAME(S) AND ADDRESS(ES)
U.S. Army Medical Research and
Materiel Command
Fort Detrick, Maryland 21702-5012

10. SPONSOR/MONITOR'S ACRONYM(S)

11. SPONSOR/MONITOR'S REPORT NUMBER(S)

12. DISTRIBUTION / AVAILABILITY STATEMENT

Approved for public release; distribution unlimited

13. SUPPLEMENTARY NOTES

14. ABSTRACT

Objective/Hypothesis: By monitoring global and local vascular oxygenation and tissue oxygen tension in breast tumors under HBO exposure with several different gas interventions, we wish to prove the following two **hypotheses:** that 1) the combination of HBO and hyperoxic intervention can largely improve breast tumor oxygenation, and that 2) tumor oxygenation remains elevated for a period of time even after HBO exposure, which may provide a unique treatment window to enhance radio-sensitivity.

Specific Aims: Aim 1: to determine the absolute values of oxygenated hemoglobin concentration, $[HbO_2]$, and hemoglobin oxygen saturation, SO_2, in solid breast tumors from the NIRS measurements. **Aim 2:** to investigate vascular oxygenation and tissue oxygen tension of breast tumors under continuous normobaric and hyperbaric oxygen exposures with several gas interventions, using both a single-channel NIRS system and 3-channel FOXY pO_2 system simultaneously. **Aim 3:** to investigate global and local dynamics of tumor vascular $[HbO_2]$ and tissue pO_2 of breast tumors immediately after HBO exposure using both three-channel NIRS and ^{19}F MR EPI imaging simultaneously.

15. SUBJECT TERMS

Technology Development, Near infrared spectroscopy, Hyperbaric Oxygen Treatment, Tumor Therapy Planning and Prognosis, Tumor Physiology Monitoring.

16. SECURITY CLASSIFICATION OF: Unclassified			17. LIMITATION OF ABSTRACT	18. NUMBER OF PAGES	19a. NAME OF RESPONSIBLE PERSON
a. REPORT	b. ABSTRACT	c. THIS PAGE			Hanli Liu (Mentor)
X				49	19b. TELEPHONE NUMBER *(include area code)* (817) 272-2054

Standard Form 298 (Rev. 8-98)
Prescribed by ANSI Std. Z39.18

Table of Contents

2004-2008 FINAL PROGRESS REPORT

This report presents the specific aims and accomplishments of our breast cancer research project during the years of funding sponsored by the US Department of the Army. It covers our activities from May 1, 2004 to April 30, 2008.

1. Introduction

The overall goal of this research project is to apply the multiple monitoring techniques, i.e. Near infrared spectroscopy (NIRS), FOXY oxygen sensor and ^{19}F MR EP imaging of Hexafluorobenzene (HFB), to prove the following hypotheses: combination of hyperbaric oxygen (HBO) intervention can significantly improve breast tumor oxygenation, and that tumor oxygenation remains elevated for a substantial period of time even after HBO exposure, which may be a novel approach to enhance radiosensitivity or chemotherapy. If our hypotheses are proven to be true, this study can lead to an optimal intervention plan to improve tumor oxygenation and to determine an optimal time interval after HBO decompression for radiotherapy. Such a novel approach will largely enhance the efficiency of non-surgical therapies for breast tumor treatment and provide a novel prognostic tool for clinical practice. This study will also provide a better understanding of tumor vasculature and tissue oxygen dynamics and spatial heterogeneity under HBO exposure.

The project has three specific aims:

Aim 1: to determine the absolute changes of oxygenated hemoglobin concentration, [HbO_2], and hemoglobin oxygen saturation, SO_2, in solid breast tumors from the NIRS measurements.

Aim 2: to investigate vascular oxygenation and tissue oxygen tension of breast tumors under continuous normobaric and hyperbaric oxygen exposures with several gas interventions, using both a single-channel NIRS system and 3-channel FOXY pO_2 system simultaneously.

Aim 3: to investigate (1) whether HBO could enhance the therapeutic efficiency of malignancy when used as a chemotherapeutic adjuvant of an anticancer agent (doxorubicin, DOX) in mammary carcinomas of rat model, and (2) the feasibility of NIRS to monitor tumor hemodynamic changes resulting from the therapeutic effect of DOX on vasculature.

This report will summarize the work we performed for the three specific aims and corresponding achievements, as given below.

2. Body of the Report

The PI and her mentor, Ms. Mengna Xia and Dr. Liu, made significant efforts from 2004-2008 to accomplish the proposed aims, resulting in multiple published journal and conference papers. This report is organized in such a way that we will combine our published papers and Dr. Xia's dissertation to give detailed descriptions of the research studies, while the papers and chapters in her dissertation are organized as Appendixes 1 to 4 for referral, as listed below:

Appendix 1: Mengna Xia, Vikram Kodibagkar, Hanli Liu, and Ralph Mason, "Tumor oxygen dynamics measured simultaneously by near-infrared spectroscopy and ^{19}F magnetic resonance imaging in rats," *Physics in Medicine and Biology* 51, 45-60 (2006).

Appendix 2: Yueqing Gu, Wei R. Chen, Mengna Xia, Sang W. Jeong, and Hanli Liu, "Effect of Photothermal therapy on breast tumor vascular contents: non-

invasive monitoring by near infrared spectroscopy," *Photochemistry and Photobiology* 81(4), 1002–1009 (2005).

Appendix 3: Jae G. Kim, Mengna Xia, and Hanli Liu, "Hemoglobin extinction coefficients: importance of correct value for near-infrared spectroscopy," *IEEE -- Engineering in Medicine and Biology magazine*, 24(2) 118-121 (2005).

Appendix 4: Mengna Xia, Hanli Liu, Ya Ren, Ralph Mason, Benjamin Levine, "Simultaneous monitoring of tumor vascular and tissue oxygen tension under hyperbaric oxygen exposure," presented at *Biomedical Optics Topical Meeting*, Fort Lauderdale, Florida, March 19-23, 2006.

2.1 Report for Aim 1

Aim 1: to determine the absolute changes of oxygenated hemoglobin concentration, [HbO_2], and hemoglobin oxygen saturation, SO_2, in solid breast tumors from the NIRS measurements.

For Aim 1, we have implemented quantification algorithms, examined their corresponding errors, and conducted animal measurements to obtain absolute changes of oxygenated hemoglobin concentration, [HbO_2], and hemoglobin oxygen saturation, SO_2, in solid breast tumors based on the NIRS measurements. The detailed descriptions can be found in **Appendixes 1 to 3**.

2.2 Report for Aim 2

Aim 2: to investigate vascular oxygenation and tissue oxygen tension of breast tumors under continuous normobaric and hyperbaric oxygen exposures with several gas interventions, using both a single-channel NIRS system and 3-channel FOXY pO_2 system simultaneously.

For Aim 2, we have reported our experimental results in **Appendixes 1 and 4** for investigation of vascular and tissue oxygenation of rat breast tumors under continuous normobaric (Appendix 1) and hyperbaric (Appendix 4) oxygen exposures with oxygen interventions, using single-change NIRS and multi-channel pO_2 sensors simultaneously. The details can be found in those two appendixes.

2.3 Report for Aim 3

Aim 3: to investigate (1) whether HBO could enhance the therapeutic efficiency of malignancy when used as a chemotherapeutic adjuvant of an anticancer agent (doxorubicin, DOX) in mammary carcinomas of rat model, and (2) the feasibility of NIRS to monitor tumor hemodynamic changes resulting from the therapeutic effect of DOX on vasculature.

For Aim 2, the PI, Dr. Mengna Xia, has reported the detailed results in her dissertation. Here we report the major findings briefly, as follows:

2.3.1 Introduction

Doxorubicin (DOX) is one of the most widely used broad-spectrum anticancer agents [1]. However, its clinical utility is limited, because this agent produces a chronic and dose-related

cardiomyopathy as its principal side effect. Therefore, it is desirable to achieve better chemotherapeutic effect with lower dosage of the agent. It is well accepted that hypoxic tumor is resistant to radiotherapy and some chemotherapy agent [2,3,4,5]. To overcome hypoxia, a variety of approaches have focused on improve oxygen delivery via oxygen-enriched gases or blood substitutes [6,7,8,9,10]. Hyperbaric oxygen was believed to improve tissue oxygenation greater than normabric oxygen because it increased oxygen tension and oxygen delivery to tissue independent of hemoglobin[11]. HBO, as a chemotherapy adjuvant in tumor treatment rather than stand alone treatment, is believed to increases cellular uptake of some chemotherapy agents and the susceptibility of cells to these agents. It has been demonstrated that HBO can increase the susceptibility of malignant cells to destruction with taxol [12], doxorubicin [13, 14] and 5-FU [15,16].

The influence of tumor oxygenation on treatment outcome has stimulated various techniques to monitor or estimate tumor oxygenation. These include microelectrodes, optical reflectance, electron paramagnetic resonance (EPR), magnetic resonance imaging (MRI) and nuclear medicine approaches, as reviewed previously [17]. As each approach has their own strength, some are highly invasive. Since its introduction in 1970s [18], Near Infrared Spectroscopy has been increasingly applied to study tissue oxygenation status non-invasively. Near infrared light can easily penetrate biological tissue, and allow for detection of specific light-absorbing chromophores in human in vivo, such as oxygenated and deoxygenated hemoglobin, water and lipid [19]. it has been used extensively for quantitative measurements of cerebral oxygenation [20] and blood oxygenation in muscles *in vivo* [21], and more recently, tumor vascular oxygenation with respect to interventions [22]. NIRS currently lack of spatial resolution, and thus, the utility of global measurement require validation, given the well-documented heterogeneity of tumor. In this regard, Xia *et al* [22] compared the spatially averaged measurement of relative tumor oxygen saturation ($_SO_2$) using NIRS with the local pO_2 measured by MRI. The sensitivity and specificity analysis suggests that NIRS may identify clinically relevant hypoxia, even when its spatial extent is below the resolution limit of the NIRS technique. Kim *et al* demonstrated that NIRS may be used as an effective tool to monitor tumor hemodynamic change induced by some vascular disrupting agent [23,24].

These studies were designed to investigate 1) whether HBO could enhance the therapeutic efficiency of malignancy when used as a chemotherapeutic adjuvant of doxorubicin in mammary carcinomas of rat model, and 2) the feasibility of NIRS to monitor tumor hemodynamic changes resulting from the therapeutic effect of DOX on vasculature.

2.3.2 Materials and Methods

2.3.2a Animal and Tumor models

Healthy female Fischer 344 rats aged 5 to 6 months were obtained from Harlan Sprague-Dawley (Indianapolis, IN). They were housed for at least a week to acclimatize and for monitoring of health before inclusion in the study. Mammary carcinomas 13762NF were implanted in the dorsum of female Fischer 344 rats weighing ~200g. Tumor volume was estimated by the formula of 6/pi *(LxWxH), Tumor diameter was measured in orthogonal axes (L,W, H). Tumor size and body weight were monitored every other day after therapeutic interventions. All animal protocols were approved by Institutional Animal Care and Use Committee at the University of Texas Southwestern Medical Center and University of Texas at Arlington.

2.3.2b Drug preparation and dose

Doxorubicin Hydrochloride was purchased from Sigma Aldrich, Inc. It was made into a solution by dissolving with saline. A single dose of DOX (2mg/kg body weight) was administrated by tail vein. The dose of doxorubicin given was the usual chemotherapeutic dose, which would not cause cardio-toxicity [13].

2.3.2c Experimental procedure

Following tumor establishment (~1 cm diameter), rats were randomly assigned to one of three groups according to different therapeutic strategies: a) DOX (n=5), b) HBO + DOX (n=5). C) control group (n=2) with saline injection. Rats were anesthetized with the mixture of ketamine hydrochloride (0.15 ml; 100mg/ml; Aveco, Fort Dodge, IA) and xylazine via i.p. After tumor hair was shaved to allow better optical contact for NIR light transmission, the rat was placed on its side in the hyperbaric chamber. Probes of SSDRS were fixed securely on the tumor of rat, and then SSDRS monitored tumor vascular oxygenation while the rat was subjected to therapeutic interventions.

DOX group was given 0.4 mg/ml doxorubicin solution intravenously after the respiratory intervention of air -O_2 - air, and then were exposed to air – O_2 - air after DOX injection. HBO + DOX group was exposed to gas intervention in a sequence of air-O_2 - HBO (30 min) prior to intravenously administration of 0.4 mg/ml doxorubicin solution, and then exposed to air - O_2 – air. Control group was subjected to the respiratory intervention of air -O_2 - air, saline solution intravenous injection and then were exposed to air – O_2 – air. To control the timing of DOX injection, an IV butterfly catheter was inserted into rat tail vein and fixed securely with tape before the rat was put into the chamber. The syringe filled with DOX solution was connected to the catheter with heparin only before DOX injection, in order to avoid the possible precipitation caused by the incompatibility of DOX and heparin [25].

2.3.2d Spectrometer for monitoring the disturbance of DOX on the absorption of tissue phantom

Because the reddish color of doxorubicin, it is reasonable to consider the bolus injection of doxorubicin may change tissue absorption. A UV/VIS spectrometer Lambda 20 (PerkinElmer Inc., Waltham, MA) was used to detect the absorption change resulting from the addition of DOX into tissue phantom, in order to verify the acute effect of DOX bolus injection on tissue absorption. A tissue phantom is composed of 100 l sheep blood mixed with phosphate buffer solution with total volume of 3.5 ml and total hemoglobin concentration of 7.1 g/L, which is in the range of total hemoglobin concentration in tissue [26]. The Hb concentration of tissue phantom was measured by Co-oximeter (Instrumentation Lab, Ramsey, MN). Since animal's total blood volume is 10% of its body weight, total blood volume = 0.2 Kg x 10% = 20 ml, with the known body weight of ~ 0.2 Kg of rats. 0.17 ml DOX solution with the concentration of 0.4 mg/ml was added into the tissue phantom. Accordingly, the volume ratio of DOX to tissue phantom is proportional to the ratio of 1 ml 0.4 mg/ml DOX to 20 ml total blood volume in rats. According to the Lambert Beer Law, the absorption in 750nm and 830nm are

$$A^{750}(0) = \varepsilon_{Hb}{}^{750}[Hb] + \varepsilon_{HbO_2}{}^{750}[HbO_2] \quad (2.1)$$

$$A^{750}(1) = \varepsilon_{Hb}{}^{750}[Hb] + \varepsilon_{HbO_2}{}^{750}[HbO_2] + \varepsilon_{DOX}{}^{750}[DOX] \quad (2.2)$$

$$A^{830}(0) = \varepsilon_{Hb}{}^{830}[Hb] + \varepsilon_{HbO_2}{}^{830}[HbO_2] \quad (2.3)$$

$$A^{830}(1) = \varepsilon_{Hb}{}^{830}[Hb] + \varepsilon_{HbO_2}{}^{830}[HbO_2] + \varepsilon_{DOX}{}^{830}[DOX] \quad (2.4)$$

where A^{750} (0) and A^{750} (1) represent the absorption at 750 nm in tissue phantom without DOX and with DOX, respectively. A^{830} (0) and A^{830} (1) represent the absorption at 830 nm in tissue phantom without DOX and with DOX, respectively.

2.3.2e Steady-state diffuse reflectance spectroscopy (SSDRS) for measuring changes in tumor vascular oxygenation (ΔHbO_2)

A broadband diffuse reflectance spectrometer was used to acquire reflectance spectra from tumor tissue. Briefly, continuous wave (CW) light from a 20 W tungsten-halogen light source (HL-2000HP, ocean optics, FL) is coupled into a 2.6-mm core diameter fiber optic bundle, the distal end of which is placed in physical contact with the surface of the tumor. After being scattered in the tumor tissue, the transmitted light is collected by a 1-mm core diameter detection fiber, the end of which is coupled to a hand-held spectrometer (USB2000, Ocean optics, FL). The broadband light diffuse spectrometer provides reflectance spectra from 400 to 900 nm.

According to the modified Beer-Lambert law, changes of oxy- and deoxy-hemoglobin concentration, $\Delta[HbO_2]$ and $\Delta[Hb]$, can be derived from the measured amplitudes at two wavelengths (750nm and 830nm), by using extinction coefficients of oxy- and deoxy-Hb published by Cope [27], as given in Equations. (2.5) and (2.6):

$$\Delta[HbO_2] = \frac{-1.532\log(\frac{A_b}{A_t})^{750} + 1.753\log(\frac{A_b}{A_t})^{830}}{DPF \cdot d} \quad (2.5)$$

$$\Delta[Hb] = \frac{1.758\log(\frac{A_b}{A_t})^{750} - 0.92\log(\frac{A_b}{A_t})^{830}}{DPF \cdot d} \quad (2.6)$$

where A_b is the baseline amplitude, A_t is the transient amplitude during the intervention, and d is the direct source-detector separation. *DPF* (differential path-length factor) is a tissue-dependent parameter and defined as the ratio between the optical path length and the physical separation between the source and detector.

2.3.3 Results

2.3.3a Disturbance of DOX on the absorption of tissue phantom

There is absorption difference between tissue phantom with and without DOX, as shown in Figure 2.1. However, the differences are relatively small. Indeed, the relative changes of absorption in wavelength of 750nm and 830nm are $\frac{A^{750}(1) - A^{750}(0)}{A^{750}(0)}$=4.85% and

$\frac{A^{830}(1) - A^{830}(0)}{A^{830}(0)}$ =4.80%, respectively. In order to investigate the disturbance of DOX on calculating oxygen saturation, absorption spectrum profiles between 700 and 900 nm were normalized by absorption values at the wavelength of 700 nm. The normalized spectra cover the wavelengths we utilized for calculating hemoglobin concentration. As shown in figure 2.2, profiles of normalized absorption spectrum in NIR range appeared to be overlaid.

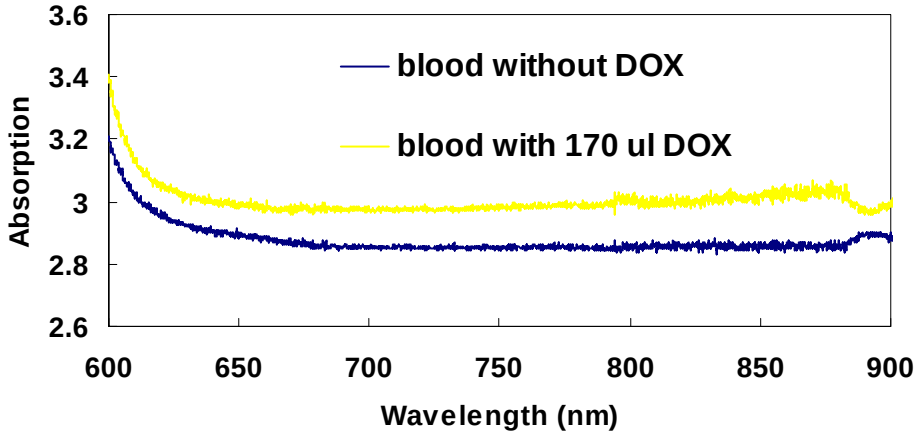

Figure 2.1 Absorption spectra of tissue phantoms with (yellow curve) or without 170 l DOX (blue curve). The unit for absorption is arbitrary unit.

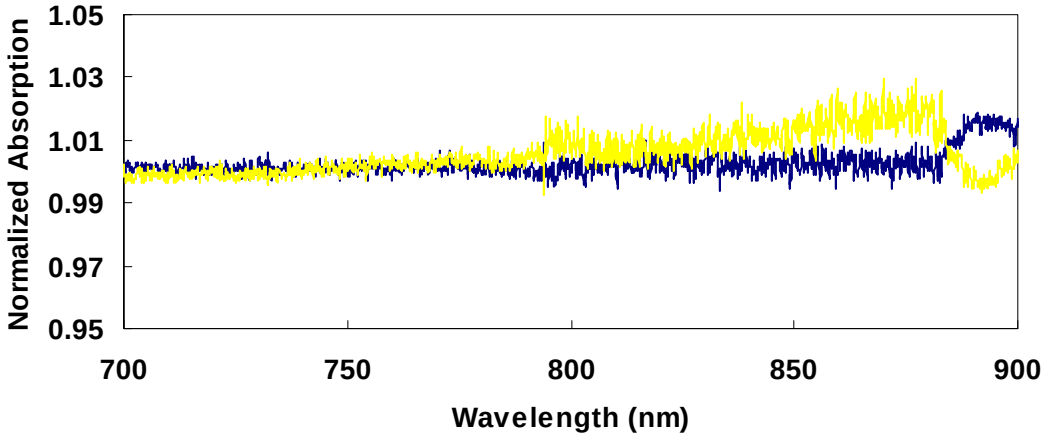

Figure 2.2 Normalized absorption spectra of tissue phantoms with (yellow curve) or without 170 l DOX (blue curve) in the wavelength range of 700 ~ 900 nm.

2.3.3b Changes in Tumor volume and body weight during chemotherapy

Tumor volume and body weight were monitored before and after DOX treatment to examine the tumor response. Changes in tumor volume and body weight were normalized by the values at day 0 (before DOX administration).

a)

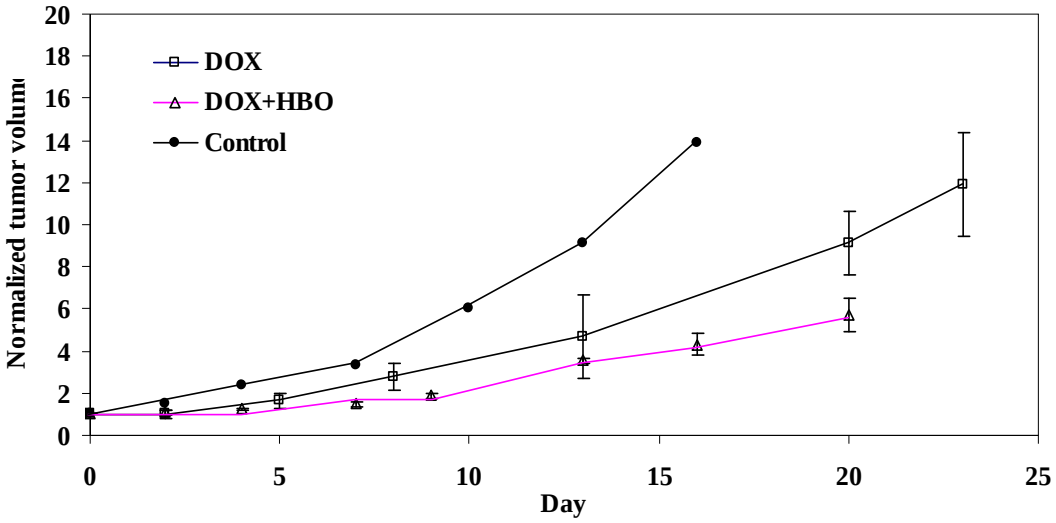

b)

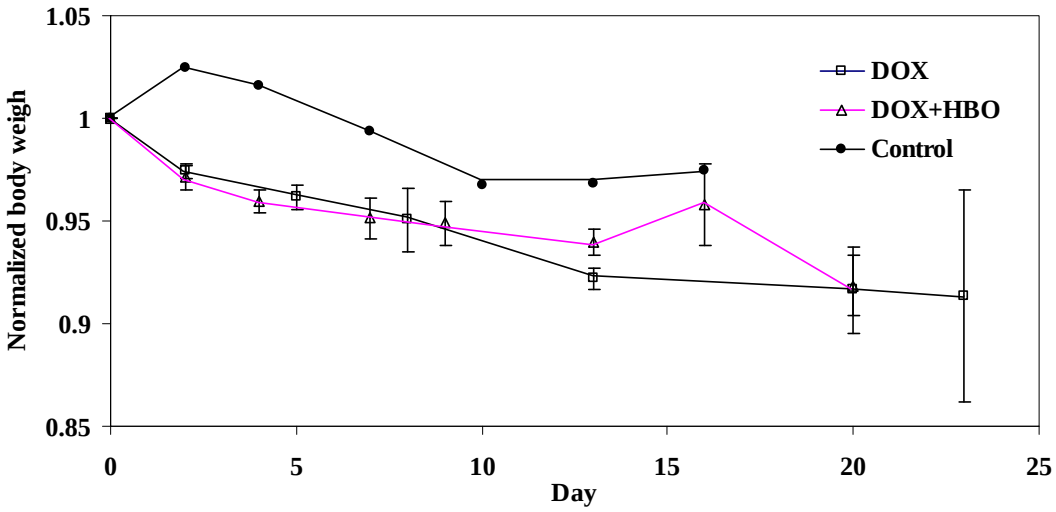

Figure 2.3 Normalized (a) tumor volume and b) body weight in rats with saline injection (●), DOX treatment (□) and HBO + DOX treatment (Δ).

Tumors in the control group grow significantly faster than tumors with treatment in the other groups ($p<0.05$), as shown in Figure 2.3a. Tumors with combined treatment of HBO and DOX grow significantly slower than those with DOX treatment except for the first two days after treatment ($p<0.05$). Basically, there is no significant difference for tumor volume in HBO + DOX and DOX groups on the 2nd day after treatment. However, significant differences are observed starting from 5th day after treatment between the DOX treated and control group ($p< 0.05$). Regarding body weight loss, figure 2.3b indicated that rats in DOX group and DOX + HBO group had significant and continuous body weight loss after day 0. Rats in control group gained weight at day 2, and started to lose weight after day 4, and then kept constant body weight thereafter.

2.3.3c Vascular hemodynamic changes of rats in DOX group

Values of $\Delta[HbO_2]$ of rats in DOX group showed increases with values in a range of 0.07 ~ 0.12 (mM/DPF), when the gas switched from air to oxygen before DOX injection. When the gas was switched from air to oxygen after DOX administration, the maximal amplitude of $\Delta[HbO_2]$ increased with values in a range of 0.02 ~ 0.04 (mM/DPF), which is significantly less than the increase achieved with O_2 inhalation before DOX administration, as shown in figure 2.4. We also noticed the signal changes during DOX i.v. injection.

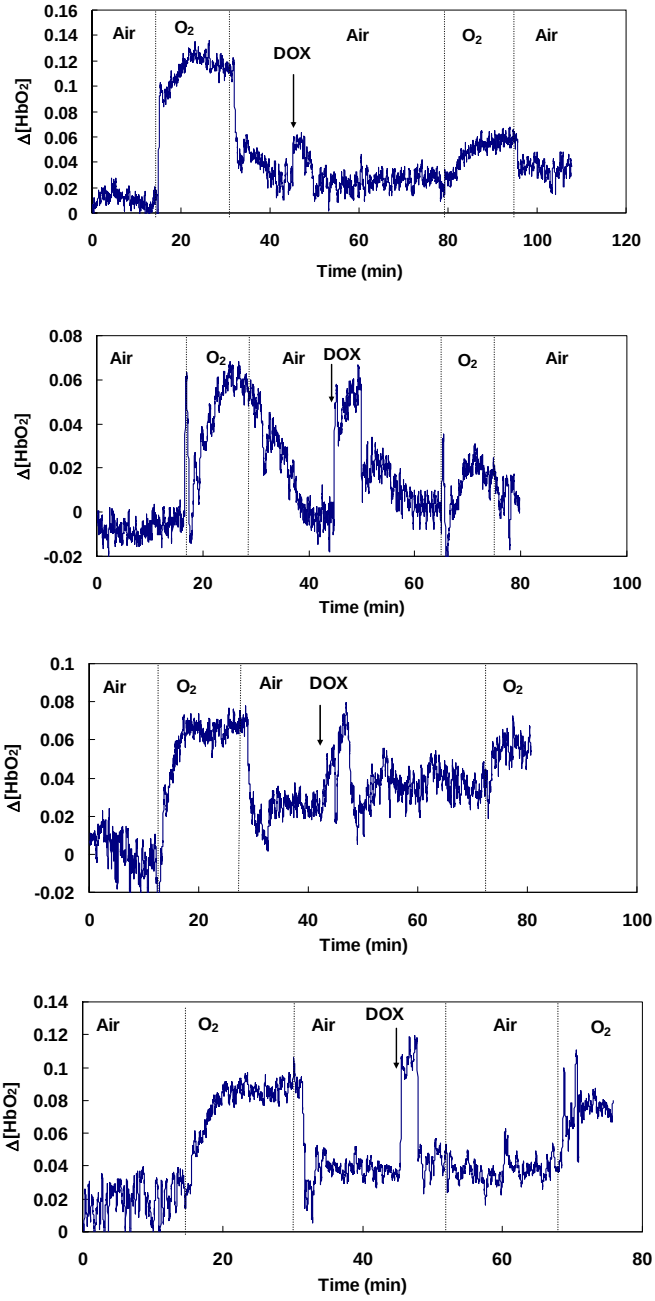

Figure 2.4 Time profile of $\Delta[HbO_2]$ of tumors (1~4) in DOX group when the rat was under gas intervention. The unit for $\Delta[HbO_2]$ is mM/DPF. $\Delta[HbO_2]$ of the 5th rat was discarded because of misplaced gas mask during the experiment due to the movement of the rat.

2.3.3d Vascular hemodynamic changes of rats in DOX +HBO group

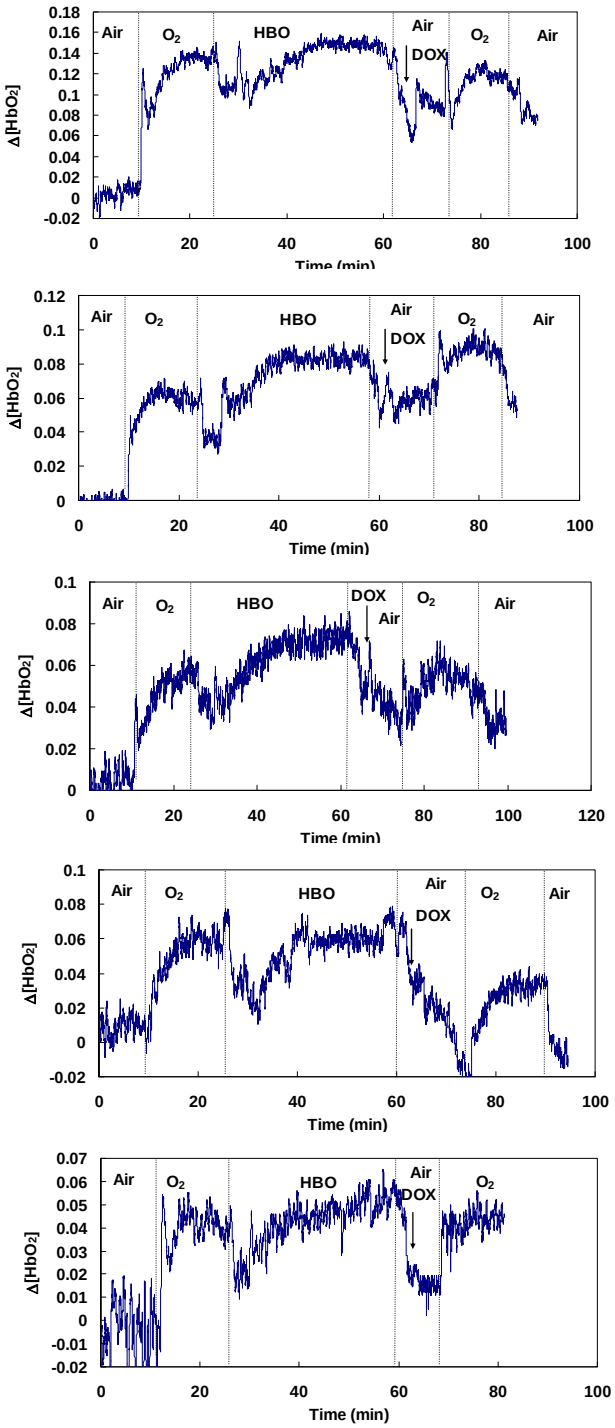

Figure 2.5 Typical time profile of $\Delta[HbO_2]$ of tumors in DOX + HBO group (n=5) when the rat was under gas intervention.

It shows a stable baseline in $\Delta[HbO_2]$ when rats were inhaling air. $\Delta[HbO_2]$ increase immediately in the first few minutes and more gradually afterwards, as shown in figure 2.5. When the rats were exposed to hyperbaric oxygen, $\Delta[HbO_2]$ has a further increase until reaching a stabilized value. DOX i.v. injection immediately after HBO caused some fluctuation of signal, but stabilized when the injection is finished. $\Delta[HbO_2]$ has a stable baseline but with values greater than air inhalation before HBO when the rats were breathing air after HBO. Similar to DOX group, the maximal amplitude of $\Delta[HbO_2]$ achieved with O_2 inhalation prior to the DOX administration is significantly greater than that achieved with O_2 inhalation after DOX administration.

2.3.3e Vascular hemodynamic changes of rats in control group

$\Delta[HbO_2]$ have stable baseline values when rats were breathing air, as shown in figure 2.6. $\Delta[HbO_2]$ increased when the gas was switching to oxygen, and decreased when the gas was switched back to air, as expected. Different from $\Delta[HbO_2]$ in DOX treated group, the change of amplitude in $\Delta[HbO_2]$ when the gas switched from air to oxygen after saline injection is similar to the change due to gas intervention before injection in both rats.

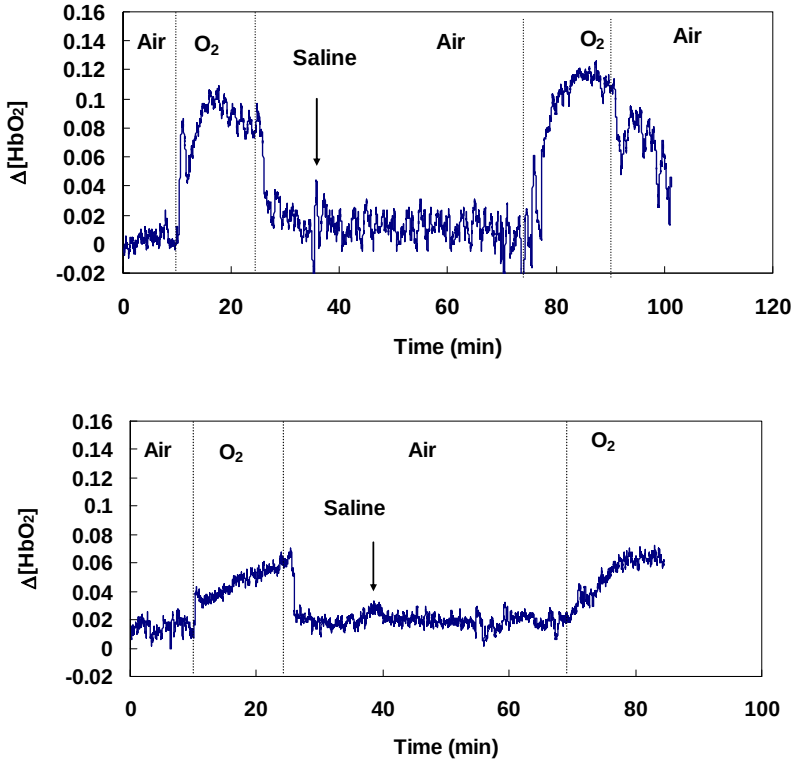

Figure 2.6 Time profile of $\Delta[HbO_2]$ of tumors in control group (n=2) when rats were subjected to gas intervention.

2.3.4 Discussion and Conclusion

In our study, we randomized breast tumors into three groups: group with DOX injection, group with DOX injection following HBO exposure at 2 atm, control group with saline injection. The result showed that tumors in HBO + DOX group grow significantly slower than those with DOX

alone. HBO enhanced chemotherapeutic response of mammary carcinoma NF13762 to DOX *in vivo* reflected by slowing down the tumor growth after treatment.

Resistance to chemotherapy is common in hypoxic tumors. HBO may help overcome chemotherapy resistance by improving both tumor perfusion and cellular sensitivity. Improving tumor oxygenation and vascularization may increase drug delivery. This has been shown experimentally and in nude mice with human epithelial ovarian cancer treated with cisplatin [28]. Reactive oxygen species (ROS), or free radicals are by-product of aerobic respiration and cellular metabolism and induced by oxidative stress during hypoxia (oxygen deficiency), reperfusion or hyperoxia (excess oxygen). ROS, at low levels, assist tumor growth but become toxic at high levels. This can be explained by the "threshold effect" whereby ROS reach a level beyond which the antioxidant capacity is inundated, resulting in irreversible damage and apoptosis [29,30]. One of the mechanisms of action of doxorubicin is production of ROS. By increasing ROS level, HBO push ROS levels past the threshold level, and thus enhanced the ROS-localized effects of doxorubicin [31,32]. Another mechanism of HBO is to push cell to enter a proliferate stage, thus sensitizing them to radiotherapy and some chemotherapy by improving oxygenation. It has been showed that HBO enhanced the chemotherapeutic effects of doxorubicin in an experimental model of pulmonary sarcoma [13]. HBO stimulated proliferation of an MCA-2 metastatic lung tumor cell line and induced cells to enter the replicating cycle compared to cells left at ambient pressure [13]. Other studies found that HBO increased the ratio of prostate cancer cells *in vitro* accumulating in G_2/M phases from the G_0 arrest phase [33]. Generally speaking, HBO therapy in combination with chemotherapy may be justified by the following: 1) improved oxygenation improves drug delivery to hypoxic regions in the tumor; 2) increasing intratumoral ROS levels beyond the threshold may induce tumor destruction; 3) improved oxygenation may also cause cell to enter a proliferate stage, thus sensitizing them to radiotherapy and some chemotherapy; 4) HBO may remove hypoxia stimulus that drives angiogenesis.

Even though the DOX dosage is reported to cause minimal cardiotoxicity, the result showed that changes in amplitudes of $\Delta[HbO_2]$ before DOX administration were much greater than the change after treatment in rats of DOX group and DOX + HBO group. It is likely that the amplitude difference results from the known cardiotoxicity reaction, the major side effect of DOX. It has been suggested that cardiac dysfunction induced by DOX resulted from the imbalances of the circulatory system such as decreases in blood pressure or the direct effects on vascular wall [34]. During the course of i.v. injection of DOX, the vasculature was exposed to high levels of DOX, and *in vitro* studies have suggested that DOX acutely induces vascular smooth muscle to release Ca^{2+} from its intracellular storage site and causes direct vasoconstrictor [35] and vasodilator effects [36]. Furthermore, the combination of doxorubicin and HBO would also be expected to enhance the agent's cardiotoxicity because of the toxicity to cardiomyocytes of HBO. Therefore, the clinical addition of HBO to doxorubicin may not change the risk-benefit ratio of the agent. NIRS, in turn, may provide a novel approach to monitor the cardiotoxicity of treatment, which may leads to an optimized therapeutic plan to minimize the side effect of treatment. We also noticed the signal fluctuation in $\Delta[HbO_2]$ during DOX injection in DOX group. DOX solution is orange-red, so it is likely that DOX bolus injection would cause the absorption change of tumor tissue in NIR range. We measured and compared the spectra of tissue phantoms before and after adding DOX, to examine the disturbance of DOX injection on the signal of $\Delta[HbO_2]$. There were absorption differences when comparing both absorption spectra (Figure 2.1). However, the normalized spectra appeared to be overlaid (Figure 2.2). Therefore, it implied that DOX would affect total hemoglobin concentration, rather than oxygen saturation.

3. Key Research Accomplishments and Reportable Outcomes

3.1 Ph.D. Dissertation:

Title: TISSUE AND VASCULAR OXYGENATION DYNAMICS DETERMINED BY OPTICAL APPROACHES AND MRI

3.2 Publications in peer-reviewed journals:

(1) **Mengna Xia**, Vikram Kodibagkar, Hanli Liu and Ralph Mason, "Tumor oxygen dynamic measured simultaneously by near infrared spectroscopy and ^{19}F magnetic resonance imaging in rats", Physics in Medicine and Biology,51: 45-60 (2006) .

(2) Jae Kim**, Mengna Xia,** Hanli Liu, **"**Extinction coefficients of hemoglobin for near-infrared spectroscopy of tissue", IEEE Engineering in Medicine and Biology magazine, 24: 118-121 (2005).

(3) Yueqing Gu, Wei R. Chen, **Mengna Xia**, Sang W. Jeong, and Hanli Liu, "Effect Of photothermal therapy On breast tumor vascular contents: non-invasive monitoring by near infrared spectroscopy", Photochemistry and Photobiology, 81: 1002-1009 (2005).

3.3 Proceeding papers and presentations:

(1) **Mengna Xia**, Benjamin Levine, Ralph Mason, Hanli Liu, "Simultaneous monitoring of tumor vascular oxygenation and tissue oxygen tension under hyperbaric oxygen exposure", in Biomedical Topical Meetings on CD-ROM (The Optical Society of America, Washington, DC, 2006).

(2) **Mengna Xia**, Vikram Kodibagkar, Ralph Mason, Benjamin Levine, Hanli Liu, "Tumor vascular and tissue oxygenation dynamics under normobaric and hyperbaric oxygen interventions", presented at the fourth Era of Hope meeting for the Department of Defense (DOD) Breast Cancer Research Program (BCRP) held on June 8-11, 2005 in Philadelphia, Pennsylvania.

(3) **Mengna Xia**, Ralph Mason, Hanli Liu, "A model of hemodynamic responses of rat tumors to hyperoxic gas challenge", Proc. SPIE- Optical Tomography and Spectroscopy of Tissue VI, 5693: 301-307 (2005).

4. Conclusions

In this 4-year study, we have learned that HBO enhances the therapeutic action of doxorubicin in our tumor model, probably by multiple physiological mechanisms. The present study reveals that DOX may be used in conjunction with HBO to obtain the same effect as higher doxorubicin doses. Meanwhile, NIRS may work as an attractive approach to monitor the treatment.

Overall, our study over the last few years has demonstrated that 1) NIRS and MRI and FOXY^{TM} oxygen sensor are complimentary approaches to monitor tumor oxygenation. 2) Tumor tissue oxygenation achieved by hyperbaric oxygenation persists over 10-20 minutes even after terminating hyperbaric oxygenation intervention. 3) Several correlations existed for both modalities (HbO_2 and pO_2) under sequences of hyperoxic gas intervention with hyperbaric oxygen exposure. Correlation of tumor vascular oxygenation and tumor tissue pO_2 determined simultaneously by those techniques could give us a better understanding on the patho-physiology of tumor and response to therapeutic interventions. 4) HBO enhanced the therapeutic action of doxorubicin in our tumor model, probably by multiple physiological mechanisms. DOX could be used in conjunction with HBO to achieve the same effect as higher doxorubicin doses. NIRS may work as an attractive approach to monitor radiation-toxicity of the treatment.

5. References

1 . Weiss, R., G. Sarosy, K. Clagett-carr, M. Russo, and B. Leyland-jones, *Anthracyline analogs: the past, present, and future.* Cancer Chemother Pharmacol, 1986. **18**: p. 185-97.

2. Brown, J.M., *The hypoxic cell: a target for selective cancer therapy--eighteenth Bruce F. Cain Memorial Award lecture.* Cancer Res., 1999. **59**(23): p. 5863-5870.

3. Hall, E., *Radiobiology for the Radiologist*. 4th ed. 1994, Philadelphia, PA: Lippincott.

4. Thews, O., D. Kelleher, and P. Vaupel, *Erythropoietin restores the anemia-induced reduction in cyclophosphamide cytotoxicity in rat tumors.* Cancer Res, 2001. **61**: p. 1358-61.

5. Bush, R., R. Jenkin, W. Allt, F. Beale, A. Dembo, and J. Pringle, *Definitive evidence for hypoxic cells influencing cure in cancer therapy.* Br J Cancer, 1978. **37**: p. 302-06.

6. Hall, E.J., *The oxygen effect and reoxygenation*, in *Radiobiology for the Radiologist*, E.J. Hall, Editor. 1994, J. B. Lippincott: Philadelphia. p. 133-152.

7. Brady, L., H. Plenk, J. Hanley, J. Glassburn, S. Kramer, and R. Parker, *Hyperbaric oxygen therapy for carcinoma of the cervix stages IIB, IIIB, and IVA: results of a randomized study by the radiation therapy oncology group.* Int J Radiat Onclo Biol Phys, 1981. **7**: p. 991-8.

8. Brizel, D., W. Hage, R. Dodge, M. Munley, C. Piantadosi, and M. Dewhirst, *Hyperbaric Oxygen Improves Tumor Radiation Response Significantly More Than carbogen/Nicotinarnid.* Radiation Res., 1997. **147**: p. 715-20.

9. Rockwell, S., M. Kelley, C. Irvin, C. Hughcs, E. Porter, H. Yabuki, and J. Fischer, *Modulation of tunlor oxygenation and radiosensitivity by a perfluorooctylbromide emulsion.* Radiother Oncol, 1991. **22**: p. 92-8.

10. Lustig, R., N. Lowe, C. Rose, J. Haas, S. Krasnow, M. Spaulding, and I. Prosnitz, *Phase 1/11 study kluosol and 100% oxygen as an adjuvant to radiation i11 the treatment of locally advanced non-small cell carcinoma of the head and neck.* Int. .I. Radiat. Oncal. Biol. Phys., 1989. **16**: p. 1587-93.

11. Xia, M., V. Kodibagkar, R. Mason, B. Levine, and H. Liu. Tumor vascular and tissue oxygenation dynamics under normobaric and hyperbaric oxygen interventions. in fourth Era of Hope meeting for the Department of Defense (DOD) Breast Cancer Research Program (BCRP). 2005. Philadelphia, PA.

12. Kalns, J., L. Krock, and E. Piepmeier, *The effect of hyperbaric oxygen on growth and chemosensitivity of metastatic prostate cancer.* Anticancer Res, 1998. **18**.

13. Petre, P., F. Baciewicz, S. Figan, and J. Spear, *Hyperbaric oxygen as a chemotherapy adjuvant in the treatment of metastatic lung tumors in a rat model.* J Thorac Cardiovasc Surg, 2003. **125**: p. 85-95.

14. Kalns, J., L. Krock, and E. Piepmeier, *The effect of hyperbaric oxygen on growth and chemosensitivity of metastatic prostate cancer.* Anticancer Res, 1998. **18**.

15. Takiguchi, N., N. Saito, M. Nunomura, K. Kouda, K. Oda, N. Furuyama, and N. Nakajima, *Use of 5-FU plus hyperbaric oxygen for treating malignant tumors:evaluation of antitumor effect and measurement of 5-FU in individual organs.* Cancer Chemother Pharmacol, 2001. **47**: p. 11-14.

16. Stuhr, L., Hyperbaric oxygen alone or combined with 5-FU attenuates growth of DMBA-induced rat mammary tumors. Cancer Lett, 2004. **210**: p. 35-40.

17. Zhao, D., L. Jiang, and R. Mason, *Measuring changes in tumor oxygenation.* Methods Enzymol, 2004. **386**: p. 378-418.

18. Jobsis, F., *Noninvasive, infrared monitoring of cerebral and myocardial oxygen sufficiency and circulatory parameters.* Science, 1977. **198**: p. 1264-7.

19. Liu, H., Y. Song, K.L. Worden, X. Jiang, A. Constantinescu, and R.P. Mason, *Noninvasive Investigation of Blood Oxygenation Dynamics of Tumors by Near-Infrared Spectroscopy. Appl. Opt.*, 2000. **39**(28): p. 5231-5243.

20. Delpy, D.T. and M. Cope, *Quantification in tissue near-infrared spectroscopy.* Phil. Trans. R. Soc. Lond. B., 1997. **352**: p. 649-659.

21. Homma, S., T. Fukunaga, and A. Kagaya, Influence of adipose tissue thickness on near-infrared spectroscopic signals in the measurement of human muscles. J. Biomed. Opt., 1996. **1**: p. 418-424.

22. Xia, M., V. Kodibagkar, H. Liu, and R.P. Mason, Tumour oxygen dynamics measured simultaneously by near-infrared spectroscopy and 19F magnetic resonance imaging in rats. Physics in medicine and biology, 2006. **51**: p. 45-60.

23. Kim, J., D. Zhao, R. Mason, and H. Liu. Acute effects of combreatastatin A4 phosphate on breast tumor hemodynamics monitored by Near Infrared Spectroscopy. in in Biomedical Optics 2006 Technical Digest (Optical Society of America, Washington, DC, 2006). 2006.

24. Kim, J., D.J. Cuccia, J. Lee, A.E. Cerussi, A.J. Durkin, and B.J. Tromberg. Monitoring of chemotherapy effects on rat breast tumors: a correlation between optical signals and histology. in SPIE. 2007. San Jose, CA.

25. Cohen, M., A. Johnston-Early, M. Hood, M. McKenzie, M. Citron, N. Jaffe, and S. Krasnow, *Drug precipitation within i.v. tubing: a potential hazard of chemotherapy administration.* Cancer Treat Rep. 1985 Nov;69(11):1325-6, 1985. **69**: p. 1325-6.

26. Esenaliev, R., Y. Petrov, O. Hartrumpf, D. Deyo, and D. Prough, Continuous, noninvasive monitoring of total hemoglobin concentration using an optoacoustic technique. Appl Opt, 2004. **43**: p. 3401-07.

27. Cope, M., *the application of near infrared spectroscopy to non invasive monitoring of cerebral oxygenation in the newborn infant*. 1991, Ph.D dissertation in University of London.

28. Alagoz, T., R. Buller, B. Anderson, K. Terrell, R. Squatrito, T. Niemann, D. Tatman, and P. Jebson, *Evaluation of hyperbaric oxygen as a chemosensitizer in the treatment of epithelial ovarian cancer in xenografts in mice.* Cancer, 1995. **75**: p. 2313-22.

29. Kong, Q., J. Beel, and K. Lillehei, *A threshold concept for cancer therapy.* Med Hpyotheses, 2000. **55**: p. 29-35.

30. Harrisona, L., M. Chadhaa, R. Hillb, K. Hua, and D. Shashaa, *Impact of tumor hypoxia and anemia on radiation therapy outcomes.* Oncologist, 2002. **7**: p. 492-508.

31. Kizaka-Kondoh, S., M. Inoue, H. Harada, and M. Hiraoka, *Tumor hypoxia: a target for selective cancer therapy.* Cancer Sci, 2003. **94**: p. 1021-28.

32. McMillan, T., K. Calhoun, J. Mader, C. Stiernberg, and S. Rajaraman, *The effect of hyperbaric oxygen on oral mucosal carcinoma.* Laryngoscope, 1989. **99**: p. 241-44.

33. Kalns, J. and E. Piepmeier, *Exposure to hyperbaric oxygen induces cell cycle perturbation in prostate cancer cells.* In Vitro Cell Dev Biol Anim, 1999. **35**: p. 98-101.

34. Murata, T., H. Yamawaki, M. Hori, K. Sato, H. Ozaki, and H. Karaki, *Chronic vascular toxicity of doxorubicin in an organ-cultured artery.* British J of Pharm, 2001. **132**: p. 1365-73.

35. Kanmura, Y., L. Raeymaekers, and R. Casteels, *Effects of doxorubicin and ruthenium red on intracellular Ca2+ stores in skiined rabbit mesenteric smooth-muscle fibres.* Cell Calcium, 1989. **10**: p. 433-39.

36. Ferrans, V., J. Clark, J. Zhang, Z. Yu, and E. Herman, *Pathogenesis and prevention of doxorubicin cardiomyopathy.* Tsitologiia, 1997. **39**: p. 928-37.

INSTITUTE OF PHYSICS PUBLISHING PHYSICS IN MEDICINE AND BIOLOGY

Phys. Med. Biol. **51** (2006) 45–60 doi:10.1088/0031-9155/51/1/004

Tumour oxygen dynamics measured simultaneously by near-infrared spectroscopy and ^{19}F magnetic resonance imaging in rats*

Mengna Xia[1], Vikram Kodibagkar[2], Hanli Liu[1] and Ralph P Mason[1,2]

[1] Joint Biomedical Engineering Graduate Program, University of Texas at Arlington/University of Texas Southwestern Medical Center at Dallas, TX 76019, USA
[2] Cancer Imaging Program, Department of Radiology, University of Texas Southwestern Medical Center at Dallas, TX 75390, USA

E-mail: Ralph.Mason@UTSouthwestern.edu

Received 1 April 2005, in final form 17 October 2005
Published 14 December 2005
Online at stacks.iop.org/PMB/51/45

Abstract

Simultaneous near-infrared spectroscopy (NIRS) and magnetic resonance imaging (MRI) were used to investigate the correlation between tumour vascular oxygenation and tissue oxygen tension dynamics in rat breast 13762NF tumours with respect to hyperoxic gas breathing. NIRS directly detected global variations in the oxygenated haemoglobin concentration ($\Delta[HbO_2]$) within tumours and oxygen tension (pO_2) maps were achieved using ^{19}F MRI of the reporter molecule hexafluorobenzene. Multiple correlations were examined between rates and magnitudes of vascular ($\Delta[HbO_2]$) and tissue (pO_2) responses. Significant correlations were found between response to oxygen and carbogen breathing using either modality. Comparison of results for the two methods showed a correlation between the vascular perfusion rate ratio and the mean pO_2 values ($R^2 > 0.7$). The initial rates of increase of $\Delta[HbO_2]$ and the slope of dynamic pO_2 response, $d(pO_2)/dt$, of well-oxygenated voxels in response to hyperoxic challenge were also correlated. These results demonstrate the feasibility of simultaneous measurements using NIRS and MRI. As expected, the rate of pO_2 response to oxygen is primarily dependent upon the well perfused rather than poorly perfused vasculature.

1. Introduction

Tumour oxygenation has been widely recognized as a pivotal factor in the efficacy of radiotherapy (Hall 1994), photodynamic therapy (Chapman *et al* 1991) and some

* Presented in part at the 12th annual meeting of the International Society of Magnetic Resonance in Medicine, Kyoto, 2004.

chemotherapies (Brown 1999), and patient stratification with respect to tumour oxygenation status could be clinically important (Hockel *et al* 1996, Fyles *et al* 1998, Welch *et al* 2003). It has been hoped that modulation of tumour oxygenation could be applied to enhance therapeutic efficacy. An attractive intervention is breathing hyperoxic gas, and, indeed, several clinical trials have examined the efficacy of normobaric or hyperbaric oxygen, to improve therapeutic outcome, but often with marginal success (Overgaard and Horsman 1996). It has been suggested that outcome might have been improved, if responsive tumours could have been identified *a priori*. Accordingly, accurate evaluation of tumour oxygenation in response to interventions at various stages of growth should provide a better understanding of tumour response to therapy, potentially allowing therapy to be tailored to individual characteristics.

Given the importance of tumour oxygenation, many techniques have been developed based on microelectrodes, optical reflectance, electron paramagnetic resonance (EPR), magnetic resonance imaging (MRI) and nuclear medicine approaches, as reviewed previously (Mason *et al* 2002, Zhao *et al* 2004). While each approach has unique strengths, some are highly invasive. Near-infrared spectroscopy (NIRS) has been developed in recent years as a promising non-invasive technique to quantify the concentration of tissue chromophores, such as oxygenated and deoxygenated haemoglobin, water and lipid (Sevick *et al* 1991, Liu *et al* 2000). Due to the deep penetration depth and biochemical specificity of NIRS, it has been widely applied for quantitative measurements of cerebral oxygenation (Delpy and Cope 1997, Yodh and Boas 2003) and blood oxygenation in muscles *in vivo* (Homma *et al* 1996). Recently, NIRS has been also used to monitor tumour vascular oxygenation with respect to interventions (Hull *et al* 1999, Liu *et al* 2000, Gu *et al* 2003). With notable exceptions (Chance 1997, Dehghani *et al* 2004, Shah *et al* 2004, Pogue *et al* 2003), NIRS currently lacks spatial resolution, and, thus, the utility of global measurements requires validation, given the well-documented heterogeneity of tumour oxygenation. In this regard, Conover *et al* (2000) compared the spatially averaged measurement of tumour oxygen saturation (SO_2) using NIRS with the local SO_2 in individual blood vessels measured by cryospectrophotometry. The sensitivity and specificity analysis suggests that NIRS may identify clinically relevant hypoxia, even when its spatial extent is below the resolution limit of the NIRS technique. We have previously investigated correlates between pO_2 assessed by electrodes (Mason *et al* 2003, Kim *et al* 2003b) or fibre-optic probes and NIRS (Gu *et al* 2003). On occasion, there was a good correlation between global vascular oxygenation and local pO_2 at individual locations, but often, disparate behaviour was observed. Sequential MRI and NIRS suggested a better relationship based on average pO_2 from multiple locations (Kim *et al* 2003b). We have now implemented simultaneous NIRS and ^{19}F MRI to examine the relationships further. Since NIRS is entirely non-invasive it would provide an attractive surrogate for monitoring tumour oxygenation, and, hence, we seek correlations with absolute pO_2 measurements observed simultaneously by MRI.

2. Materials and methods

Investigations were approved by the Institutional Animal Care and Use Committee.

2.1. Animal preparation and experimental set-up

Mammary adenocarcinomas 13762NF (cells originally obtained from the Division of Cancer Therapeutics, NCI) were implanted in skin pedicles (Hahn *et al* 1993) on the foreback of ten adult female Fisher 344 rats (∼150 g). When the tumours reached ∼1 cm in diameter, the rats were anaesthetized with ketamine hydrochloride i.p. (100 mg kg^{-1} body weight, Aveco, Fort

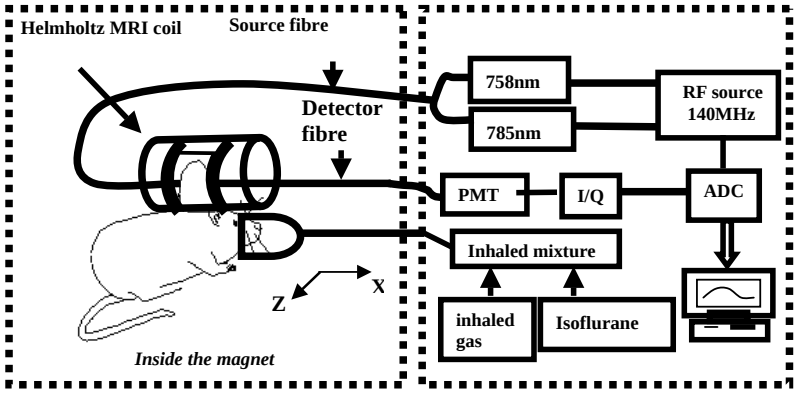

Figure 1. Schematic of experimental set-up. Z is along the bore of the magnet, and X along the axis of the RF coil. PMT represents a photomultiplier tube, I/Q represents an In-phase and quadrature (I/Q) demodulator chip and ADC represents an analogue-to-digital converter.

Dodge, IA) and were maintained under general gaseous anaesthesia (air and 1% isoflurane; Baxter International Inc, Deerfield, IL). Tumour hair was trimmed to give good optical contact for NIR light transmission. Hexafluorobenzene (HFB, 50 μl, 99.9%, Lancaster Co, Pelham, NH) was administered along two or three tracks in central and peripheral regions of the tumours in a single plane (transverse to the rat's tumour, and in the region of NIR photon pathway) using a Hamilton syringe with a 32 G needle. The needle was inserted manually to penetrate across the tumour and was withdrawn $\sim$1 mm to reduce pressure and 3–4 μl of HFB were deposited. The needle was then repeatedly withdrawn 1–2 mm and further HFB deposited at each point, as described in detail previously (Zhao *et al* 2004).

The tumour was placed inside a size-matched Helmholtz coil, specially designed for the simultaneous MRI-NIRS study. The tumour was inserted between the two loops of the Helmholtz coil and two NIRS probes were introduced through the ends of the coil along the coil axis (figure 1). The probes were positioned to be in the same plane as the HFB injection. The rats were placed in the magnet on their side, and body temperature was maintained using a warm water blanket. A total of ten rats were used in the study: seven rats were subjected to respiratory challenge in the sequence of air–oxygen–air–carbogen–air, one rat breathed air–carbogen–air–oxygen–air, one rat breathed air–carbogen–air, and one breathed air–oxygen–air.

2.2. NIRS for measuring $\Delta[HbO_2]$

A homodyne frequency-domain system (NIM, Philadelphia, PA) was used to monitor the global change of deoxy- and oxyhaemoglobin concentration ($\Delta[HbO_2]$) in the tumour, as described previously (Yang *et al* 1997), though with minor modifications to ensure MR compatibility (figure 1). Briefly, the laser light, which was emitted from two laser diodes (at 758 nm and 785 nm), was amplitude-modulated at 140 MHz and time gated on and off sequentially. The two time-shared laser beams illuminated the tumour surface alternately through a light-delivery fibre bundle (source fibre) with a 7 m length and a 3 mm bundle diameter. The long fibre bundle ensured the separation of the NIRS hardware from the magnet. After being absorbed and scattered in the tumour tissue, the transmitted light was collected on the opposite side of the tumour by another fibre bundle (detector fibre) of same length and diameter as those of source

fibre. The collected optical signal was detected and amplified by a photomultiplier tube (PMT). The probe sheaths at the fibre tips were made of nylon for MR compatibility. An In-phase and quadrature (I/Q) demodulator chip was used to demodulate the amplitude-modulated signal from the PMT.

In principle, since the I/Q system could give both phase and amplitude values, it should be possible to calculate absolute HbO_2, Hb and SO_2 (Yang *et al* 1997). However, given the tumour's small size and large spatial heterogeneity, we are currently unable to achieve reliable absolute quantification using the conventional algorithm (Fishkin and Gratton 1993) based on the diffusion approximation. Instead, based on modified Beer–Lambert's law, we simply use the amplitude of the light transmitted through the tumour to calculate concentration changes in HbO_2, Hb and Hb_t of the tumour caused by respiratory intervention. Namely, changes of oxy- and deoxyhaemoglobin concentration, $\Delta[HbO_2]$ and $\Delta[Hb]$, respectively, can be derived from the measured amplitudes at the two wavelengths (758 nm and 785 nm) (Kim *et al* 2003b)

$$\Delta[HbO_2] = \frac{-10.63 \log\left(\frac{A_b}{A_t}\right)^{758} + 14.97 \log\left(\frac{A_b}{A_t}\right)^{785}}{\mathrm{DPF} \cdot d} \tag{1}$$

$$\Delta[Hb] = \frac{8.95 \log\left(\frac{A_b}{A_t}\right)^{758} - 6.73 \log\left(\frac{A_b}{A_t}\right)^{785}}{\mathrm{DPF} \cdot d} \tag{2}$$

where A_b is the baseline amplitude, A_t is the transient amplitude during measurement and d is the direct source–detector separation. DPF (differential path-length factor) is a tissue-dependent parameter and is defined as the ratio between the optical path length and the physical separation between the source and detector. The units for $\Delta[HbO_2]$, $\Delta[Hb]$ and $\Delta[Hb]_{total}$ are mM. DPF is a variable depending on tissue type and wavelengths and it is currently difficult to quantify DPF for tumours. Since this study focuses on dynamic changes of $[HbO_2]$, $\Delta[HbO_2]$ values may be scaled by a factor of DPF (in units of mM/DPF), to obtain characteristic features of tumour oxygen dynamics (Liu *et al* 2000).

2.3. Mathematical model for blood oxygenation dynamics of tumours

Based on our previous experimental study, we derived a simple mathematical model (Liu *et al* 2000) to examine tumour vascular dynamics during oxygen intervention, by analogy to the method used to quantify regional cerebral blood flow (rCBF) with diffusible radiotracers, originally developed by Kety (1951). Accordingly, changes of oxyhaemoglobin concentration in tumour vasculature induced by hyperoxic gas intervention, $\Delta[HbO_2]$, can be expressed as

$$\Delta[HbO_2(t)]^{\text{vasculature}} = \gamma H_0 \left[1 - \exp\left(-\frac{ft}{\gamma}\right)\right] = A\left[1 - \exp\left(-\frac{t}{\tau}\right)\right] \tag{3}$$

where $\Delta[HbO_2]$ corresponds to the changes in oxyhaemoglobin concentration from tumour vasculature measured by NIRS, H_0 is the arterial oxygenation input for $\Delta HbO_2^{\text{artery}}$ after time 0, f is the blood perfusion rate and γ is the vascular coefficient of the tumour, defined as the ratio of $[HbO_2]$ changes in the vascular bed to that in the veins. Specifically, $\gamma = \Delta[HbO_2]^{\text{vasculature}}/\Delta[HbO_2]^{\text{vein}}$, τ is the time constant $(= \gamma/f)$ and $A = \gamma H_0$.

Given that solid tumours often develop hypoxic regions, which are poorly perfused (Jiang *et al* 2004, Mason *et al* 1994, Mazurchuk *et al* 1999, Song *et al* 2002), we hypothesized that the observed, bi-phasic feature of $\Delta[HbO_2]$ came from two different perfusion regions (well- and poorly perfused regions). Therefore, it is reasonable to define two different blood

perfusion rates (f_1, f_2) with two different vascular coefficients (γ_1, γ_2) in the mathematical model. Consequently, equation (3) has been modified to a summation of two exponential expressions, representing two perfusion regions, as

$$\begin{aligned}\Delta[\mathrm{HbO}_2(t)]^{\text{vasculature}} &= \gamma_1 H_0\left[1-\exp\left(-\frac{f_1 t}{\gamma_1}\right)\right]+\gamma_2 H_0\left[1-\exp\left(-\frac{f_2 t}{\gamma_2}\right)\right]\\ &= A_1\left[1-\exp\left(-\frac{t}{\tau_1}\right)\right]+A_2\left[1-\exp\left(-\frac{t}{\tau_2}\right)\right]\end{aligned} \tag{4}$$

where f_1 and γ_1 are the blood perfusion rate and the vasculature coefficient, respectively, in the well-perfused region, and f_2 and γ_2 represent the same respective meanings in the poorly perfused region. Also, it follows that $A_1 = \gamma_1 H_0$, $A_2 = \gamma_2 H_0$, $\tau_1 = \gamma_1/f_1$ and $\tau_2 = \gamma_2/f_2$. Since A_1, A_2, τ_1 and τ_2 can be determined by curve-fitting equation (4) to the dynamic NIRS measurements, we can obtain the ratios for two vascular coefficients and two blood perfusion rates, as follows (Liu *et al* 2000):

$$\frac{\gamma_1}{\gamma_2}=\frac{A_1}{A_2}, \qquad \frac{f_1}{f_2}=\frac{A_1/\tau_1}{A_2/\tau_2}. \tag{5}$$

These two ratios provide insight into tumour vascular structures and blood perfusion rates. Specifically, γ_1/γ_2 may be associated with the vascular volume fraction between the two regions, and f_1/f_2 reflects the perfusion ratio between the two regions. For example, if f_1/f_2 is substantially greater than 1, the two compartments have significantly different perfusion rates.

This mathematical model is consistent with experimental animal studies (Liu *et al* 2000, Gu *et al* 2003, Kim *et al* 2003b). Moreover, it is supported by computer simulations (Kim and Liu 2005) and a phantom study (Kim and Liu 2004) each of which shows that the bi-phasic or bi-exponential feature can be present if both a slow and a fast perfusion of flow co-exist within the interrogated volume.

2.4. FREDOM *for measuring* pO_2

MRI was performed using a Varian Inova 4.7 T horizontal bore system equipped with actively shielded gradients. Shimming was performed on the tumour tissue water signal to reduce the line-width to less than 100 Hz. ^{1}H MRI (200.1 MHz) T1-weighted reference images were acquired with TR/TE of 150/10 ms and 40 × 40 mm^2 field of view. Following ^{1}H MRI, corresponding ^{19}F MR images (188.3 MHz) with a matrix size of 32 × 32 (1.25 mm per pixel) were obtained to show the distribution of HFB in the tumour. A single 10 mm thick slice was chosen to include all the injected HFB, as the plane of injection was not always perfectly aligned with the imaging plane. The actual volume interrogated is defined by the distribution of the reporter molecule in the third dimension rather than the imaging gradients (Zhao *et al* 2004). The *FREDOM* (*F*luorocarbon *R*elaxometry by *E*cho-planar imaging for *D*ynamic *O*xygen *M*apping) approach was used to measure pO_2, as described in detail previously (Hunjan *et al* 2001). The spin lattice relaxation rate (R1 = 1/T1) of HFB is highly sensitive to changes in pO_2, but not sensitive to temperature variations: a deviation of 1 ^{o}C in temperature will introduce a deviation of only 0.13 Torr in the pO_2 estimate, when pO_2 is about 5 Torr (Zhao *et al* 2004). T1 maps were computed on a voxel-by-voxel basis using nonlinear least-squares data fitting by the Gauss–Newton method. We applied a threshold to the raw T1 data in order to remove random noise, i.e., voxels with T1 error >3.6 s or T1 error/T1 >50% were disregarded. Maps of pO_2 values with 1.25 mm pixel size were obtained from the T1 maps using the equation, $pO_2 = (1/\mathrm{T1} - 0.0835)/0.001\,876$ (Hunjan *et al* 2001).

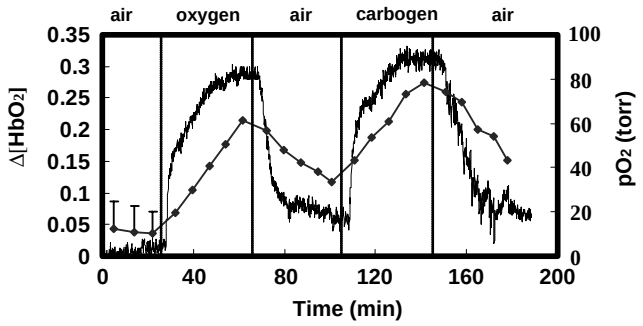

Figure 2. Temporal profiles of $\Delta[HbO_2]$ (curve only) and mean pO_2 (curve with ♦) in response to respiratory challenge. Both $\Delta[HbO_2]$ and pO_2 are group-averaged data from seven 13762NF rat breast tumours with an intervention sequence of air–oxygen–air–carbogen–air, measured simultaneously by NIRS and *FREDOM*. The standard deviations of the volume-averaged pO_2 from seven tumours are indicated for baseline, but became very large in response to interventions and are omitted. $\Delta[HbO_2]$ has units of mM/DPF.

Each pO_2 map was acquired in $6\frac{1}{2}$ min. Three baseline pO_2 data sets were acquired over 24 min for all tumours, while the rats breathed air, after which the rats were repeatedly exposed to oxygen or carbogen (95% O_2 and 5% CO_2) interventions. Five pO_2 maps were obtained during each subsequent gas switch period. Typically, for a five gas-intervention sequence (e.g., air–oxygen–air–carbogen–air), a total of 23 pO_2 maps were obtained over a period of 3 h. Due to thresholding, some voxels did not appear in all pO_2 maps and these were discarded. For temporal analysis, voxels were selected as only those which provided consistently reliable data (i.e., satisfied all the thresholding criteria specified above) for all 23 measurements over the time course with a range of 5–44 acceptable voxels for the ten tumours. The slope of dynamic pO_2 changes (rate) was defined as $\mathrm{d}(pO_2)/\mathrm{d}t$ and $\mathrm{d}(pO_2')/\mathrm{d}t$ in response to increasing or decreasing inhaled FO_2 (Fraction of O_2), respectively.

2.5. Statistical analysis

Linear regression analysis was used to calculate the correlation between the NIRS-derived tumour haemodynamic parameters (i.e., $\Delta[HbO_2]$, A_1/τ_1, A_2/τ_2, f_1/f_2) and the *FREDOM*-determined tumour parameters (i.e., pO_2, $\mathrm{d}(pO_2)/\mathrm{d}t$, $\mathrm{d}(pO_2')/\mathrm{d}t$). Data are presented as mean $\pm$ standard deviation (SD) and paired Student-*t* tests compared the effects of oxygen and carbogen on $\Delta[HbO_2]$ and pO_2.

3. Results

3.1. Dynamic response of $\Delta[HbO_2]$ measured by NIRS

Figure 2 shows a group-averaged, temporal profile of $\Delta[HbO_2]$ from seven 13762NF rat breast tumours with air–oxygen–air–carbogen–air intervention, displaying apparent biphasic responses to both interventions. Both single (equation (3)) and double-exponential (equation (4)) curve fitting were tested for the carbogen intervention in one representative tumour (1.6 cm^3), as in figure 3(A). The maximal $\Delta[HbO_2]$ achieved with oxygen challenge was compared with that of carbogen, and revealed no significant difference between oxygen and carbogen interventions ($p > 0.3$); indeed, there was a strong correlation between the

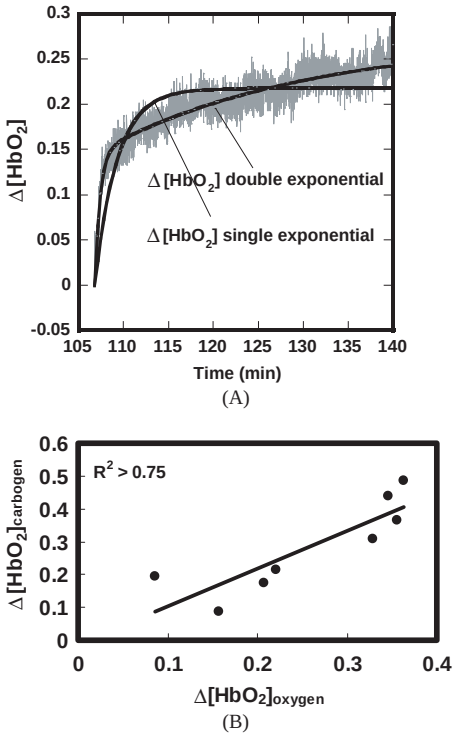

Figure 3. (A) Dynamic responses of $\Delta[HbO_2]$ (mM/DPF) to gas intervention (carbogen). Single exponential curve fitting yielded $\Delta[HbO_2] = 0.22\{1 - \exp[-(t - 106.8)/2.5]\}$ ($R^2 = 0.64$), and double exponential fitting resulted in $\Delta[HbO_2] = 0.15\{1 - \exp[-(t - 106.8)/0.58]\} + 0.13\{1 - \exp[-(t - 106.8)/23.2]\}$ ($R^2 = 0.88$). (B) Relationship of maximum $\Delta[HbO_2]$ (mM/DPF) in breast tumours in response to switching from air to oxygen and to carbogen ($R^2 > 0.75$).

maximal $\Delta[HbO_2]$ values with these two interventions ($R^2 > 0.75$, figure 3(B)), consistent with our previous observations (Gu *et al* 2003). No correlation was found between the perfusion rate ratio (f_1/f_2) and tumour size ($R^2 = 0.16$). Vascular oxygen dynamics in response to interventions are provided for individual tumours in table 2.

3.2. pO_2 measurements by FREDOM

Overlay of ^{19}F and ^{1}H MR images demonstrated that HFB was distributed in both central and peripheral regions of tumours (not shown). Individual pO_2 values taken from each voxel ranged from hypoxic (<1 Torr) to 35 Torr under baseline conditions (figure 4). Mean baseline pO_2 values, which are averaged over all voxels in a given tumour in the first three pO_2 maps, ranged from hypoxic (<5 Torr) to 27 Torr with a hypoxic fraction (HF_5; fractional voxels that are less than 5 Torr) ranging from 0 to 100% (mean 36%) and summarized in table 1. A strong correlation was found between mean baseline pO_2 and HF_5 ($R^2 > 0.85$, figure 5). Administration of oxygen or carbogen produced significant increases in tumour pO_2, as shown in the pO_2 maps, graphs and table. The tumour pO_2 values were averaged over the entire slice and responses to respiratory challenge for the group of seven tumours, measured simultaneously by *FREDOM* and NIRS, are shown in figure 2. Baseline measurements (breathing air) were generally stable, and altering the inhaled gas to oxygen or carbogen

Table 1. Oxygen tension (pO_2) in ten rat mammary 13762NF adenocarcinomas. pO_2 in baseline is the average value of all voxels in the first three maps, while pO_2 for oxygen or carbogen is the average value of all voxels in the final three pO_2 maps during exposure to the hyperoxic gas. Hypoxic fraction (HF) is the percentage of voxels with pO_2 values less than 5 Torr (HF_5) or 10 Torr (HF_{10}) and HF_5 and HF_{10} are the average values of final three maps in baseline, oxygen or carbogen respectively. The mean pO_2 increased significantly with both oxygen and carbogen and the value was significantly higher with carbogen. HF_5 was significantly reduced with oxygen or carbogen.

Tumour			Baseline (air)			Oxygen challenge			Carbogen challenge		
			pO_2 (Torr)			pO_2 (Torr)			pO_2 (Torr)		
No	Volume (cm^3)	Voxels[a]	Mean ± SD	HF_5 (%)	HF_{10} (%)	Mean ± SD	HF_5 (%)	HF_{10} (%)	Mean ± SD	HF_5 (%)	HF_{10} (%)
1	1.6	26	12 ± 3	24 ± 14	49 ± 15	56 ± 10	22 ± 2	29 ± 8	66 ± 3	0	0
2	0.3	10	12 ± 2	6 ± 12	53 ± 15	62 ± 15	0	0	79 ± 6	0	0
3	0.5	5	4 ± 4	60 ± 20	80 ± 0	14 ± 1	33 ± 12	53 ± 12	3 ± 1	73 ± 12	73 ± 12
4	1.3	14	<1 Torr[b]	100 ± 0	100 ± 0	14 ± 7	19 ± 11	48 ± 30	61 ± 21	0	0
5	0.9	24	24 ± 4	0 ± 0	8 ± 4	47 ± 10	0	0	71 ± 11	0	0
6	1.2	8	4 ± 1	58 ± 7	63 ± 0	43 ± 12	50 ± 22	63 ± 0	73 ± 10	0	0
7	0.8	24	27 ± 2	0 ± 0	3 ± 2	122 ± 21	0	0	142 ± 26	0	0
8	0.6	8	9 ± 6	50 ± 22	63 ± 22	103 ± 26	0	0	118 ± 37	0	0
9	0.7	44	25 ± 1	10 ± 5	26 ± 3	–	–	–	35 ± 3	0	3 ± 3
10	0.7	8	7 ± 6	54 ± 19	75 ± 22	52 ± 18	0	0	–	–	–
Mean ± SD	0.9 ± 0.4	17 ± 12	12 ± 10	36 ± 33	52 ± 31	57 ± 36[c]	14 ± 1[d]	21 ± 27	72 ± 41[b]	8 ± 24[b]	8 ± 24

[a] Number of voxels that provide acceptable data for all 23 pO_2 maps.
[b] $p < 0.01$.
[c] $p < 0.005$.
[d] $p < 0.05$.

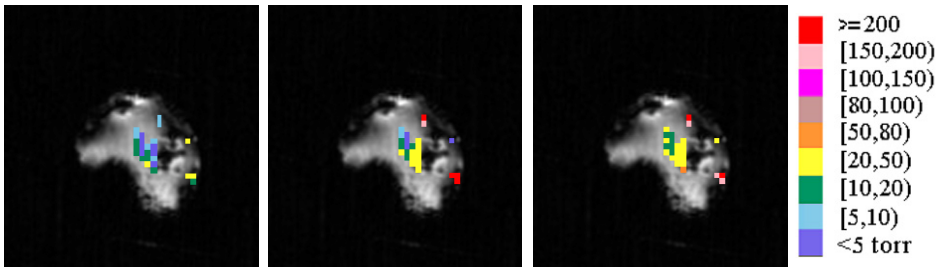

Figure 4. pO_2 maps (1.25 mm resolution) obtained using *FREDOM* overlaid on the ^{1}H anatomic image of a tumour (FOV = 4 cm × 4 cm). (Left) rat breathing air, (centre) breathing 100% O_2 (fifth map after switching from air), (right) breathing carbogen (95% O_2 + 5% CO_2) (fifth map after switching from air). The pO_2 maps show distinct heterogeneity.

(This figure is in colour only in the electronic version)

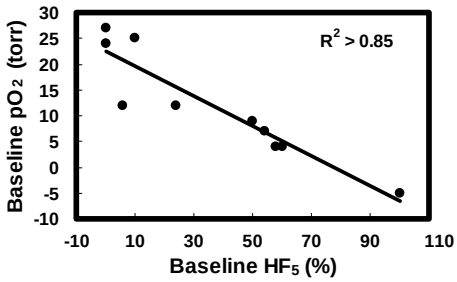

Figure 5. Correlation between baseline pO_2 and hypoxic fraction (HF_5) measured using *FREDOM* ($R^2 > 0.85$).

induced rapid and significant changes in both pO_2 and $\Delta[HbO_2]$ ($p < 0.001$). Upon return to air (baseline), $\Delta[HbO_2]$ dropped quickly and significantly within 16 min, and then more slowly, for the next 24 min, whereas the pO_2 decrease was more gradual. Altering the inhaled gas to carbogen also produced a rapid increase in both pO_2 and $\Delta[HbO_2]$. Upon return to air breathing from carbogen, both $\Delta[HbO_2]$ and pO_2 showed a similar trend to that following oxygen. As expected, all ten tumours showed a significant increase in pO_2 (average over entire slice), and decrease in hypoxic fraction (HF) in response to oxygen or carbogen inhalation. The magnitude of response to either hyperoxic gas was correlated ($R^2 > 0.79$), as was the maximum volume-averaged pO_2 achieved with either gas ($R^2 > 0.83$). The rate of increase with oxygen challenge, $d(pO_2)/dt$, was significantly faster than the return to baseline, $d(pO_2')/dt$, for oxygen intervention ($p < 0.02$), but no difference was observed for carbogen ($p > 0.1$, figure 6). The mean pO_2 values of individual tumours averaged over the final three pO_2 maps during exposure to carbogen breathing were significantly higher than oxygen ($p < 0.01$), and the tumour hypoxic fraction was generally eliminated during carbogen breathing ($n = 7$ of 9 tumours, table 1).

3.3. The relationship between pO_2 and $\Delta[HbO_2]$ with respect to hyperoxic gas

Taken as a group of ten tumours, there was no apparent relationship between the magnitude of the change in tumour vascular oxygenation ($\Delta[HbO_2]$) and change in pO_2 ($R^2 < 0.1$). However, if tumours were divided into two sub-populations, then two separate correlations

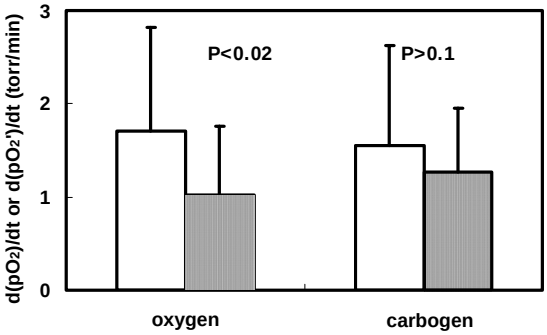

Figure 6. Mean $d(pO_2)/dt$ (open) and $d(pO_2')/dt$ (shaded) $\pm$ SD for eight tumours with both interventions, when gas was switched from air to the hyperoxic gas and back to air, respectively. pO_2 is the mean value of all acceptable voxels appearing in the five maps during the oxygen or carbogen intervention. $d(pO_2)/dt$ is the slope of regression line of five pO_2 readings versus time when switching from air to oxygen or carbogen, and $d(pO_2')/dt$ is the slope of regression line for five pO_2 readings during the switch back to air. The rates showed a significant difference with oxygen ($p < 0.02$), but not with carbogen ($p > 0.1$).

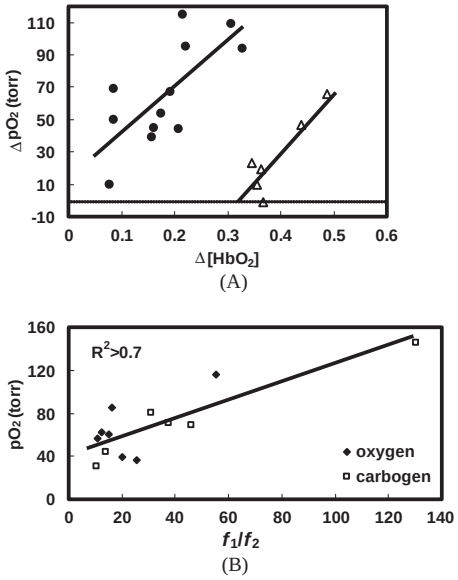

Figure 7. (A) Correlation between maximum $\Delta[HbO_2]$ and change in pO_2 with respect to hyperoxic gas intervention for two groups of tumours (•) (group 1: no 1, 2, 6, 7, 8, 9, 10; $R^2 > 0.51$) and (Δ) (group 2: no 3, 4, 5; $R^2 > 0.82$). The unit for $\Delta[HbO_2]$ is mM/DPF. (B) Correlation between mean pO_2 achieved with hyperoxic gas breathing and perfusion rate ratio (f_1/f_2) for tumours with biphasic response to intervention ($R^2 > 0.7$). pO_2 is the mean value for the final three pO_2 maps under hyperoxic intervention, selected from all voxels appearing in the final three pO_2 maps during oxygen (♦) or carbogen (□) intervention.

were found each with similar slope (figure 7(A)). There was also a correlation ($R^2 > 0.7$) between the perfusion rate ratio, f_1/f_2, derived from fitting the $\Delta[HbO_2]$ curve and the mean pO_2 values achieved with hyperoxic gas intervention (figure 7(B)). Assessment of f_1/f_2 is

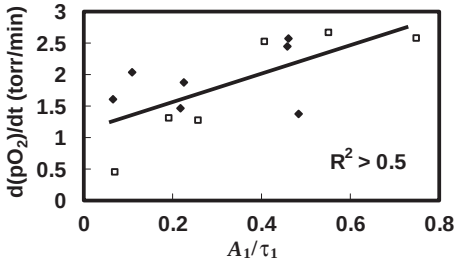

Figure 8. $d(pO_2)/dt$ versus A_1/τ_1 (determined from $\Delta[HbO_2]$ for tumours with biphasic response to interventions) showing a positive correlation ($R^2 > 0.5$). pO_2 values are the mean value of all well-oxygenated voxels (i.e., the maximum $pO_2 > 10$ Torr under oxygen or carbogen intervention) appearing in the five pO_2 maps during oxygen (♦) or carbogen (□) intervention.

Table 2. Summary of vascular oxygen dynamics for the experimental tumours. Two amplitudes (A_1, A_2) and two time constants (τ_1, τ_2) were determined by curve-fitting the dynamic NIRS measurements using a double-exponential expression. Nine out of ten tumours were observed to have double-exponential features with either oxygen or carbogen intervention. A_1 is significantly smaller than A_2 with oxygen ($p < 0.01$), but no significant differences in carbogen ($p > 0.19$).

Tumour		Double exponential fitting				
No	Intervention	A_1 (AU)	A_2 (AU)	τ_1 (min)	τ_2 (min)	R
1[a]	Oxygen	0.11 ± 0.002	0.12 ± 0.002	0.49 ± 0.02	6.6 ± 0.2	0.94
	Carbogen	0.15 ± 0.001	0.13 ± 0.002	0.58 ± 0.01	23.2 ± 1.1	0.94
2[a]	Oxygen	0.03 ± 0.002	0.11 ± 0.005	0.46 ± 0.18	25.6 ± 2.9	0.91
	Carbogen	–	–	–	–	–
3[a]	Oxygen	0.15 ± 0.001	0.38 ± 0.003	0.31 ± 0.02	20.1 ± 0.39	0.98
	Carbogen	0.23 ± 0.005	0.2 ± 0.004	1.2 ± 0.04	10.8 ± 0.45	0.95
4[a]	Oxygen	–	–	–	–	–
	Carbogen	0.16 ± 0.002	2.3 ± 0.27	0.29 ± 0.02	155.8 ± 21	0.97
5[a]	Oxygen	0.12 ± 0.002	0.23 ± 0.002	0.55 ± 0.03	11.6 ± 0.27	0.94
	Carbogen	–	–	–	–	–
6[a]	Oxygen	0.06 ± 0.001	0.26 ± 0.005	0.13 ± 0.01	31.2 ± 1.1	0.96
	Carbogen	0.03 ± 0.001	0.08 ± 0.001	0.04 ± 0.02	13.9 ± 0.6	0.78
7[a]	Oxygen	–	–	–	–	–
	Carbogen	–	–	–	–	–
8[b]	Oxygen	0.11 ± 0.002	0.2 ± 0.001	0.24 ± 0.02	7.1 ± 0.1	0.96
	Carbogen	0.2 ± 0.002	0.12 ± 0.001	0.49 ± 0.01	9.1 ± 0.2	0.95
9[c]	Carbogen	0.01 ± 0.0004	0.02 ± 0.0004	0.14 ± 0.02	3.9 ± 0.12	0.64
10[d]	Oxygen	0.05 ± 0.002	0.03 ± 0.002	0.46 ± 0.05	5.6 ± 0.56	0.68
Mean ± SD	–	0.11 ± 0.068	0.32 ± 0.59	0.42 ± 0.3	24.9 ± 40.2	–

[a] Air → O_2 → air → carbogen → air.
[b] Air → carbogen → air → O_2 → air.
[c] Air → carbogen → air.
[d] Air → oxygen → air.

predicated on biphasic behaviour with respect to interventions, which was observed in most cases (13 of 16 measurements). There was also a positive correlation between A_1/τ_1 (the fast component of biphasic $\Delta[HbO_2]$) and the $d(pO_2)/dt$ of well-oxygenated voxels (i.e., those with pO_2 values >10 Torr under oxygen or carbogen intervention) ($R^2 > 0.5$, figure 8). However, no correlation was found between $d(pO_2)/dt$ and A_2/τ_2 (the slow component).

4. Discussion

Integration of diverse imaging techniques can be technically challenging, since each modality has specific technical constraints and requirements. Here, the NIR system was modified to use longer optical fibres and any metal components were eliminated from the fibre tips. Due to the spatial restrictions within the bore of the magnet a Helmholtz coil was built specifically providing access to both the tumour and fibres. The fibres required sufficient flexibility to allow them to be bent through requisite angles within the confines of the magnet bore. To date there have been few reports of simultaneous data acquisition by NIR and MRI, e.g., studies of phantoms (Pogue *et al* 2003), human brain (Toronov *et al* 2001, Chen *et al* 2003) and breast (Ntziachristos *et al* 2000, Gulsen *et al* 2002, Ntziachristos *et al* 2002, Gu *et al* 2004).

In the present study, global average $\Delta[HbO_2]$ was measured by NIRS, and pO_2 maps were obtained simultaneously by ^{19}F MRI. We used transmission mode NIRS in order to interrogate deep tumour tissue. While NIRS is a global measurement, the region sampled by it is predominantly a banana-shaped region joining the locations of the source and detector (Arridge 1995, Arridge and Schweiger 1995), and we recently showed that typically 15 to 30% of the vascular volumes of rat tumours are interrogated by NIR using this configuration (Gu *et al* 2005). We positioned the NIRS probes (source and detector) to be in the same plane as the HFB injection to ensure maximum overlap between the regions sampled by the two techniques. Utilizing our previously developed mathematical model (Liu *et al* 2000), multiple haemodynamic parameters were derived for $\Delta[HbO_2]$ (A_1/τ_1, A_2/τ_2 and f_1/f_2) to be compared with pO_2. Our results demonstrate that oxygenation parameters measured from both techniques show significant and consistent elevation in tumour oxygenation during the hyperoxic gas interventions. As reported previously, the magnitude of the vascular response was similar with both hyperoxic gases (Gu *et al* 2003). As expected, $\Delta[HbO_2]$ increased much faster than pO_2 in all ten tumours, indicating that change in tumour vascular oxygenation precedes tumour tissue oxygenation. This observation is consistent with our previous studies in this tumour type measured simultaneously by NIRS and fibre-optic probes (Gu *et al* 2003), as well in the Dunning prostate R3327-AT1 tumours measured sequentially by NIRS and ^{19}F MRI (Kim *et al* 2003b).

We have previously demonstrated the application of *FREDOM* to monitor tumour oxygen dynamics in diverse rat prostate tumours (Zhao *et al* 2001, 2002), human tumour xenografts (Mason *et al* 2002) and a few breast tumours (Song *et al* 2002). Here, the mean baseline was $pO_2 = 12 \pm 10$ Torr for the ten tumours, which is lower than reported previously (Song *et al* 2002), but entirely consistent with the newer anaesthetic protocol (air or 21% oxygen, as opposed to 33% O_2 previously). There was a strong correlation between baseline pO_2 and hypoxic fraction (figure 5), as we have previously found using Dunning prostate R3327-HI tumours (Zhao *et al* 2001). The pO_2 achieved with carbogen in this study was significantly higher than with oxygen and carbogen appeared to be more effective at eliminating the hypoxic fraction (table 1). However, carbogen was generally applied second in our experimental protocols, and it is highly likely that the initial oxygen primed the tumour. Indeed, while oxyhaemoglobin generally returned to baseline during the air breathing episode between hyperoxic gases, it is clear that pO_2 remained elevated (figure 2). Both ΔpO_2 and the

maximum pO_2 achieved with either gas were closely correlated. Similar behaviour was reported previously based on measurements using fibre optic probes (Gu *et al* 2003). For the group of tumours in this study, mean baseline pO_2 did not provide a good indication of response to hyperoxic gas (ΔpO_2 or pO_{2max}). However, considering the fate of individual voxels in separate tumours with respect to intervention, strong linear correlation was observed in some tumours (tumour no 3, 4, 6 and 9) between initial mean baseline pO_2 and the maximum pO_2 at the same location (voxel) in response to carbogen or oxygen breathing consistent with the results of Song *et al* (2002). Other tumours showed no correlation.

The rate of pO_2 response to either gas was similar (figure 6), but decrease upon return to air was significantly faster in the case of oxygen, but not carbogen. While the relationships between ΔpO_2 and $\Delta[HbO_2]$ are not obvious, there exists a significant correlation between f_1/f_2 and mean pO_2 values achieved with hyperoxic gas intervention. Most f_1/f_2 values are between 5 and 60 (figure 7(B)), implying that the blood perfusion rate in the well-perfused region is much higher than that from the poorly perfused region. Not surprisingly the higher the ratio of well perfused to poorly perfused regions, the higher the mean pO_2 values achieved by the hyperoxic gas interventions.

Previous studies have demonstrated that tumour tissue oxygenation could be strongly affected by changes in tumour blood flow measured locally by laser Doppler flowmetry (Vaupel *et al* 1994). It was also reported that spontaneous fluctuations in flow and perivascular pO_2 are correlated at the micro-regional level (Kimura *et al* 1996, Braun *et al* 1999). In our study, we are able to derive the perfusion rate ratios between the well perfused and poorly perfused regions from the haemoglobin concentration responses to the intervention measured by NIRS. We found that there was a significant correlation between $d(pO_2)/dt$ and A_1/τ_1 (f_1, proportional to A_1/τ_1), but not $d(pO_2)/dt$ and A_2/τ_2 (f_2, proportional to A_2/τ_2), provided that the pO_2 readings were selected from well-oxygenated or responsive voxels (figure 8). This linear correlation suggests that the rate of change in pO_2 is closely related to the perfusion rate in the well-perfused region, f_1. In other words, the dynamic changes in pO_2 of those regions responsive to hyperoxic gas intervention may be attributed to fast tumour vascular perfusion, rather than to the slow perfusion in tumour vasculature. We believe these results provide a valuable association between tumour vascular oxygenation and tumour pO_2 determined simultaneously by the optical and NMR measurements.

A goal had been to develop a low-cost, simple, fast surrogate measurement of pO_2 based on NIRS of the oxygenation status of endogenous haemoglobin. Both figures 7(B) and 8 suggest that there exist linear relationships of pO_2 with the NIRS measurable parameters f_1/f_2 and with A_1/τ_1. However, the correlation between ΔpO_2 and $\Delta[HbO_2]$ (figure 7(A)) seems to be more complex with a separation of the tumours into two groups. It may be noteworthy that the majority (6 of 7) of the tumours associated with the correlation on the left-hand side of the graph had a high initial global pO_2 (i.e., mean baseline $pO_2 > 5$ Torr), whereas 2 out of 3 of the tumours on the right had low initial global pO_2. A possible interpretation relates to the shape of the haemoglobin–oxygen dissociation curve (the Hill curve). A given pO_2 response can correspond to different changes in haemoglobin saturation depending on where the change occurs on the Hill curve. At lower initial pO_2 there may be a substantial ΔpO_2 with little $\Delta[HbO_2]$. By contrast, at higher initial pO_2 the same increase in pO_2 could produce a greater effect on the saturation. While $\Delta[HbO_2]$ is proportional to the change of SO_2 (with the assumption of little change in total haemoglobin concentration during intervention), two subpopulations of tumours in the relationship between ΔpO_2 and $\Delta[HbO_2]$ could be the result of different initial pO_2. Similarly, two subpopulations of tumours were observed in the relationship between initial SO_2 and the carbogen-induced change in saturation in the study of Hull *et al* (1999). Such an effect also confounds the direct correlation of BOLD MRI response

to changes in pO_2 (Baudelet and Gallez 2002). Significantly, preliminary data reported by Gu *et al* (2004) for simultaneous BOLD MRI and NIR in tumours showed a strong linear correlation in response to hyperoxic gas challenge, as also reported by Chen *et al* (2003) in the rat brain.

A major concern is tumour heterogeneity, as recognized throughout the literature and shown here by ^{19}F MRI (figure 4). Indeed, we have obtained some preliminary data using a single NIR source and three detectors placed on various regions across a tumour (Kim *et al* 2003a), showing that each region of the tumour responded differently to hyperoxic gas, in terms of the extent and rate, indicating the heterogeneity of tumour vasculature. Spatial discrimination will be even more critical, if such studies are transferred to human breast cancer, where the tumour is surrounded by normal tissue (Brooksby *et al* 2003). Nevertheless, we believe this haemodynamic model and correlation between tumour vascular oxygenation and pO_2 provides valuable insight into the tumour compartment of such a mixed system and explores dynamic signatures of breast tumours, which could, in turn, enhance/assist human breast cancer diagnosis and prognosis.

In summary, by studying tumour vascular oxygenation concomitantly with changes in tumour oxygen tension, we found several significant correlations between rates and magnitudes of vascular and tissue responses. This study also demonstrates the feasibility of conducting simultaneous NIRS and MRI oximetry. We believe the correlation of tumour vascular oxygenation and tumour tissue pO_2 can provide valuable insights into tumour pathophysiology and response to interventions.

Acknowledgments

This work was supported in part by the Department of Defense Pre-doctoral Research Fellowship W81XWH-04-1-0411 (MX), Breast Cancer Initiative grant DAMD17-00-1-0459 (HL), NIH R01 CA79515/EB002762 (RPM) and Cancer Imaging Program NIH P20 CA086354 (RPM). The MR investigations were performed at the Mary Nell and Ralph B Rogers NMR Center, a NIH BRTP facility (#P41RR02584). We are grateful to Vincent Bourke and Drs Anca Constantinescu, Yueqing Gu and Luis Saez for valuable discussions and technical assistance.

References

Arridge S R 1995 Photon measurement density functions: I. Analytical forms *Appl. Opt.* **34** 7395–409

Arridge S R and Schweiger M 1995 Photon measurement density functions: II. Finite element method calculations *Appl. Opt.* **34** 8026–37

Baudelet C and Gallez B 2002 How does blood oxygen level-dependent (BOLD) contrast correlate with oxygen partial pressure (pO_2) inside tumors? *Magn. Reson. Med.* **48** 980–6

Braun R D, Lanzen J L and Dewhirst M W 1999 Fourier analysis of fluctuations of oxygen tension and blood flow in R3230Ac tumors and muscle in rats *Am. J. Physiol.* **277** H551–68

Brooksby B A, Dehghani H, Pogue B W and Paulsen K D 2003 Near infrared (NIR) tomography breast image reconstruction with a priori structural information from MRI: algorithm development for reconstructing heterogeneities *IEEE J. Sel. Top. Quantum Electron.* **9** 199–209

Brown J M 1999 The hypoxic cell: a target for selective cancer therapy—eighteenth Bruce F Cain Memorial Award lecture *Cancer Res.* **59** 5863–70

Chance B 1997 Near infrared images using continuous, phase modulated and pulsed light with quantitation of blood and oxygenation *Ann. New Acad. Sci.* **838** 29–45

Chapman J D, Stobbe C C, Arnfield M R, Santus R, Lee J and McPhee M S 1991 Oxygen dependency of tumor cell killing *in vitro* by light-activated Photofrin II *Radiat. Res.* **126** 73–9

Chen Y, Tailor D R, Intes X and Chance B 2003 Correlation between near-infrared spectroscopy and magnetic resonance imaging of rat brain oxygenation modulation *Phys. Med. Biol.* **48** 417–27

Conover D L, Fenton B M, Foster T H and Hull E L 2000 An evaluation of near infrared spectroscopy and cryospectrophotometry estimates of haemoglobin oxygen saturation in a rodent mammary tumour model *Phys. Med. Biol.* **45** 2685–700

Dehghani H, Doyley M M, Pogue B W, Jiang S, Geng J and Paulsen K D 2004 Breast deformation modeling for image reconstruction in near infrared optical tomography *Phys. Med. Biol.* **49** 1131–45

Delpy D T and Cope M 1997 Quantification in tissue near-infrared spectroscopy *Phil. Trans. R. Soc. Lond.* B **352** 649–59

Fishkin J B and Gratton E 1993 Propagation of photon-density waves in strongly scattering media containing an absorbing semi-infinite plane bounded by a straight edge *J. Opt. Soc. Am.* A **10** 127–40

Fyles A W et al 1998 Oxygenation predicts radiation response and survival in patients with cervix cancer *Radiother. Oncol.* **48** 149–56

Gu Y, Bourke V A, Kim J G, Constantinescu A, Mason R P and Liu H 2003 Dynamic response of breast tumor oxygenation to hyperoxic respiratory challenge monitored with three oxygen-sensitive parameters *Appl. Opt.* **42** 2960–7

Gu Y, Mason R P and Liu H 2005 Estimated fraction of tumor vascular blood contents sampled by near infrared spectroscopy and ^{19}F magnetic resonance spectroscopy *Opt. Express* **13** 1724–33

Gu Y, Xia M, Liu H, Kodibagkar V D, Constantinescu A and Mason R P 2004 Correlation of NIR spectroscopy with BOLD MR imaging of assessing breast tumor vascular oxygen status *Biomedical Topical Meetings on CD-ROM (Washington, DC: The Optical Society of America)* FB6

Gulsen G, Yu H, Wang J, Nalcioglu O, Merritt S, Bevilacqua F, Durkin A, Cuccia D J, Lanning R and Tromberg B J 2002 Congruent MRI and near-infrared spectroscopy for functional and structural imaging of tumors *Technol. Cancer Res. Treat.* **1** 497–505

Hahn E W, Peschke P, Mason R P, Babcock E E and Antich P P 1993 Isolated tumor growth in a surgically formed skin pedicle in the rat: a new tumor model for NMR studies *Magn. Reson. Imaging* **11** 1007–17

Hall E J 1994 The oxygen effect and reoxygenation *Radiobiology for the Radiologist* (Philadelphia, PA: J B Lippincott) pp 133–52

Hockel M, Schlenger K, Aral B, Mitze M, Schaffer U and Vaupel P 1996 Association between tumor hypoxia and malignant progression in advanced cancer of the uterine cervix *Cancer Res.* **56** 4509–15

Homma S, Fukunaga T and Kagaya A 1996 Influence of adipose tissue thickness on near-infrared spectroscopic signals in the measurement of human muscles *J. Biomed. Opt.* **1** 418–24

Hull E L, Conover D L and Foster T H 1999 Carbogen-induced changes in rat mammary tumour oxygenation reported by near infrared spectroscopy *Br. J. Cancer* **79** 1709–16

Hunjan S, Zhao D, Constantinescu A, Hahn E W, Antich P P and Mason R P 2001 Tumor oximetry: demonstration of an enhanced dynamic mapping procedure using fluorine-19 echo planar magnetic resonance imaging in the Dunning prostate R3327-AT1 rat tumor *Int. J. Radiat. Oncol. Biol. Phys.* **49** 1097–108

Jiang L, Zhao D, Constantinescu A and Mason R P 2004 Comparison of BOLD contrast and Gd-DTPA dynamic contrast enhanced imaging in rat prostate tumor *Magn. Reson. Med.* **51** 953–60

Kety S S 1951 The theory and applications of the exchange of inert gas at the lungs and tissues *Pharmacol. Rev.* **3** 1–41

Kim J G, Gu Y, Constantinescu A, Mason R P and Liu H 2003a Non-uniform tumor vascular oxygen dynamics monitored by three-channel near-infrared spectroscopy *Proc. SPIE* **4955** 388–96

Kim J G and Liu H 2004 Investigation of breast tumor hemodynamics using tumor vascular phantoms and FEM simulations *Proc. Biomedical Topical Meetings CD-ROM* (Washington, DC: The Optical Society of America) WF16

Kim J and Liu H 2005 Investigation of bi-phasic tumor oxygen dynamics induced by hyperoxic gas intervention: a numerical study *Opt. Express* **13** 4465–75

Kim J G, Zhao D, Song Y, Constantinescu A, Mason R P and Liu H 2003b Interplay of tumor vascular oxygenation and tumor pO_2 observed using near-infrared spectroscopy, an oxygen needle electrode, and ^{19}F MR pO_2 mapping *J. Biomed. Opt.* **8** 53–62

Kimura H, Braun R D, Ong E T, Hsu R, Secomb T W, Papahadjopoulos D, Hong K and Dewhirst M W 1996 Fluctuations in red cell flux in tumor microvessels can lead to transient hypoxia and reoxygenation in tumor parenchyma *Cancer Res.* **56** 5522–8

Liu H, Song Y, Worden K L, Jiang X, Constantinescu A and Mason R P 2000 Noninvasive investigation of blood oxygenation dynamics of tumors by near-infrared spectroscopy *Appl. Opt.* **39** 5231–43

Mason R P, Antich P P, Babcock E E, Constantinescu A, Peschke P and Hahn E W 1994 Non-invasive determination of tumor oxygen tension and local variation with growth *Int. J. Radiat. Oncol. Biol. Phys.* **29** 95–103

Mason R P, Hunjan S, Constantinescu A, Song Y, Zhao D, Hahn E W, Antich P P and Peschke P 2003 Tumor oximetry: comparison of ^{19}F MR EPI and electrodes *Adv. Exp. Med. Biol.* **530** 19–27

Mason R P, Ran S and Thorpe P E 2002 Quantitative assessment of tumor oxygen dynamics: molecular imaging for prognostic radiology *J. Cell Biochem.* **39** 45–53

Mazurchuk R, Zhou R, Straubinger R M, Chau R and Grossman Z 1999 Functional magnetic resonance (FMRI) imaging of a rat brain tumor model: implications for evaluation of tumor microvasculature and therapeutic response *Magn. Reson. Imaging* **17** 537–48

Ntziachristos V, Yodh A G, Schnall M and Chance B 2000 Concurrent MRI and diffuse optical tomography of breast after indocyanine green enhancement *Proc. Natl Acad. Sci. USA* **97** 2767–72

Ntziachristos V, Yodh A G, Schnall M and Chance B 2002 MRI-guided diffuse optical spectroscopy of malignant and benign breast lesions *Neoplasia* **4** 347–54

Overgaard J and Horsman M R 1996 Modification of hypoxia-induced radioresistance in tumors by the use of oxygen and sensitizers *Semin. Radiat. Oncol.* **6** 10–21

Pogue B W, Zhu H, Nwaigwe C, McBride T O, Osterberg U L, Paulsen K D and Dunn J F 2003 Hemoglobin imaging with hybrid magnetic resonance and near-infrared diffuse tomography *Adv. Exp. Med. Biol.* **530** 215–24

Sevick E M, Chance B, Leigh J, Nioka S and Maris M 1991 Quantitation of time- and frequency-resolved optical spectra for the determination of tissue oxygenation *Anal. Biochem.* **195** 330–51

Shah N, Cerussi A, Jakubowski D, Hsiang D, Butler J and Tromberg B J 2004 Spatial variations in optical and physiological properties of healthy breast tissue *J. Biomed. Opt.* **9** 534–40

Song Y, Constantinescu A and Mason R P 2002 Dynamic breast tumor oximetry: the development of prognostic radiology *Technol. Cancer Res. Treat.* **1** 471–8

Toronov V, Webb A, Choi J, Wolf M, Michalos A, Gratton E and Hueber D 2001 Investigation of human brain hemodynamics by simultaneous near-infrared spectroscopy and functional magnetic resonance imaging *Med. Phys.* **28** 521–7

Vaupel P, Kelleher D K and Engel T 1994 Do changes in tumor blood flow necessarily lead to changes in tissue oxygenation and in bioenergetic status? *Adv. Exp. Med. Biol.* **361** 607–11

Welch M J, Halpern H and Kurdziel K A 2003 Example of imaging solutions to multi-disease biological challenge—imaging of hypoxia *Acad. Radiol.* **10** 887–90

Yang Y, Liu H, Li X and Chance B 1997 Low-cost frequency-domain photon migration instrument for tissue spectroscopy, oximetry, and imaging *Opt. Eng.* **36** 1562–9

Yodh A G and Boas D A 2003 Functional imaging with diffusing light *Biomedical Photonics Handbook* ed V Tuan (Boca Raton, FL: CRC Press)

Zhao D, Constantinescu A, Hahn E W and Mason R P 2001 Tumor oxygen dynamics with respect to growth and respiratory challenge: investigation of the Dunning prostate R3327-HI tumor *Radiat. Res.* **156** 510–20

Zhao D, Constantinescu A, Hahn E W and Mason R P 2002 Differential oxygen dynamics in two diverse dunning prostate R3327 rat tumor sublines (MAT-Lu and HI) with respect to growth and respiratory challenge *Int. J. Radiat. Oncol. Biol. Phys.* **53** 744–56

Zhao D, Jiang L and Mason R P 2004 Measuring changes in tumor oxygenation *Methods Enzymol.* **386** 378–418

Photochemistry and Photobiology, 2005, 81: 000–000

Effect of Photothermal Therapy on Breast Tumor Vascular Contents: Noninvasive Monitoring by Near-infrared Spectroscopy¶

Yueqing Gu[1,3], Wei R. Chen[2], Mengna Xia[1], Sang W. Jeong[2], and Hanli Liu*[1]

[1]Biomedical Engineering Program, University of Texas at Arlington, Arlington, TX
[2]Biomedical Engineering Program, Department of Physics and Engineering, University of Central Oklahoma, Edmond, OK
[3]Biomedical Engineering Laboratory, China Pharmaceutical University, Nanjing, P.R. China

Received 16 March 2005; accepted 20 March 2005

ABSTRACT

?1 **The goal of this study was to investigate the effect of photothermal laser irradiation on rat breast tumor (DMBA-4) vascular contents. An 805-nm diode laser was used in our experiment with a power density ranging from 0.32 to 1.27 W/cm^2. The dynamic changes of oxygenated hemoglobin and total hemoglobin concentrations, $\Delta[HbO_2]$ and $\Delta[Hb]_{total}$, in rat tumors during photothermal irradiation were *noninvasively* monitored by a near-infrared spectroscopy system. A multichannel thermal detection system was also used simultaneously to record temperatures at different locations within the tumors. Our experimental results showed that: (1) photoirradiation did have the ability to induce hyperthermic effects inside the rat breast tumors in a single exponential trend; (2) the significant changes ($P < 0.005$) of $\Delta[HbO_2]$ and $\Delta[Hb]_{total}$ in response to a low dosage of laser irradiation (0.32 W/cm^2) have a single exponential increasing trend, similar to that seen in the tumor interior temperature; and (3) the increase in magnitude of $\Delta[HbO_2]$ is nearly two times greater than that of $\Delta[Hb]_{total}$, suggesting that photoirradiation may enhance tumor vascular oxygenation. The last observation may be important to reveal the hidden mechanism of photoirradiation on tumors, leading to improvement of tumor treatment efficiency.**

INTRODUCTION

Laser phototherapy, a nonsurgical modality for cancer treatment, is gaining widespread acceptance because of precise energy delivery into the tumor tissue (1–3). The laser energy delivered to the targeted tumors can induce localized photomechanical, photochemical and photothermal reactions, thus killing tumor cells. In general, photochemical reactions may cause the change of chemical bonds and form toxic radicals, such as release of singlet oxygen, leading to the death of organized tissues. Photomechanical reactions may induce tissue stress, resulting in the disruption of tissue cells and ejection of material. Photothermal reactions may induce hyperthermia and coagulation, causing cell destruction (4). In particular, thermal cytotoxicity effects are found to be more profound under acidotic (low pH) conditions, which are often present in poorly oxygenated tissues (5–7), such as in tumors. Many research studies have reported the existence of acute/chronic hypoxic regions within the majority of solid tumors (8–10). As a result, cytotoxicity induced by selective photothermal irradiation can be more effective in tumor tissue than in normal tissue. To further enhance the desirable photothermal effects, selective absorbers are often used in the targeted tumor tissue along with laser irradiation to cause selective and localized photon–tissue interactions (11,12). In addition, administration of an immunoadjuvant has been proved to increase systemic cancer cure and long-term resistance to cancer of the same origin, when combined with the selective photochemical treatment (13,14). Chen *et al*. have developed a laser immunotherapy by combining laser irradiation, a laser-absorbing dye and an immunoadjuvant to improve cancer therapy efficiency (11,12,15,16). The previous experimental results have demonstrated that this unique approach has positive effects on both primary and metastatic tumors.

Although the underlying mechanism of the laser irradiation has been intensively studied (17–20), the hemodynamic and physiological properties inside the tumors during phototherapy are poorly understood. Measuring the reduction of tumor size and survival rates is the current practice to evaluate the therapeutic outcome of therapy. Obviously, noninvasive, real-time monitoring of tumor hemodynamic characteristics before, during and after therapy is highly desirable. Such a technique may help reveal the tumor physiology and therapeutic process caused by the therapy, providing treatment prognoses and guidance to optimize the light dosimetry so as to improve the therapeutic outcome. Near-infrared spectroscopy (NIRS) has been demonstrated in our recent studies to be such a noninvasive means in monitoring tumor vascular oxygenation during therapeutic interventions (21–23).

In this study, we investigated the effects of photothermal therapy on tumor vascular contents and tumor temperature. An 805-nm diode laser was used for photothermal irradiation of mammary tumors in rats. The dynamic changes caused by the laser irradiation in oxygenated, deoxygenated and total hemoglobin concentrations, $\Delta[HbO_2]$, $\Delta[Hb]$, and $\Delta[Hb]_{total}$, in the tumor vasculature were

¶Posted on the website on ???

*To whom correspondence should be addressed: Biomedical Engineering Graduate Program, 501 West First, ELB-220, P.O. Box 19138, University of Texas at Arlington, Arlington, TX 76019, USA. Fax: 817-272-2251; e-mail: Hanli@uta.edu

Abbreviations: NIR, near infrared; NIRS, near-infrared spectroscopy; I&Q, in phase and quadrature phase; $[HbO_2]$, oxygenated hemoglobin concentration; [Hb], deoxygenated hemoglobin concentration; $[Hb]_{total}$, total hemoglobin concentration.

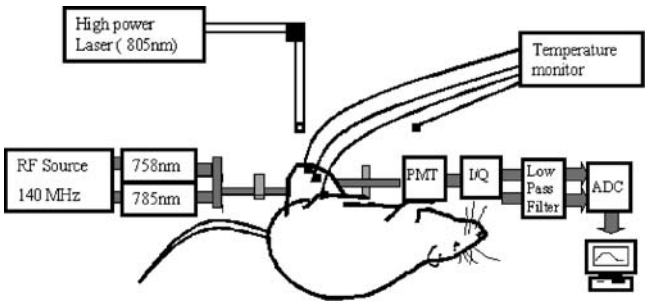

Figure 1. Experimental setup for the simultaneous NIRS and thermal measurements of breast tumors under photothermal therapy. PMT represents a photomultiplier tube; I&Q is an in-phase and quadrature-phase demodulator for retrieving amplitude and phase information. The thermal detection system comprises multiple thermal sensing probes, three of which are inserted into different regions of the tumor, and one probe was used to measure room temperature. The power-adjustable laser light (805 nm) is vertically delivered to tumor surface with a 2-cm beam diameter for photoirradiation.

monitored by an NIRS system. A multichannel, thermal monitor was also used simultaneously to record the temperatures at three different locations inside the breast tumors. The correlations between the optical irradiation dosages, tumor temperatures, and tumor vascular contents were studied. The dynamic features of tumor temperature and vascular oxygenation were quantified to reveal the dynamic effects within the tumors under the laser irradiation.

MATERIALS AND METHODS

NIRS. The changes of oxygenated, deoxygenated and total hemoglobin concentrations, $\Delta[HbO_2]$, $\Delta[Hb]$ and $\Delta[Hb]_{total}$, in tumor tissue caused by laser irradiation were determined by a near-infrared, homodyne, frequency-domain spectroscopy system (NIM, Philadelphia, PA), which has been described in detail elsewhere (21–23). Briefly, the amplitude-modulated light at 140 MHz at wavelengths of 758 nm and 785 nm illuminated the tumor surface through a light-delivery fiber bundle with output powers of 9 mW and 11 mW at 785 nm and 758 nm wavelengths, respectively, measured at the tip of the bundle by an optical power meter. The experimental setup is shown in Fig. 1. The 805-nm laser light was vertically applied on the tumor surface. The delivering and detecting fiber bundles of the NIRS system were placed horizontally and in good contact with the surface of the tumors in a transmittance mode, without compressing the tumors. The diffused light through the tumor tissue was collected and filtered by a sharp low-pass optical filter, which cut off the optical signal above 805 nm from the laser irradiation, and then propagated into a photomultiplier tube (PMT) through the detecting fiber bundle. The signal detected by the PMT was demodulated through an in-phase and quadrature-phase (I&Q) circuit, and the amplitude and phase of the signal were recorded.

Algorithms for calculations of $\Delta[HbO_2]$, $\Delta[Hb]$, and $\Delta[Hb]_{total}$. On the basis of the Beer-Lambert law, light attenuation, represented by optical density (OD), through a sample is proportional to the concentration of hemoglobin inside the sample (24–28),

$$\mathrm{OD} = \mathrm{Log}(A_0/A) = \varepsilon c l \tag{1}$$

where A_0 and A are light intensities of the incident and transmitted light, respectively, ε is the extinction coefficient of hemoglobin, c is the concentration of hemoglobin, and l is the length of light path through the measured sample. When the measured sample has a mixture of oxygenated and deoxygenated hemoglobin, Eq. (1) can be further evolved to (28–30),

$$\mathrm{OD}(\lambda) = \{\varepsilon_{Hb}(\lambda)[Hb] + \varepsilon_{HbO2}(\lambda)[HbO_2]\}l \tag{2}$$

where $\mathrm{OD}(\lambda)$ is the optical density at wavelength λ, $\varepsilon_{Hb}(\lambda)$ and $\varepsilon_{HbO2}(\lambda)$ are the extinction coefficients at wavelength λ for molar concentrations of deoxygenated hemoglobin, [Hb], and oxygenated hemoglobin, $[HbO_2]$, respectively, assuming ferrihemoglobin is minimal. By using two wavelengths, both $[HbO_2]$ and [Hb] can be determined by measuring the OD values at the two specific wavelengths, provided that the values for $\varepsilon_{Hb}(\lambda)$ and $\varepsilon_{HbO2}(\lambda)$ are known:

$$[HbO_2] = \frac{\varepsilon_{Hb}(\lambda_2)\mathrm{OD}(\lambda_1) - \varepsilon_{Hb}(\lambda_1)\mathrm{OD}(\lambda_2)}{l[\varepsilon_{Hb}(\lambda_2)\varepsilon_{HbO2}(\lambda_1) - \varepsilon_{Hb}(\lambda_1)\varepsilon_{HbO2}(\lambda_2)]}, \tag{3}$$

$$[Hb] = \frac{\varepsilon_{HbO2}(\lambda_2)\mathrm{OD}(\lambda_1) - \varepsilon_{HbO2}(\lambda_1)\mathrm{OD}(\lambda_2)}{l[\varepsilon_{Hb}(\lambda_1)\varepsilon_{HbO2}(\lambda_2) - \varepsilon_{Hb}(\lambda_2)\varepsilon_{HbO2}(\lambda_1)]}. \tag{4}$$

It follows that changes in [Hb] and $[HbO_2]$ can be consequently given as:

$$\Delta[HbO_2] = \frac{\varepsilon_{Hb}(\lambda_2)\Delta\mathrm{OD}(\lambda_1) - \varepsilon_{Hb}(\lambda_1)\Delta\mathrm{OD}(\lambda_2)}{l[\varepsilon_{Hb}(\lambda_2)\varepsilon_{HbO2}(\lambda_1) - \varepsilon_{Hb}(\lambda_1)\varepsilon_{HbO2}(\lambda_2)]}, \tag{5}$$

$$\Delta[Hb] = \frac{\varepsilon_{HbO2}(\lambda_2)\Delta\mathrm{OD}(\lambda_1) - \varepsilon_{HbO2}(\lambda_1)\Delta\mathrm{OD}(\lambda_2)}{l[\varepsilon_{Hb}(\lambda_1)\varepsilon_{HbO2}(\lambda_2) - \varepsilon_{Hb}(\lambda_2)\varepsilon_{HbO2}(\lambda_2)]}, \tag{6}$$

where $\Delta\mathrm{OD}(\lambda)$ represents a change in optical density at the specific wavelength, λ, and equals $\log(A_B/A_T)$. A_B and A_T correspond to light intensities measured under the baseline and transient conditions.

Note that in principle, l represents the optical path length between the source and detector. Whereas l is simply the physical separation, d, between the source and detector through a nonscattering medium, exact quantification of l for an intact tissue or organ is complex because of light scattering in tissue. Since l is in proportion to the separation, d, we can associate l to d as $l = DPF*d$, where DPF is a differential path length factor to account for light scattering. It has been well accepted that together with DPF, Eq. (2) can be treated as modified Beer–Lambert law; and consequently, Eqs. (5) and (6) can be correctly used to quantify changes in [Hb] and $[HbO_2]$ in highly scattering media (29,30), such as in intact tissue or organs.

To be consistent with our previous work, we adopted in this paper the ε values published by Zijlstra *et al*. (31). We had to interpolate the ε values at the two wavelengths used in our study, followed by certain corrections due to the interpolation errors by phantom calibration measurements (22). Specifically, we included two factors, β_1 and β_2, for the calibrated algorithm, as given below:

$$\Delta[HbO_2] = \frac{\frac{\varepsilon_{Hb}(785\ \mathrm{nm})}{\beta_1} \times \mathrm{OD}(758\ \mathrm{nm}) - \varepsilon_{Hb}(758\ \mathrm{nm}) \times \mathrm{OD}(785\ \mathrm{nm})}{l[\varepsilon_{Hb}(785\ \mathrm{nm})\varepsilon_{HbO2}(758\ \mathrm{nm}) - \varepsilon_{Hb}(758\ \mathrm{nm})\varepsilon_{HbO2}(785\ \mathrm{nm})]}, \tag{7}$$

$$\Delta[Hb] = \frac{\frac{\varepsilon_{HbO2}(785\ \mathrm{nm})}{\beta_2} \times \mathrm{OD}(758\ \mathrm{nm}) - \varepsilon_{HbO2}(758\ \mathrm{nm}) \times \mathrm{OD}(785\ \mathrm{nm})}{l[\varepsilon_{Hb}(785\ \mathrm{nm})\varepsilon_{HbO2}(758\ \mathrm{nm}) - \varepsilon_{Hb}(758\ \mathrm{nm})\varepsilon_{HbO2}(785\ \mathrm{nm})]}, \tag{8}$$

where $\varepsilon_{Hb}(758\ \mathrm{nm}) = 1.418$, $\varepsilon_{HbO2}(758\ \mathrm{nm}) = 0.6372$, $\varepsilon_{Hb}(785\ \mathrm{nm}) = 1.111$, and $\varepsilon_{HbO2}(785\ \mathrm{nm}) = 0.766$, all in $\mathrm{mM^{-1}cm^{-1}}$. Note that a factor of four has been multiplied for each of the εs at the respective wavelengths to account for light absorption from four hemes per hemoglobin molecule (34) since the extinction coefficients published in the field of biochemistry were expressed on a heme basis (24–28). Furthermore, we have used $\beta_1 = 1.103$ and $\beta_2 = 0.9035$ according to our phantom study (22). After substituting all of the parameters into Eqs. (7) and (8), we have arrived at the final equations to quantify changes in hemoglobin concentration: **?2**

$$\Delta[HbO_2] = \frac{-2.658 \cdot \mathrm{OD}(758\ \mathrm{nm}) + 3.743 \cdot \mathrm{OD}(785\ \mathrm{nm})}{d}, \tag{9}$$

$$\Delta[Hb] = \frac{2.238 \cdot \mathrm{OD}(758\ \mathrm{nm}) - 1.683 \cdot \mathrm{OD}(785\ \mathrm{nm})}{d}. \tag{10}$$

$\Delta[Hb]_{total}$ can also be obtained by adding Eqs. (9) and (10),

$$\begin{aligned}\Delta[Hb]_{total} &= \Delta[HbO_2] + \Delta[Hb] \\ &= \frac{-0.42 \cdot \mathrm{OD}(758\ \mathrm{nm}) + 2.06 \cdot \mathrm{OD}(785\ \mathrm{nm})}{d}.\end{aligned} \tag{11}$$

Notice that the units for $\Delta[HbO_2]$, $\Delta[Hb]$, and $\Delta[Hb]_{total}$ are mM; however, the values obtained from Eqs. (9) to (11) are scaled by a factor of

DPF. Since DPF is so far an unknown parameter for tumors, we include it within the unit as mM/DPF.

Laser photothermal irradiation system. The system used for the photothermal therapy consisted of an NIR diode laser, DIOMED 25 (DIOMEDICS, The Woodlands, TX), with an emitting peak wavelength at 805 nm and a maximum power output of 25 W. The laser light was coupled into an optical fiber, fitted with a microlens at the tip (Pioneer Optics, Windsor Locks, CT) to ensure a uniform beam density, and delivered onto the tumor surface. The laser beam diameter projected on the tumor surface was set as 2 cm in all the measurements by using the visible aiming light in the laser system. After the beam diameter was adjusted, the aiming light was turned off during NIR measurements.

Multichannel thermal monitor. A multichannel thermal monitor (Omega, Stamford, CT), incorporating an OM-700 Omega engineering data acquisition and control unit, was used simultaneously with the NIRS observation to monitor the internal temperatures at several locations within the tumors. Specifically, three thermal probes were inserted at the top (immediately below the overlaying skin), middle and bottom positions of the tumors, and one probe was located outside the tumor for room temperature recording. The data of each probe were recorded continuously, and the middle thermal probe recorded the internal tumor temperature near the center of the optical field of NIRS.

Animal model. The transplantable, metastatic mammary tumor cells (DMBA-4) (33–35) were implanted in one of the inguinal fat pads of female Wistar Furth rats (Harlan Sprague Dawley, Indianapolis, IN). Once the tumors reached 0.5 to 0.8 cm in diameter, the rats were anesthetized for the experiments. Hairs around tumors were removed for better probe contact in the NIRS measurement and for more efficient tumor exposure to the laser irradiation. The tumor diameters along the three major orthogonal axes (*a, b, c*) were measured to determine the volume of the tumors by using an ellipsoid approximation with the formula of $V = (\pi/6)abc$.

In this study, 16 rat breast tumors were used in two different treatment protocols. Ten rat tumors were first exposed to a single laser irradiation with a laser power of 0.32 W/cm^2 (1 W laser power in a 2-cm-diameter beam) for 10 min. Three or four days later, four of the treated tumors, along with other six untreated tumors, were exposed to repeated laser irradiations with a power density of 0.32, 0.64, 0.96 and 1.27 W/cm^2 (1 W, 2 W, 3 W, and 4 W in 2-cm-diameter beam) for 10 min with a recovery period of 10 min between two adjacent irradiations. Tumor temperatures, tumor vascular $\Delta[HbO_2]$, and $\Delta[Hb]_{total}$ were measured simultaneously in all the experiments.

Statistic analysis. A Student's *t*-test was applied in data analysis to determine whether the paired samples are significantly different. We considered $P < 0.05$ as the criteria for significant difference between the two sample groups. In addition, a mean and standard deviation (mean ± sd) were usually used to express the measured data and their dispersions.

RESULTS

Dynamic responses of $\Delta[HbO_2]$, $\Delta[Hb]_{total}$ and temperature to photothermal treatment

Using the experimental setup shown in Fig. 1 and Eqs. (9) and (11), tumor vascular $\Delta[HbO_2]$, $\Delta[Hb]_{total}$ and internal temperatures were quantified simultaneously. Figure 2 shows the temporal profiles of $\Delta[HbO_2]$, $\Delta[Hb]_{total}$ and the internal temperatures of a rat tumor under photothermal irradiation with a laser power density of 0.32 W/cm^2. The experimental data consisted of four temporal periods, as labeled in the Fig. In period 1, without irradiation, the thermal probes recorded the baseline temperatures at three different locations inside the tumor for about 6 min. In period 2, the NIRS system was turned on while the thermal recording continued, and the recorded thermal readings showed no obvious perturbation from the NIRS. After the NIRS signals were stabilized, a 10-min laser irradiation started. During the laser treatment, the tumor temperatures, $\Delta[HbO_2]$, and $\Delta[Hb]_{total}$ showed significant elevation (period 3 in Fig. 2a). Tumor temperatures increased significantly ($P < 0.0001$) with the irradiation. The tumor volumes near the tumor surface had more significant thermal effects: the temperature at the top (T-top) varied from 25.3 ± 0.1°C to 30.3 ± 0.1°C (mean ± sd), while the temperatures at the middle and bottom (T-middle and T-bottom) of the tumor were elevated from 26.1 ± 0.1°C to 29.8 ± 0.1°C and from 27.5 ± 0.1°C to 28.9 ± 0.1°C, respectively. The maximal changes in T-top, T-middle and T-bottom caused by the laser irradiation were 5.0 ± 0.1°C, 3.7 ± 0.1°C and 1.4 ± 0.1°C, respectively. Similarly, both $\Delta[HbO_2]$ and $\Delta[Hb]_{total}$ displayed significant increases over the entire irradiation period ($P < 0.005$), with the mean elevations of 0.04 ± 0.01 mM/DPF and 0.02 ± 0.01 mM/DPF, respectively. Notice that the maximal values of $\Delta[HbO_2]$ and $\Delta[Hb]_{total}$ shown in Fig. 2a are ~0.1 and 0.05 mM/DPF. When the laser beam was turned off in period 4, $\Delta[HbO_2]$, $\Delta[Hb]_{total}$ and temperatures all decreased, with the temperatures reaching the baselines quickly and $\Delta[HbO_2]$ and $\Delta[Hb]_{total}$ declining more gradually and not quite reaching the baselines within the 10-min recovery period.

To quantify the dynamic behaviors observed in Fig. 2a, single-exponential functions were applied to T-top, T-middle, $\Delta[HbO_2]$, and $\Delta[Hb]_{total}$ on both rising and falling periods, as shown in Fig. 2b,c. The time constants obtained from such fittings reveal the dynamic responses of signals to the initiation and termination of photothermal irradiation. As shown in Fig. 2b, T-top (time constant of 4.5 ± 0.5 min) has a faster response to laser irradiation than T-middle (time constant as 14.4 ± 0.6 min). The time constants for $\Delta[HbO_2]$ and $\Delta[Hb]_{total}$ are 3.85 ± 0.03 min and 3.95 ± 0.06 min, respectively. In response to the termination of laser irradiation, T-top and T-middle have a time constant of 3.9 ± 0.5 min and 12.3 ± 0.6 min, respectively (Fig. 2c). It is clearly seen that the dynamic thermal responses of the tumor to laser irradiation and to the termination of laser irradiation are well matched both at the tumor surface and within the tumor. However, the time constants for $\Delta[HbO_2]$ and $\Delta[Hb]_{total}$ to return to the baseline are much longer in the falling period, with 18.5 ± 0.5 min and 24.3 ± 0.8 min, respectively, also shown in Fig. 2c.

Similar protocols and measurements were performed on the other nine tumors. Figure 3 shows the average increases of the temperature at different locations. Temperatures near the tumor surface have maximal increases, whereas local temperatures near the bottom of the tumors have minimal increases observed from all the 10 tumors. The average elevations for T-top and T-bottom are 7 ± 3°C and 3 ± 2°C, respectively. The thermal readings from the middle position (T-middle) represent the average temperatures in the tumor volumes probed by the NIRS beams, and the average increase in T-middle for the 10 rats is 5 ± 2°C. The statistical analysis indicates significant differences between T-top, T-middle, and T-bottom ($P < 0.05$).

To investigate dynamic behaviors of the tumors in response to the initiation and termination of laser irradiation, the time constants of T-top, T-middle, $\Delta[HbO_2]$, and $\Delta[Hb]_{total}$ obtained from the rising and falling periods are summarized in Table 1. The results demonstrate several points: (1) an average dynamic change in T-top is significantly ($P < 0.05$) faster than that in T-middle in the rising period, with a time constant of 3.7 ± 1.1 min for T-top and 6.4 ± 3.2 min for T-middle. A similar significant difference ($P < 0.01$) also holds in the falling period with a time constant of 3.8 ± 1.2 min for T-top and 6.6 ± 2.7 min for T-middle, respectively. (2) The dynamic responses of $\Delta[HbO_2]$, $\Delta[Hb]_{total}$, and T-middle have no significant differences during the initiation of photoirradiation ($P > 0.4$). (3) The average time constant of T-top in the rising period is similar ($P > 0.9$) to that in the falling period, and so is that of T-middle ($P > 0.7$). However, (4) the dynamic response of

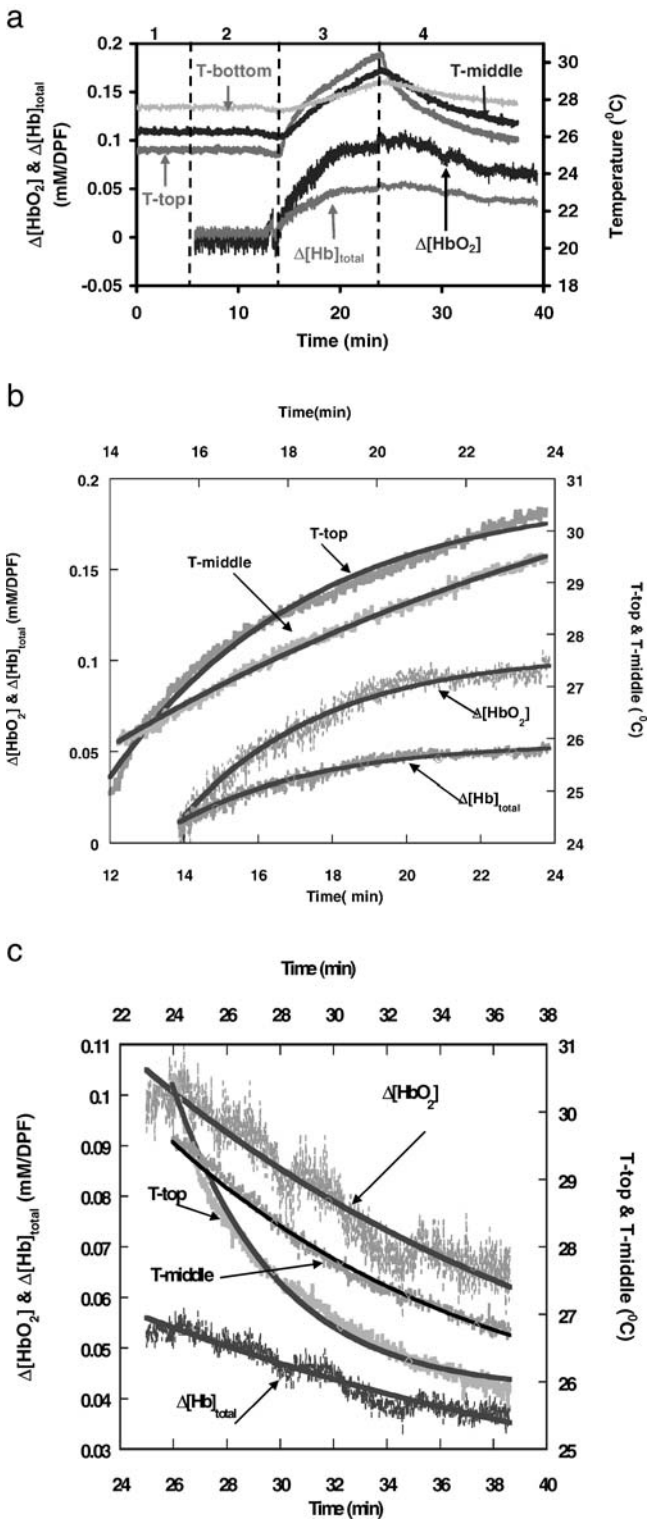

Figure 2. (a) Temporal profiles of the changes in tumor oxygenation and total hemoglobin concentrations, $\Delta[HbO_2]$ and $\Delta[Hb]_{total}$, and three intratumor temperatures during photothermal intervention in a representative DMBA-4 rat breast tumor (2.4 cm^3). The profile is divided into four periods, and the laser irradiation was applied only in period 3. (b) Respective single-exponential curve fittings for the rising period of T-top, T-middle, $\Delta[HbO_2]$ and $\Delta[Hb]_{total}$ displayed in (a). The top *x*-axis is used for the T-top and T-middle curves, whereas the bottom *x*-axis is for $\Delta[HbO_2]$ and $\Delta[Hb]_{total}$. Single exponential fitting yields: T-top = 5.76*(1 − exp[−{*t* − 147}/4.49]) + 24.95 with R = 0.99; T-middle = 7.28*(1 − exp[−{*t* − 14}/14.3]) + 25.98 with R = 0.99; $\Delta[HbO_2]$ = 0.093*(1 − exp[−{*t* − 14}/3.85]) + 0.013 with R = 0.98; $\Delta[Hb]_{total}$ = 0.044*(1 − exp[−{*t* − 14}/3.95]) + 0.012 with R = 0.98; (c) Respective single-exponential curve fittings for the falling period of T-top, T-middle, $\Delta[HbO_2]$ and $\Delta[Hb]_{total}$ displayed in (a). Single exponential fitting yields: T-top = –4.48*(1 − exp[−{*t* − 25}/3.86]) + 29.23 with R = 0.98; T-middle = –3.83*(1 − exp[−{*t* − 25}/12.29]) + 30.42 with R = 0.99; $\Delta[HbO_2]$ = –0.163*(1 − exp[−{*t* − 25}/18.5]) + 0.10 with R = 0.94; $\Delta[Hb]_{total}$] = –0.114*(1 − exp[−{*t* − 25}/24.3]) + 0.06 with R = 0.92.

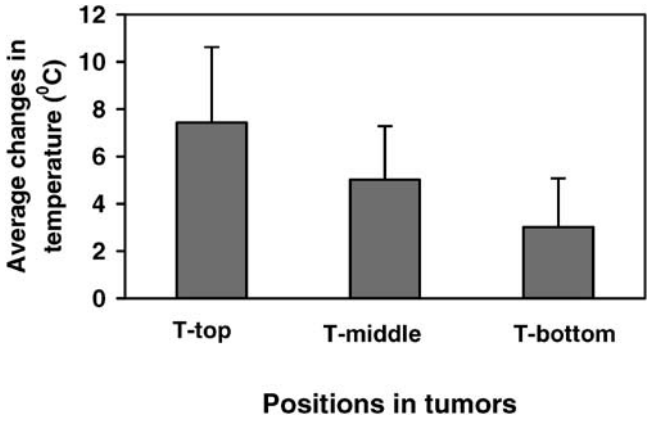

Figure 3. Average changes in temperature from the 10 rats for T-top, T-middle and T-bottom.

$\Delta[HbO_2]$ in the falling period (a time constant of 28 ± 22 min) is significantly slower ($P < 0.01$) than that in the rising period (a time constant of 5.3 ± 2.8 min), and so is $\Delta[Hb]_{total}$ response, with a time constant of 6.2 ± 3.7 min and 41 ± 32 min for the rising and falling periods, respectively ($P < 0.01$).

Furthermore, although $\Delta[HbO_2]$ and $\Delta[Hb]_{total}$ have similar dynamic trends in response to photoirradiation, a difference between their magnitudes exists. A strong correlation ($R^2 = 0.95$) between $\Delta[HbO_2]$ and $\Delta[Hb]_{total}$ has been observed, as shown in Fig. 4, where the amplitude in $\Delta[HbO_2]$ is nearly twice that of $\Delta[Hb]_{total}$ for all 10 tumors (with a slope of the fitted curve being 0.54).

Effect of the optical power density on tumor $\Delta[HbO_2]$, $\Delta[Hb]_{total}$ and temperatures

Repeated laser irradiation was applied to the 10 tumors, 4 of which were used in the previous single-irradiation treatment 3 or 4 days earlier. Figure 5a shows the profiles of the tumor vascular $\Delta[HbO_2]$, $\Delta[Hb]_{total}$ and tumor temperatures in response to irradiations under power densities of 0.32, 0.64, 0.96 and 1.27 W/cm^2, with an irradiation period of 10 min and a recovery period of 10 min between each treatment. Tumor temperatures (T-top, T-middle and T-bottom) increased significantly ($P < 0.0001$) from the baseline to different maximum values under different laser powers. The maximal changes in temperature in the middle of the tumor (T-middle) due to consecutive irradiation displayed a strong linear dependence on the laser power density, as shown in Fig. 5b. However, $\Delta[HbO_2]$ and $\Delta[Hb]_{total}$ showed interesting behaviors in response to the thermal irradiation at different light dosages. Under relatively low laser power irradiations (0.32, 0.64, 0.96 W/cm^2), both $\Delta[HbO_2]$ and $\Delta[Hb]_{total}$ increased significantly ($P < 0.0001$) with respect to the baselines, and they both declined significantly under a high laser power irradiation (1.27 W/cm^2), as shown in

Table 1. Time constants (minutes) of T-top, T-middle, $\Delta[HbO_2]$, and $\Delta[Hb]_{total}$ with respect to photoirradiation and termination

Tumor size(cm^3)	Rising part (in response to irradiation)				Falling part (in response to termination)			
	T-top	Tmiddle	$\Delta[HbO_2]$	$\Delta[Hb]_{total}$	T-top	Tmiddle	$\Delta[HbO_2]$	$\Delta[Hb]_{total}$
2.4	4.49	14.3	3.85	3.95	3.86	12.29	18.5	24.3
2.5	2.47	6.77	1.99	1.53	3.17	8.27	50	74
0.68	4.83	4.83	1.76	1.66	3.87	4.45	20	25
0.53	4.61	7.62	1.84	1.91	4.56	8.37	3.63	2.75
1.2	3.28	5.17	6.9	9.8	4.20	6.30	80	120
3.3	4.70	6.65	7.34	7.83	3.58	4.45	11.3	29.9
1.9	1.89	3.85	10.0	12.0	1.30	3.43	28	37
3.4	2.69	3.13	6.76	7.81	2.96	4.58	35	45
2.1	3.25	4.31	7.32	7.58	4.52	5.65	23.5	30
3.0	4.50	7.80	5.60	8.40	5.50	8.30	15.5	23.4
Average	3.7	6.4	5.3	6.2	3.8	6.6	28.	41
SD*	1.1	3.2	2.8	3.7	1.2	2.7	22.	33

*SD = standard deviation.

Fig. 5b. Similar to the feature observed in single irradiation, $\Delta[HbO_2]$ values had greater magnitude than $\Delta[Hb]_{total}$, whereas their dynamic trends were consistent.

To investigate the accumulative effects on $\Delta[HbO_2]$ and $\Delta[Hb]_{total}$ from several thermal irradiations given 10 min apart (Fig. 5a), we had also taken a direct reading for $\Delta[HbO_2]$ and $\Delta[Hb]_{total}$ with a high laser power of 1.27 W/cm^2 without any preirradiation. Figure 5c shows an example of this case, demonstrating that $\Delta[HbO_2]$ indeed decreases after an initial increase for a few minutes, whereas $\Delta[Hb]_{total}$ has less trend to drop within the 10-min treatment. The similarity for the ratio of $\Delta[HbO_2]$ to $\Delta[Hb]_{total}$ close to a factor of 2 still exists.

Temperature data for all 10 tumors under different power irradiations are plotted in Fig. 6a. The maximum changes in T-middle increase linearly with the optical radiation dosages, with a correlation of $R^2 > 0.91$ for all the cases and having an average slope of 13 ± 3 (°C/[W/cm^2]). To distinguish the tumors pretreated and nonpretreated with a single low-power irradiation (0.32 W/cm^2) 3 or 4 days before, the slopes of the linear regression for each of the tumors shown in Fig. 6a were classified into two groups, *i.e.* without pretreatment and with pretreatment (Fig. 6b). A Student's *t*-test showed that there is no significant difference ($P = 0.95$) between the two groups of slopes.

DISCUSSION

In this study, we have investigated vascular $\Delta[HbO_2]$, $\Delta[Hb]_{total}$ and internal temperature in response to photothermal therapy simultaneously in rat breast tumors by using an NIRS system and a thermal monitor, respectively. The results obtained in this study clearly demonstrate the compatibility of the NIRS system with the temperature monitoring system, without noticeable interference between the two systems (Fig. 2). The NIRS system offers a real-time measurement of $\Delta[HbO_2]$ and $\Delta[Hb]_{total}$ in tumor vasculature within the optical field of the NIR probes, while the multichannel thermal monitor records the temperatures at specific locations within the tumors in real time. The compatibility of the two systems permits simultaneous determinations of thermal and vascular characteristics of treated tumors under photothermal therapy, providing valuable insight into the dynamic relationship between the tumor vascular contents and the thermal effect in treated tumor tissues.

Thermal treatment to tumors has been demonstrated to cause cellular cytotoxicity, and thus, to destroy the tumor cells (36–38). Laser irradiation applied in this study proves its ability to induce photothermal effects inside the rat breast tumors. The single exponential increase in tumor temperature obtained in our results indicates that an extended exposure period to the laser beam may gradually stabilize the tumor temperature at a certain level, depending on both the laser power density and the individual tumors (as seen in Figs. 2a and 5a). Manipulation of the laser power may help adjust the internal tumor temperature, resulting in optimal tissue destruction. Although a strong linear relation between the maximum temperature increase within the tumors and the irradiation power density has been observed for all the tumors, the actual dependence of tumor temperature on the laser power density does vary from tumor to tumor (Fig. 6). Such intertumor variability demonstrates the necessity of real-time monitoring for tumor temperature under photothermal therapy. Moreover, the tumor temperatures near the surface (T-top) respond to the photoirradiation more rapidly and with a greater increase than those within deeper tumor tissue (T-middle) (as seen in Figs. 2, 3, and 5a, and Table 1). Such large thermal effects can cause tissue damage at the tumor surface. To avoid such thermal damage,

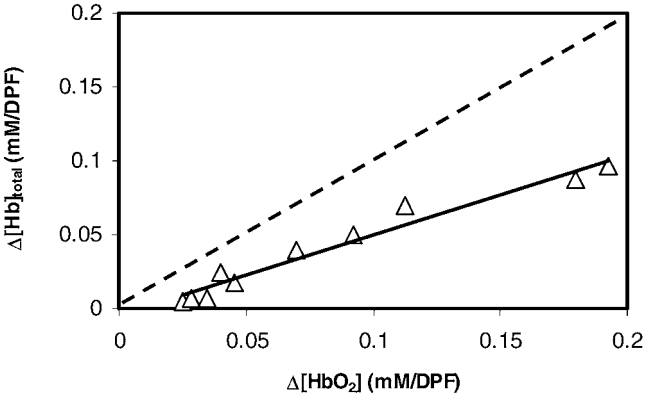

Figure 4. Relationship between $\Delta[HbO_2]$ and $\Delta[Hb]_{total}$ for the 10 rat tumors under single laser irradiation treatment (0.32 W/cm^2 for 10 min) with a linear fit of $\Delta[Hb]_{total} = 0.54*\Delta[HbO_2] - 0.0039$ (the solid curve) and a correlation of $R^2 = 0.96$. The dashed line represents the situation of $\Delta[HbO_2] = \Delta[Hb]_{total}$.

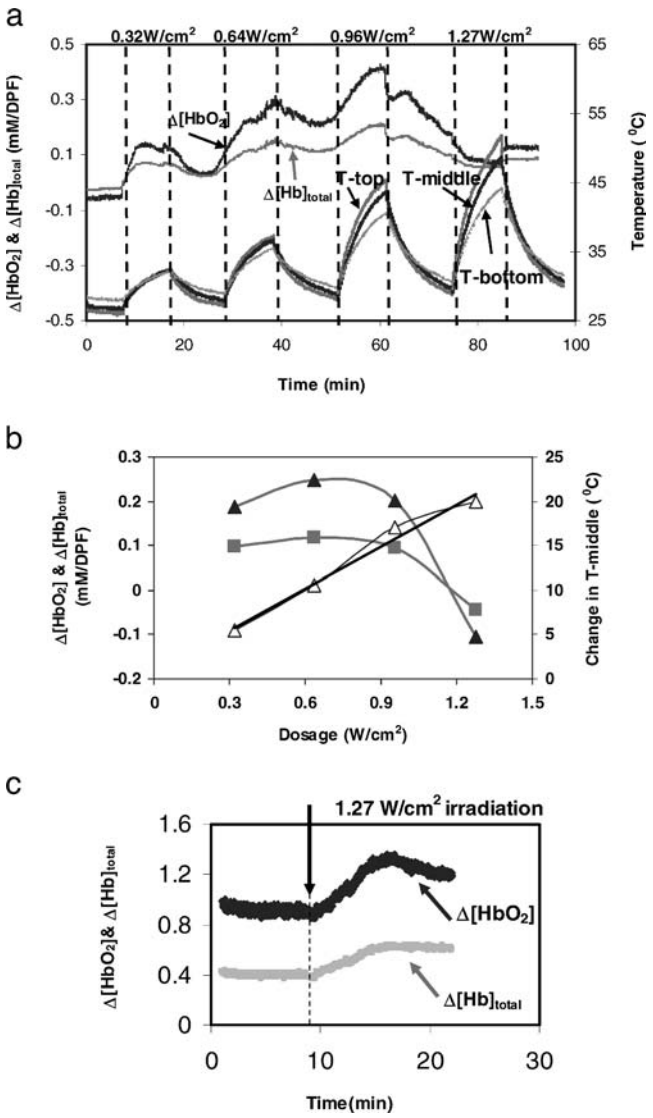

Figure 5. (a) The temporal profiles of vascular $\Delta[HbO_2]$, $\Delta[Hb]_{total}$ and temperatures of a tumor (#6, 3.0 cm^3) in response to repeated laser irradiations with different laser power densities (0.32, 0.64, 0.96 and 1.27 W/cm^2) for a 10-min treatment cycle with a 10-min recovery period between each treatment. (b). The correlations between the changes in $\Delta[HbO_2]$ (solid triangles), $\Delta[Hb]_{total}$ (squares), T-middle (open triangles), and laser irradiation power densities in the tumors. The thick straight line is the best-fitting curve for the tumor temperature increases as function of laser dosage. (c) The temporal profiles of vascular $\Delta[HbO_2]$ and $\Delta[Hb]_{total}$ of a tumor irradiated with a single laser power density of 1.27 W/cm^2.

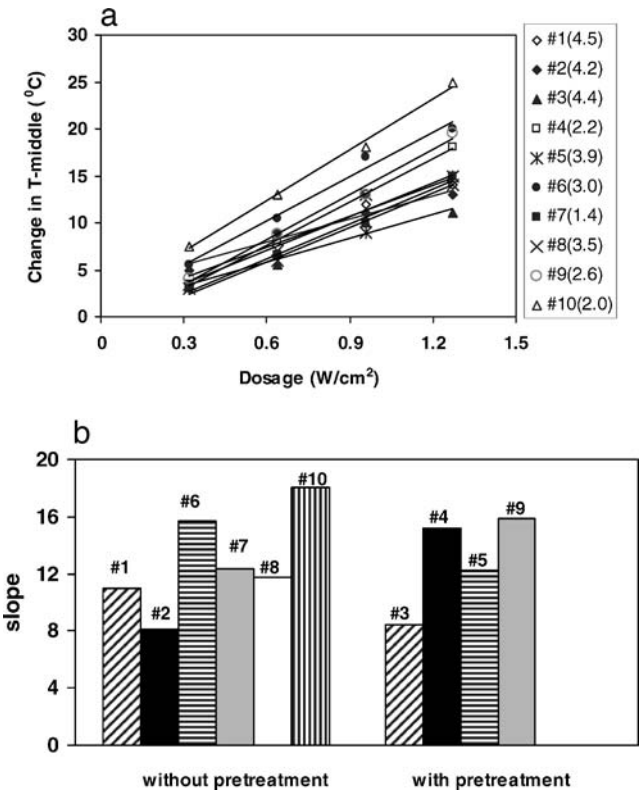

Figure 6. (a) Correlations between the maximum changes in T-middle reached at the end of each photothermal treatment cycle and the optical irradiation power density from the 10 treated rats. The numbers after the symbol ''#'' are labels for different tumors. The numbers inside the parentheses indicate the tumor volume, with unit of cm^3. Note that there are four tumors that had preirradiations 3–4 days earlier, and their tumor volumes have been possibly changed in comparison to those listed in Table 1. (b). The slopes in (a) for all the tumors were classified into two groups: without pretreatment and with pretreatment. A *t*-test between these two groups of slopes gives rise to $P = 0.95$.

intratumoral injection of selective absorbers, such as indocyanine green, has been used by Chen *et al*. to selectively manipulate the temperature within the tumor without severe damage at the tumor surface (11,12,39).

It is seen clearly in this study that tumor vascular contents, *i.e*. oxygenated and deoxygenated hemoglobin, are greatly affected by photothermal therapy. When the photothermal irradiation with a low power density (0.32 W/cm^2) was applied to the breast tumors, both $\Delta[HbO_2]$ and $\Delta[Hb]_{total}$ increased significantly ($P < 0.005$) in all the tumors (Figs. 2a, 4 and 5a). The dynamic behaviors of $\Delta[HbO_2]$ and $\Delta[Hb]_{total}$ in response to photo-irradiation, quantified by the time constants, are in the same order as those of tumor interior temperature, T-middle, while their behaviors in response to the termination of photoirradiation are much slower than those of T-middle (Fig. 2 and Table 1). In contrast to the lower laser power irradiation, higher laser power densities could cause interesting responses in tumor vascular contents. As seen in Fig. 5b,c, $\Delta[HbO_2]$ started to decrease when the laser power approached a certain level, either with or without preirradiation. Intriguingly, although $\Delta[HbO_2]$ has the same dynamic trend as $\Delta[Hb]_{total}$ in response to photoirradiation, the magnitude of $\Delta[HbO_2]$ is more profound than that of $\Delta[Hb]_{total}$ (Figs. 4, 5).

The analysis on the dynamic behaviors of tumor vascular contents and interior tumor temperature in response to photoirradiation allows us to better understand the mechanism of photothermal therapy. The time constants of $\Delta[HbO_2]$ as well as of $\Delta[Hb]_{total}$ have the same order as those of interior tumor temperature. We may speculate that an increase in tumor temperature may lead to vessel dilation within tumor vasculature, and thus, resulting in an increase in blood inflow. Such an increase in blood inflow will give rise to an increase in $\Delta[Hb]_{total}$ as well as $\Delta[HbO_2]$.

Besides thermal effects, it is reasonable to expect other photoactivation processes involved in the laser irradiation. It is known that direct exposure of vascular tissue to visible light causes vasodilation (40), whereas the thermal effect from visible light is minor. Photoactivation has also been reported to cause

upregulation of nitric oxide, and thus, produce vasodilation (41–43). The increase of tumor blood contents due to laser irradiation observed in our study may be attributed to the vessel dilation induced by the direct effect of heating as well as photoactivation. Consistently, the single-exponential trend of both $\Delta[Hb]_{total}$ and $\Delta[HbO_2]$ in response to laser irradiation indicated the existence of vessel dilation. The fact that the time constants of $\Delta[HbO_2]$ and $\Delta[Hb]_{total}$ in response to the laser termination are longer than those in response to the laser initiation (Table 1, Figs. 2a, 5a) implies a longer settling time needed for the recovery of dilated vessels.

In the laser thermal treatment, we realized that $\Delta[HbO_2]$ as well as $\Delta[Hb]_{total}$ did not completely return to the baseline during each of the recovery periods (Figs. 2a, 5a). Figure 5c was taken from a tumor that was exposed to a single high-power laser irradiation (1.27 W/cm^2), displaying somewhat different behavior in comparison to that under consecutive repeated treatments: the $\Delta[HbO_2]$ signals increased, followed by an obvious decrease. These phenomena lead us to a speculation that the previous laser exposure ''preconditions'' the treated tumor, with respect to consecutive treatments, and affects the response of tumor to subsequent high irradiation exposure, although the single lower-power irradiation pretreated 3 or 4 days earlier has no obvious influence on the later treatment (Fig. 6b). It is reasonable to believe that the ''preconditioning'' can be minimal if the time intervals between two repeated irradiations are two to three times longer than the time constants during the recovery periods, such as in the order of 1–1.5 h.

The interesting phenomenon, *i.e.* changes of oxygenated hemoglobin concentration are nearly two times greater than those of total hemoglobin concentration, allures us to speculate that the increase in $\Delta[HbO_2]$ comes partly from the increase of $\Delta[Hb]_{total}$, and partly from the conversion of deoxygenated hemoglobin to oxygenated hemoglobin. The correlation of magnitude between $\Delta[HbO_2]$ and $\Delta[Hb]_{total}$ unambiguously demonstrates that the increased total hemoglobin concentration, due to blood vessel dilation, is mostly oxygenated after the irradiation starts. It basically implies that photoirradiation may increase the tumor oxygenation, which will be beneficial to some nonsurgical treatments, such as chemotherapy and radiotherapy (37).

In summary, changes in breast tumor temperature and vascular oxygenation have been simultaneously measured using a multichannel thermal monitor and an NIRS system, while the tumors were under photothermal irradiation. The results have demonstrated that: (1) the compatibility of thermal monitoring system and the NIR system permits simultaneous determinations of thermal and vascular characteristics of the treated tumors; (2) photoirradiation did have the ability to induce thermal effects inside the rat breast tumors in a single exponential trend, thus leading to destruction of the tumor cells; (3) the response of $\Delta[HbO_2]$ and $\Delta[Hb]_{total}$ to photoirradiation may be attributed to vessel dilation under both thermal and photo effect; (4) low-power laser irradiations predelivered 3 or 4 days earlier have no effect on the later treatments; the previous laser exposures within a time interval of 10 min do influence the response of tumor vascular contents to subsequent high irradiation; (5) the fact that the change in the magnitude of $\Delta[HbO_2]$ is nearly two times greater than that of $\Delta[Hb]_{total}$ suggests that photoirradiation may enhance tumor vascular oxygenation. The primary results from this study clearly indicate that besides a considerable thermal effect, low-power density irradiation could also result in a significant enhancement of tumor vascular oxygenation; this enhancement may lead to improvement of treatment efficiency.

Acknowledgements—The authors acknowledge the support in part by the Department of Defense Breast Cancer Research Programs DAMD17-01-1-0423 (Y.G.) and DAMD17-00-1-0459 (H.L.), in part by Chinese National Science Foundation Committee (NSFC 30371362), in part by the Oklahoma Center for Advancement of Science and Technology (OCAST) AP01-016 (W.R.C.) and from the University of Central Oklahoma (W.R.C.), and in part by the National Institutes of Health P20 RR016478, the INBRE Program of the National Center for Research Resources (W.R.C.).

REFERENCES

1. Jacques, S. L. (1992) Laser-tissue interactions. Photochemical, photothermal, and photomechanical. *Surg. Clin. North Am.* **72**, 531–558.
2. Thomsen, S. L. (1991) Pathologic analysis of photothermal and photomechanical effects of laser–tissue interactions. *Photochem. Photobiol.* **53**, 825–835.
3. Chen, W. R., R. L. Adams, S. Heaton, D. T. Dickey, K. E. Bartels and R. E. Nordquist (1995) Chromophore-enhanced laser-tumor tissue photo-thermal interaction using an 808-nm diode laser. *Cancer Lett.* **88**, 15–19.
4. Chen, W. R., R. L. Adams, K. E. Bartels and R. E. Nordquist (1995) Chromophore enhanced in vivo tumor cell destruction using an 808-nm diode laser. *Cancer Lett.* **94**, 125–131.
5. Thistlethwaite, A. J., D. B. Leeper, D. J. Moylan and R. E. Nerlinger (1986) pH distribution in human tumors. *Int. J. Radiat. Oncol. Biol. Phys.* **11**, 1647–1652.
6. Reinhold, H. S. and B. Endrich (1986) Tumor microcirculation as a target for hyperthermia: a review. *Int. J. Hyperthermia* **2**, 111–137.
7. Anghileri, L. J. and J. Robert (1986) *Hyperthermia in Cancer Treatment*. CRC Press, Boca Raton, FL.
8. Thews, O., D. K. Kelleher and P. Vaupel (2002) Dynamics of tumor oxygenation and red blood cell flux in response to inspiratory hyperoxia combined with different levels of inspiratory hypercapnia. *Radiother. Oncol.* **62**, 77–85.
9. Hockel, M. and P. Vaupel (2001) Biological consequences of tumor hypoxia. *Semin. Oncol.* **28**, 36–41.
10. Wouters, B. G., S. A. Weppler, M. Koritzinsky, W. Landuyt, S. Nuyts, J. Theys, P. K. Chiu and P. Lambin (2002) Hypoxia as a target for combined modality treatments. *Eur. J. Cancer* **38**, 240–257.
11. Chen, W. R., R. L. Adams, R. Carubelli and R. E. Nordquist (1997) Laser-photosensitizer assisted immunotherapy: a novel modality for cancer treatment. *Cancer Lett.* **115**, 25–30.
12. Chen, W. R., H. Liu, J. W. Ritchey, K. E. Bartels, M. D. Lucroy and R. E. Nordquist (2002) Effect of different components of laser immunotherapy in treatment of metastatic tumors in rats. *Cancer Res.* **62**, 4295–4299.
13. Korbelik, M., V. R. Naraparaju, and N. Yamamoto (1997) Macrophage-directed immunotherapy as adjuvant to photodynamic therapy of cancer. *Br. J. Cancer.* **75**, 202–207.
14. Curry, P. M., A. J. Steward., L. Hardwicke, C. Smith and J. R. North (2001) Augmentation of tumor immunity with ENHANZYN adjuvant following verteporfin PDT: photodynamic vaccination (PDV). *SPIE* **4257**, 9–18.
15. Chen, W. R., A. K. Singhal, H. Liu and R. E. Nordquist (2001) Antitumor immunity induced by laser immunotherapy and its adoptive transfer. *Cancer Res.* **61**, 459–461.
16. Chen, W. R., W. G. Zhu, J. R. Dynlacht, H. Liu and R. E. Nordquist (1999) Long-term tumor resistance induced by laser photo-immunotherapy. *Int. J. Cancer* **81**, 808–812.
17. Fingar, V. H., T. J. Wieman and K. W. Doak (1991) Mechanistic studies of PDT-induced vascular damage: evidence that eicosanoids mediate this process. *Int. J. Radiat. Biol.* **60**, 303–309.
18. Yu, W., J. Naim and R. Lanzafame (1994) The effect of laser irradiation on the release of bFGF from 3T3 Fibroblasts. *Photochem. Photobiol.* **59**, 167–170.
19. Karu, T. (1988) Molecular mechanism of the therapeutic effect of low intensity laser radiation. *Laser Life Sci.* **2**, 53–74.
20. Margaret, T. T., W. Riley, X. Bai, E. Buchmann and H. T. Whelan (2001) Light-emitting diode treatment reverses the effect of TTX on cytochrome oxidase in neurons. *Neuroreport* **12**, 3033–3037.
21. Liu, H., Y. Song, K. L. Worden, X. Jiang, A. Constantinescu and R. P. Mason (2000) Noninvasive investigation of blood oxygenation

dynamics of tumors by near infrared spectroscopy. *Appl. Opt.* **39**, 5231–5243.
22. Kim, J. G., Y. Song, D. Zhao, A. Constantinescu, R. P. Mason and H. Liu (2003) Interplay of tumor vascular oxygenation and pO_2 in tumors using NIRS, ^{19}F MR pO_2 mapping, and pO_2 needle electrode. *J. Biomed. Opt.* **8**, 53–62.
23. Gu, Y., V. Bourke, J. G. Kim, A. Constantinescu, R. P. Mason and H. Liu (2003) Dynamic response of breast tumor oxygenation to hyperoxic respiratory challenge monitored with three oxygen-sensitive parameters. *Appl. Opt.* **42**, 2960–2967.
24. Horecker, B. L. (1943) The absorption spectra of hemoglobin and its derivatives in the visible and near infrared regions. *J. Biol. Chem.* **148**, 173–183.
25. Van Kampen, E. J. and W. G. Zijlstra (1965) Determination of hemoglobin and its derivatives. *Adv. Clin. Chem.* **8**, 141–187.
26. Benesch, R., G. Macduff and R. E. Benesch (1965) Determination of oxygen equilibria with a versatile new tonometer. *Anal. Biochem.* **11**, 81–87.
27. Benesch, R. E., R. Benesch and S. Yung (1973) Equations for the spectrophotometric analysis of hemoglobin mixtures. *Anal. Biochem.* **55**, 245–248.
28. Van Assendelft, O. W. and W. G. Zijlstra (1975) Extinction coefficients for use in equations for the spectrophotometric analysis of haemoglobin mixtures. *Anal. Biochem.* **69**, 43–48.
29. Sevick, E. M., B. Chance, J. Leigh, S. Nioka and M. Maris (1991) Quantitation of time- and frequency-resolved optical spectra for the determination of tissue oxygenation. *Anal. Biochem.* **195**, 330–351.
30. Gu, Y., Z. Qian, J. Chen, D. Blessington, N. Ramanujam and B. Chance (2002) High resolution three dimensional scanning optical image system for intrinsic and extrinsic contrast agents in tissue. *Rev. Sci. Instrum.* **73**, 172–178.
31. Zijlstra, W. G., A. Buursma, H. E. Falke and J. F. Catsburg (1994) Spectrophotometry of hemoglobin: absorption spectra of rat oxyhemoglobin, deoxyhemoglobin, carboxyhemoglobin, and methemoglobin. *Comp. Biochem. Physiol.* **107B**, 161–166.
?3 32. Cope, M. (1991) The application of near infrared spectroscopy to non invasive monitoring of cerebral oxygenation in the newborn infant. Ph.D. dissertation, University College London.
33. Chatterjee, S. K. and U. Kim (1976) Biochemical properties of cyclic nucleotide phosphodiesterase in metastasizing and nonmetastasizing rat mammary carcinomas. *J. Natl. Cancer Inst.* **56**, 105–110.
34. Chatterjee, S. K. and U. Kim (1977) Galactosyltransferase activity in metastasizing and nonmetastasizing rat mammary carcinomas and its possible relationship with tumor cell surface antigen shedding. *J. Natl. Cancer Inst.* **58**, 273–280.
35. Chatterjee, S. K. and U. Kim (1978) Fucosyltransferase activity in metastasizing and nonmetastasizing rat mammary carcinomas. *J. Natl. Cancer Inst.* **61**, 151–162.
36. Song, C. W., A. lokshina, J. G. Rhee, M. Patten and S. H. Levitt (1984) Implication of blood flow in hyperthermic treatment of tumors. *IEEE Trans. Biomed. Eng.* **31**, 9–16.
37. Dewey, E. C., L. E. Hopwood, S. A. Sapareto and L. E. Gerweck (1977) Cellular responses to combination of hyperthermia and radiation. *Radiology* **123**, 463–474.
38. Sapareto, S. A. and W. C. Dewey (1984) Thermal dose determination in cancer therapy. *Int. J. Radiat. Oncol. Biol. Phys.* **10**, 787–800.
39. Liu, V. G., T. M. Cowan, S. W. Jeong, S. L. Jacques, E. C. Lemley and W. R. Chen (2002) Selective photothermal interaction using an 805nm diode laser and indocyanine green in gel phantom and chicken breast tissue. *Lasers Med. Sci.* **17**, 272–279.
40. Furchgott, R. F., S. J. Ehrreich and E. Greenblatt (1961) The photoactivated relaxation of smooth muscle of rabbit aorta. *J. Gen. Physiol.* **44**, 499–518.
41. Chang, K.C., E. B. Koo, G. W. Lee, Y. J. Kang and H. Y. Lee (1998) Comparison of relaxations evoked by photoactivation of NO-containing compounds and nitrergic nerve stimulation in 5-hydroxytryptamine and potassium contracted rat gastric fundus. *Gen. Pharmacol.* **30**, 585–591.
42. Venturini, C. M., R. M. J. Palmer and S. Moncada (1993) Vascular smooth muscle contains a depletable store of a vasodilator which is light-activated and restored by donors of nitric oxide. *J. Pharmacol. Exp. Therap.* **266**, 1497–1500.
43. Matsunaga, K. R. and F. Furchgott (1991) Response of rabbit aorta to nitric oxide and superoxide generated by ultraviolet irradiation of solutions containing inorganic nitrite. *J. Pharmacol. Exp. Ter.* **259**, 1140–1146.

extinction coefficients of hemoglobin for near-infrared spectroscopy of tissue

Jae G. Kim, Mengna Xia, and Hanli Liu

Extinction coefficients of hemoglobin have been studied for five decades by clinical chemists and biochemists, particularly for laboratory spectrophotometric measurements. A representative list of literature can be found in [1]–[12], and the studies on the temperature dependence of extinction coefficients of hemoglobin can be found in [13] and [14].

However, during the last ten to 15 years, near infrared spectroscopy (NIRS) and imaging for tissue vascular oxygenation, breast tumor detection, and functional brain imaging have been intensively developed for in vivo measurements by groups of physicists, biomedical engineers, and mathematicians. In the approach of NIRS, NIR light in the wavelength range of 650–900 nm is utilized to illuminate tissue in vivo, and the transmitted or reflected light through tissue is recorded for the quantification of hemoglobin concentrations of the measured tissue vasculature. In order to achieve mathematical conversion from the detected light intensity at different wavelengths to hemoglobin concentration, extinction coefficients of hemoglobin, ε, must be used.

While the engineers and physicists working in the NIR field have found the correct ε values to use, there has been controversy on what ε values should be used for in vivo NIRS in comparison with the conventional ε that most biochemists have used in the laboratories for in vitro measurements. The purpose of this article is to address this issue and help biomedical engineers and physicists gain a better understanding of ε to be used for NIRS and NIR imaging.

Spectrophotometric Measurements to Determine Hemoglobin Concentration

Hemoglobin is a molecule in the red blood cells that has a role of delivering oxygen to tissue cells. Hemoglobin is composed of four heme groups and a protein group, known as a globin. Historically, for spectrophotometric experiments, biological chemists and biochemists utilized Beer-Lambert's law and developed the notation of absorbance to express light absorption as a function of hemoglobin concentration as given in [1]–[5]:

$$\mathrm{OD} = \mathrm{Log}(I_0/I) = \varepsilon \mathrm{c} L \qquad (1)$$

where OD is the optical density, I_0 is the light intensity of incident light, I is the light intensity of transmitted light, ε is the extinction coefficient of hemoblogin, c is the concentration of hemoglobin, and L is the length of light path through solution.

When the measured sample has a mixture of oxygenated and deoxygenated hemoglobin, (1) can be further expanded as [3]–[5],

$$\mathrm{OD}^{\lambda} = \{\varepsilon_{\mathrm{Hb}}{}^{\lambda}[\mathrm{Hb}] + \varepsilon_{\mathrm{HbO_2}}{}^{\lambda}[\mathrm{HbO_2}]\}\mathrm{L} \qquad (2)$$

where OD^{λ} is the optical density or absorbance at wavelength λ and $\varepsilon_{\mathrm{Hb}}(\lambda)$ and $\varepsilon_{\mathrm{HbO_2}}(\lambda)$ are the extinction coefficients at wavelength λ for molar concentrations of deoxygenated hemoglobin, [Hb], and oxygenated hemoglobin, [$\mathrm{HbO_2}$], respectively, assuming ferrihemoglobin is minimal. In some references, the light path, L, was taken as 1 cm without mentioning the definition of L each time [3]–[5]. Both [$\mathrm{HbO_2}$] and [Hb] can be determined by measuring the light absorbance at the two specific wavelengths, provided that the values for $\varepsilon_{\mathrm{Hb}}(\lambda)$ and $\varepsilon_{\mathrm{HbO_2}}(\lambda)$ are known, as expressed below.

$$[\mathrm{HbO_2}] = \frac{\varepsilon_{\mathrm{Hb}}{}^{\lambda_2}\mathrm{OD}^{\lambda_1} - \varepsilon_{\mathrm{Hb}}{}^{\lambda_1}\mathrm{OD}^{\lambda_2}}{\mathrm{L}(\varepsilon_{\mathrm{Hb}}{}^{\lambda_2}\varepsilon_{\mathrm{HbO_2}}{}^{\lambda_1} - \varepsilon_{\mathrm{Hb}}{}^{\lambda_1}\varepsilon_{\mathrm{HbO_2}}{}^{\lambda_2})} \qquad (3)$$

$$[\mathrm{Hb}] = \frac{\varepsilon_{\mathrm{HbO_2}}{}^{\lambda_2}\mathrm{OD}^{\lambda_1} - \varepsilon_{\mathrm{HbO_2}}{}^{\lambda_1}\mathrm{OD}^{\lambda_2}}{\mathrm{L}(\varepsilon_{\mathrm{Hb}}{}^{\lambda_1}\varepsilon_{\mathrm{HbO_2}}{}^{\lambda_2} - \varepsilon_{\mathrm{Hb}}{}^{\lambda_2}\varepsilon_{\mathrm{HbO_2}}{}^{\lambda_1})}. \qquad (4)$$

It follows that changes in [Hb] and [$\mathrm{HbO_2}$] can be consequently given as

$$\Delta[\mathrm{HbO_2}] = \frac{\varepsilon_{\mathrm{Hb}}{}^{\lambda_2}\Delta\mathrm{OD}^{\lambda_1} - \varepsilon_{\mathrm{Hb}}{}^{\lambda_1}\Delta\mathrm{OD}^{\lambda_2}}{\mathrm{L}(\varepsilon_{\mathrm{Hb}}{}^{\lambda_2}\varepsilon_{\mathrm{HbO_2}}{}^{\lambda_1} - \varepsilon_{\mathrm{Hb}}{}^{\lambda_2}\varepsilon_{\mathrm{HbO_2}}{}^{\lambda_2})} \qquad (5)$$

$$\Delta[\mathrm{Hb}] = \frac{\varepsilon_{\mathrm{HbO_2}}{}^{\lambda_2}\Delta\mathrm{OD}^{\lambda_1} - \varepsilon_{\mathrm{HbO_2}}{}^{\lambda_1}\Delta\mathrm{OD}^{\lambda_2}}{\mathrm{L}(\varepsilon_{\mathrm{Hb}}{}^{\lambda_1}\varepsilon_{\mathrm{HbO_2}}{}^{\lambda_2} - \varepsilon_{\mathrm{Hb}}{}^{\lambda_2}\varepsilon_{\mathrm{HbO_2}}{}^{\lambda_1})} \qquad (6)$$

$$\Delta[\mathrm{Hb}]_{\mathrm{total}} = \Delta[\mathrm{Hb}] + \Delta[\mathrm{HbO_2}], \qquad (7)$$

where $\Delta\mathrm{OD}^{\lambda}$ represents a change in optical density at the specific wavelength, λ, and equals $\log(\mathrm{I_B}/\mathrm{I_T})$. $\mathrm{I_B}$ and $\mathrm{I_T}$ correspond to light intensities measured under the baseline and transient conditions.

These spectrophotometric calculations seem straightforward mathematically and have been used for several decades by biochemists to quantify [Hb] and [$\mathrm{HbO_2}$] in the laboratory measurements. However, close attention must be paid to the definition and accuracy of ε since biochemical details in obtaining ε

 0739-5175/05/$20.00©2005IEEE

values give rise to the different quantification of hemoglobin concentration. In early publications on spectrophotometry of hemoglobin [3], it was clearly stated that all extinction coefficients were expressed on a heme basis, using a term of equivalent, where per equivalent of hemoglobin was assumed to be 66,800/4 or 16,700 gm, i.e., one-quarter of the molecular weight of the hemoglobin molecule [12]. While spectroscopic absorption measurements became a popular methodology for biochemists to quantify [Hb] and [HbO_2] in laboratories [5], [6], [12] the notation of extinction coefficients being based on one heme group (or per equivalent) gradually has not been mentioned and has become conventionally understood by biological chemists for the last two to three decades.

Near-Infrared Spectroscopy Used to Determine Hemoglobin Concentration

For the last 15 or more years, significant research efforts have been conducted using NIRS for in vivo quantification of hemoglobin concentrations from intact living tissues. At the early stage of development, direct utilization of (3) and (4) was performed to obtain values or changes of oxygenated and deoxygenated hemoglobin concentration from living tissues in vivo [15]–[18], without particularly noticing that most of the ε values published in biological literature were extinction coefficients for hemoglobin per equivalent (or per one heme of hemoglobin). Such confusion was propagated in some recent publications [19], including our own studies [20]–[22], where the ε values given by Zijlstra et al. have been applied [7].

It gradually becomes clear to the authors that for NIRS of hemoglobin quantification, a factor of four needs to be multiplied by the ε values published by the conventional biochemistry methods. This is a conversion factor to account for four hemes per hemoglobin molecule, which has been demonstrated by Mark Cope [10]. In this way, more meaningful results for concentrations of [Hb] and [HbO_2] can be arrived from the NIR absorption measurements.

During the last ten to 15 years, near infrared spectroscopy (NIRS) and imaging for tissue vascular oxygenation, breast tumor detection, and functional brain imaging have been intensively developed for in vivo measurements.

Furthermore, accurate determination of [Hb] and [HbO_2], or Δ[Hb] and Δ[HbO_2], is highly sensitive to the accuracy of ε values, and intensive studies have been conducted over decades on how to determine accurate ε values [6]–[8], [13]–[14]. The ε values used in our earlier publications were obtained using data interpolation from Zijlstra's ε table [7]. However, such data interpolation for ε at different wavelengths contained potential errors because of the nonlinearity of ε. Therefore, a calibration procedure was necessary and correction factors had to be applied in our earlier algorithm development [21]. On the other hand, Mark Cope has generated a complete ε table at each wavelength between 650 and 999 nm, while taking four hemes into consideration. Such an ε table has been recently well accepted and used [23]–[25].

Comparison of Published Extinction Coefficients for NIRS Given by Two Groups

Since Hoppe-Seyler first described the visible bands of oxyhemoglobin in 1862 [26], numerous reports on hemo-

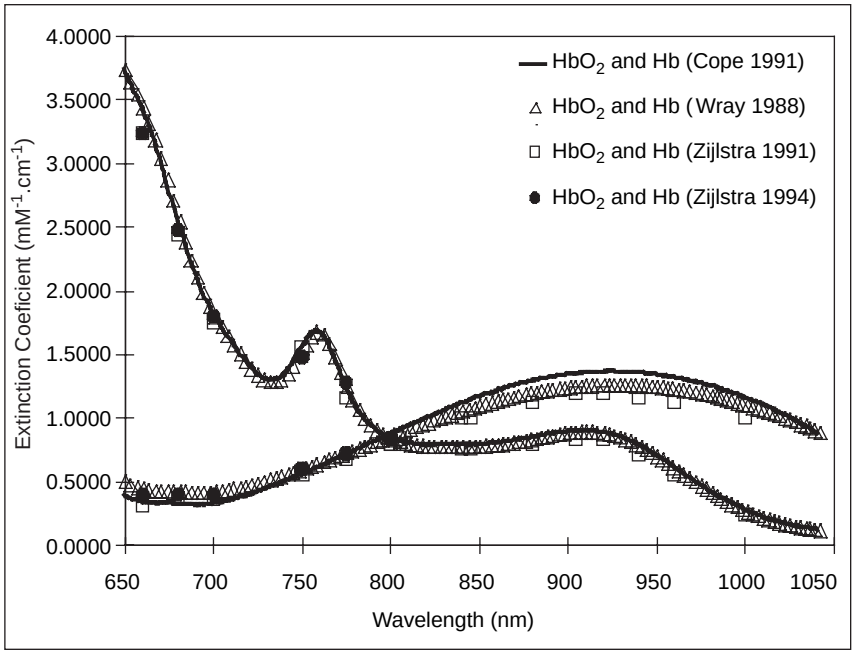

Fig. 1. Absorption spectra of oxy- and deoxyhemoglobin from Wray (9), Cope (10), and Zijlstra (7), (8).

Table 1: Hemoglobin extinction coefficients from two different sources.

Wavelength (nm)	ε_{Hb} ($mM^{-1}\cdot cm^{-1}$)				ε_{HbO_2} ($mM^{-1}\cdot cm^{-1}$)			
	Human (7)	Human (8)	Human (10)	Difference (Absolute)	Human (7)	Human (8)	Human (10)	Difference (Absolute)
750	0.39	0.37	0.3865	0.0165	0.14	0.15	0.1374	0.0126
758		0.354	0.4205	0.0665		0.1596	0.1494	0.0102
775	0.29	0.32	0.3120	0.008	0.17	0.18	0.1759	0.0041
785		0.276	0.2494	0.0266		0.192	0.192	0
800	0.20	0.21	0.2099	0.0001	0.20	0.21	0.2163	0.0063
805	0.20		0.2037		0.21		0.2243	
840	0.19		0.1954		0.25		0.2768	

globin absorption spectra have appeared in the literature. However, only a few have tabular forms of hemoglobin extinction coefficients. In particular, two groups have reported tabular forms of hemoglobin extinction coefficients in a broad range of the NIR spectrum. Zijlstra et al. reported ε values for human blood [7], followed by another publication for updated human ε values with a comparison to those of rat blood [8]. Moreover, Cope has generated a complete ε table at each wavelength between 650 and 999 nm, while taking four hemes into account for in vivo NIRS measurements. Cope also compared his own experiments with other previous reports, finding that the isobestic point of hemoglobin is shifted to 798 ± 1.5 nm from 800 nm reported by Horecker [1], 805 nm by Barlow [27] and 815 nm by van Assendelft [28].

It is worthwhile to note that the determination of ε values has resulted in a range of accuracy claims, even for values reported from the same group. For example, according to Zijlstra et al., a value of ε_{Hb} at 560 nm in [29] was 12.72 ($mM^{-1}cm^{-1}$), while it was later changed to 13.09 ($mM^{-1}cm^{-1}$) in [7]; a value of ε_{HbO_2} at 630 nm was 0.11 ($mM^{-1}cm^{-1}$) as given in [7], while it was also reported as 0.14 ($mM^{-1}cm^{-1}$) in [8]. From Cope's group, their published reports show that ε_{Hb} and ε_{HbO_2} at 752 nm are 1.574 ($mM^{-1}cm^{-1}$) and 0.608 ($mM^{-1}cm^{-1}$), respectively, as given in [9], while the corresponding ε values are 1.5938 ($mM^{-1}cm^{-1}$) and 0.5613 ($mM^{-1}cm^{-1}$) in [10]. A complete comparison of ε values based on [7]–[10] by Zijlstra et al., Wray et al., and Cope is plotted in Figure 1, showing the similarities and differences among the reported extinction coefficients of oxy- and deoxyhemoglobin. Notice that the values plotted from Zijlstra's group have been multiplied by a factor of four to account for four hemes per hemoglobin molecule for in vivo measurements. It is obvious that certain variations among different sets of ε values exist, while the basic trends are the same.

Table 1, on the other hand, shows the tabular form of hemoglobin extinction coefficients from these two groups. Extinction coefficients in the left two columns of ε_{Hb} and ε_{HbO_2} are from Zijlstra's two reports [7], [8] and those in the third column of ε_{Hb} and ε_{HbO_2} are from Cope's report [10]. Since the tabular form of extinction coefficients from Zijlstra does not have values of 758 and 785 nm, the extinction coefficients of 758 and 785 nm were obtained by linear interpolation between 750 and 775 nm and between 775 and 800 nm, respectively. The hemoglobin extinction coefficients from Cope were divided by four to be "per equivalent" so that they could be compared to those from Zijlstra et al. The differences listed in the last column are the differences between Cope's ε values and the values from Zijlstra et al [8].

While the differences in ε values seem small among the published data, they can result in ~20% variation in quantification of hemoglobin concentration, i.e., [Hb], [HbO_2], and $[Hb]_{total}$ for the NIRS determined values. The error range varies, depending on the actual wavelengths used. We are currently conducting more quantitative error analysis to demonstrate the importance of accurate ε for NIRS. Meanwhile, we wish in this report to help biomedical engineers better understand the extinction coefficients of hemoglobin and to further draw attention to the dependence of NIRS accuracy on the extinction coefficients of hemoglobin.

Acknowledgments

This work was supported in part by the U.S. Department of Defense Breast Cancer Research grants of DAMD17-03-1-0353 (JGK), W81XWH-04-1-0411 (MX), and DAMD17-00-1-0459 (HL).

References

[1] B.L. Horecker, "The absorption spectra of hemoglobin and its derivatives in the visible and near

infrared regions," *J. Biol. Chem.*, vol. 148, no. 1, pp. 173–183, 1943.
[2] E.J. van Kampen and W.G. Zijlstra, "Determination of hemoglobin and its derivatives," *Adv. Clin. Chem.*, vol. 8, pp. 141–187, 1965.
[3] R. Benesch, G. Macduff, and R.E. Benesch, "Determination of oxygen equilibria with a versatile new tonometer," *Anal. Biochem.*, vol. 11, no. 1, pp. 81–87, 1965.
[4] R.E. Benesch, R. Benesch, and S. Yung, "Equations for the spectrophotometric analysis of hemoglobin mixtures," *Anal. Biochem.*, vol. 55, no. 1, pp. 245–248, 1973.
[5] O.W. van Assendelft and W.G. Zijlstra, "Extinction coefficients for use in equations for the spectrophotometric analysis of haemoglobin mixtures," *Anal. Biochem.*, vol. 69, pp. 43–48, 1975.
[6] W.G. Zijlstra, A. Buursma, and A. Zwart, "Molar absorptivities of human hemoglobin in the visible spectral range," *J. Appl. Physiol.: Respirat. Environ. Exercise Physiol.*, vol. 54, no. 5, pp. 1287–1291, 1983.
[7] W.G. Zijlstra, A. Buursma, and W.P. Meeuwsen-van der Roest, "Absorption spectra of human fetal and adult oxyhemoglobin, de-oxyhemoglobin, carboxyhemoglobin, and methemoglobin," *Clin. Chem.*, vol. 37, no. 9, pp. 1633–1638, 1991.
[8] W.G. Zijlstra, A. Buursma, H.E. Falke, and J.F. Catsburg, "Spectrophotometry of hemoglobin: Absorption spectra of rat oxyhemoglobin, deoxyhemoglobin, carboxyhemoglobin, and methemoglobin," *Comp. Biochem. Physiol.*, vol. 107B, no. 1, pp. 161–166, 1994.
[9] S. Wray, M. Cope, D.T. Delpy, J.S. Wyatt, and E. Osmund R. Reynolds, "Characterization of the near infrared absorption spectra of cytochrome aa3 and haemoglobin for the non-invasive monitoring of cerebral oxygenation," *Biochimica et Biophysica Acta*, vol. 933, no. 1, pp. 184–192, 1988.
[10] M. Cope, "The application of near infrared spectroscopy to non invasive monitoring of cerebral oxygenation in the newborn infant," Ph.D. thesis, Appendix B, pp. 316–323, University College London, 1991.
[11] S.J. Matcher, C.E. Elwell, C.E. Cooper, M. Cope, and D.T. Delpy, "Performance comparison of several published tissue near-infrared spectroscopy algorithms," *Anal. Biochem.*, vol. 227, no. 1, pp. 54–68, 1995.
[12] Y. Mendelson and J.C. Kent, "Variations in optical absorption spectra of adult and fetal hemoglobins and its effect on pulse oximetry," *IEEE Trans. Biomed. Eng.*, vol. 36, no. 8, pp. 844–848, 1989.
[13] L. Cordone, A. Cupane, M. Leone and E. Vitrano, "Optical absorption spectra of deoxy- and oxyhemoglobin in the temperature range 300-20 K," *Biophys. Chem.*, vol. 24, no. 3, pp. 259–275, 1986.
[14] J.M. Steinke and A.P. Shepherd, "Effects of temperature on optical absorbance spectra of oxy-, carboxy-, and deoxyhemoglobin," *Clin. Chem.*, vol. 38, no. 7, pp. 1360–1364, 1992.
[15] E.M. Sevick, B. Chance, J. Leigh, S. Nioka, and M. Maris, "Quantitation of time- and frequency-resolved optical spectra for the determination of tissue oxygenation," *Anal. Biochem.*, vol. 195, no. 2, pp. 330–351, 1991.
[16] M. Miwa, Y. Ueda, and B. Chance, "Development of time resolved spectroscopy system for quantitative non-invasive tissue measurement," *Proc. SPIE-Int. Soc. Opt. Eng.*, vol. 2389, p. 142, 1995.
[17] H. Liu, A.H. Hielscher, F.K. Tittel, S.L. Jacques, and B. Chance, "Influence of blood vessels on the measurement of hemoglobin oxygenation as determined by time-resolved reflectance spectroscopy," *Med. Phys.*, vol. 22, no. 8, pp. 1209–1217, 1995.
[18] S. Fantini, M.A. Franceschini-Fantini, J.S. Maier, S.A. Walker, B. Barbieri, and E. Gratton, "Frequency-domain multichannel optical detector for noninvasive tissue spectroscopy and oximetry," *Opt. Eng.*, vol. 34, no. 1, pp. 32–42, 1995.
[19] C.D. Kurth and W.S. Thayer, "A multiwavelength frequency-domain near-infrared cerebral oximeter," *Phys. Med. Biol.*, vol. 44, no. 3, pp. 727–740, 1999.
[20] H. Liu, Y. Song, K.L. Worden, X. Jiang, A. Constantinescu, and R.P. Mason, "Noninvasive investigation of blood oxygenation dynamics of tumors by near infrared spectroscopy," *Appl. Opt.*, vol. 39, no. 28, pp. 5231–5243, 2000.
[21] J.G. Kim, Y. Song, D. Zhao, A. Constantinescu, R.P. Mason, and H. Liu, "Interplay of tumor vascular oxygenation and tumor pO_2 observed using near infrared spectroscopy, an oxygen needle electrode, and ^{19}F MR pO_2 mapping," *J. Biomed. Opt.*, vol. 8, no. 1, pp. 53–62, 2003.
[22] Y. Gu, V. Bourke, J.G. Kim, A. Constantinescu, R.P. Mason, and H. Liu, "Dynamic response of breast tumor oxygenation to hyperoxic respiratory challenge monitored with three oxygen-sensitive parameters," *Appl. Opt.*, vol. 42, no. 16, pp. 2960–2967, 2003.
[23] J.B. Fishkin, O. Coquoz, E.R. Anderson, M. Brenner, and B.J. Tromberg, "Frequency-domain photon migration measurements of normal and malignant tissue optical properties in a human subject," *Appl. Opt.*, vol. 36, no. 1, pp. 10–20, 1997.
[24] E.L. Hull, D.L. Conover, and T. Foster, "Carbogen-induced changes in rat mammary tumour oxygenation reported by near infrared spectroscopy," *British J. of Cancer*, vol. 79, no. 11/12, pp. 1709–1716, 1999.
[25] D.A. Boas, M.A. Franceschini, A.K. Dunn, and G. Strangman, "Noninvasive imaging of cerebral activation with diffuse optical tomography," in *In-vivo Optical Imaging of Brain Function*, R.D. Frostig, Ed. New York: CRC Press, 2000.
[26] H.S. Newcomer, "Absorption spectra of acid hematin, oxyhemoglobin, and carbon monoxide hemoglobin," *J. Biol. Chem.*, vol. 37. no. 3, pp. 465–496, 1919.
[27] R.B. Barlow and M.L. Polanyi, "Absorption measurements for oxygenated and reduced hemoglobin in the range 0.6–1.88 microns," *Clin. Chem.*, vol. 8, no. 1, pp. 67–71, 1962.
[28] O.W. van Assendelft, "Spectrophotometry of haemoglobin derivatives," Ph.D. thesis, Univ. of Groningen, The Netherlands, 1970.
[29] W.G. Zijlstra and A. Buursma, "Spectrophotometry of hemoglobin: A comparison of dog and man," *Comp. Biochem. Physiol.*, vol. 88B, no. 1, pp. 251–255, 1987.

Address for Correspondence: Hanli Liu, Joint Graduate Program in Biomedical Engineering, The University of Texas at Arlington and The University of Texas Southwestern Medical Center at Dallas Arlington, TX 76019 USA. Phone: +1 817 272 2054. Fax: +1 817 272 2251. E-mail: hanli@uta.edu.

COMAR Reports *(continued from page 117)*

membership and by the IEEE EMBS Executive Committee.

Sources and Further Reading

[1] IEEE C95.1-1991, Standard for Safety Levels with Respect to Human Exposure to Radio Frequency Electromagnetic Fields, 3 kHz to 300 GHz, (1999 edition).

[2] International Commission on Non-Ionizing Radiation Protection, "Guidelines for limiting exposure to time-varying electric, magnetic and electromagnetic fields (up to 300 GHz)," *Health Physics*, vol. 74, no. 4, pp. 494–522, 1998.

[3] J. M. Osepchuk and R. C. Petersen, "Safety standards for exposure to electromagnetic fields," *IEEE Microwave Magazine*, vol. 2, no. 2, pp. 57–69, June 2001.

[4] "Reviews of the Effects of RF Fields on Various Aspects of Human Health," *Bioelectromagnetics*, vol. 24, no. S6, 2003.

[5] *Welcome to IEEE standards development online* [Online]. Available: http://standards.ieee.org/resources/development/index.html

[6] *IEEE international committee on electromagnetic safety* [Online]. Available: http://grouper.ieee.org/groups/scc28/

[7] K. R. Foster, "Limiting Technology: Issues in Setting Exposure Guidelines for Radiofrequency Energy," in Ma Jian-Guo, Ed. 3rd Generation Mobile Communication Systems: Future Developments and Advanced Topics, Springer, Sept. 2003.

[8] *Framework for harmonization of standards* [Online]. Available: http://www.who.int/peh-emf/standards/framework/en/

Simultaneous monitoring of tumor vascular oxygenation and tissue oxygen tension under hyperbaric oxygen exposure

Mengna Xia, Hanli Liu
Biomedical Engineering Graduate Program, University of Texas at Arlington, Arlington, TX 76013
Tel: (817) 272-2054; Fax: (817) 272-2251; email address: hanli@ uta.edu
Ya Ren, Ralph Mason
Department of Radiology, UT Southwestern Medical Center at Dallas, Dallas, Texas, United States
Tel: (214) 648-8926; Fax: (214) 648-4538; email address: Ralph.Mason@UTSouthwestern.edu
Benjamin Levine
Institute of Exercise and Environmental medicine, UT Southwestern Medical Center at Dallas, Dallas, Texas, United States
Tel: (214) 345-4619; Fax: (214) 345-4618; email address: benjaminlevine@texashealth.org

Abstract: We demonstrate the ability to investigate breast tumor oxygen dynamics simultaneously by steady-state diffuse reflectance spectroscopy and FOXY oxygen sensor in response to hyperbaric oxygen intervention.

OCIS codes: (170.1470) blood/tissue constituent monitoring; (170.6510) Spectroscopy, tissue diagnostics

1. Introduction

Tumor hypoxia has proven to have a prognostic impact in cancers and is associated with poor response to radiotherapy [1,2]. Hyperbaric oxygenation offers an approach to overcome tissue or tumor hypoxia. Several randomized studies investigating hyperbaric oxygenation as a radiosensitizer were performed 30-40 years ago [3-5]. However, hyperbaric oxygenation was largely abandoned. Recently, a few groups have developed and demonstrated a new strategy to combine hyperbaric oxygenation and radiotherapy, based on the finding that tumors maintained elevated oxygenation even after exposure to hyperbaric oxygen [6-8]. Accordingly, accurate evaluation of tumor oxygenation could be crucial for determination of radio-sensitivity. In our study, we applied two monitoring techniques simultaneously, i.e., steady-state diffuse reflectance spectroscopy (SSDRS) to monitor tumor vascular oxygenation and a multi-channel FOXY oxygen sensor to measure regional tumor oxygen tension when the rats were under hyperbaric oxygen exposure. The objective of study was to investigate breast tumor oxygen dynamics in response to hyperbaric oxygenation and to examine whether a possible improvement in tumor oxygenation is maintained after hyperbaric oxygenation.

2. Materials and Methods

2.1 Animal Preparation and experimental setup

Female Fischer 344 rats were used with subcutaneously growing mammary adenocarcinoma 13762NF (originally obtained from DCT, NIH) on the dorsum of the thigh. When the tumors reached ~1 cm in diameter, the rats were anesthetized with ketamine hydrochloride (1.5ml; 100mg/ml; Aveco, Fort Dodge, IA) and xylazine by intraperitoneal injection. Tumor hair was trimmed for the ease of optical contact for transmitting NIR light and FOXY probe insertion. The rats were placed in the hyperbaric chamber on their sides, and then the probes of SSDRS and FOXY were fixed securely on the tumor. Tumor oxygenation parameters were measured simultaneously by SSDRS and FOXY during respiratory challenge with hyperbaric oxygen (HBO) or carbogen (HBCB).

During the experiments, the rats were exposed to hyperbaric oxygen in an acrylic hyperbaric chamber. The chamber was flushed with air for 15 min, followed by normobaric 100% oxygen or carbogen for 15 min, then followed by a pressure increase to 2 atmospheres absolute (HBO) for 30 min. The chamber pressure was then reduced to ambient, followed by a flushing with air. Gas exchange (air to oxygen/carbogen) was accomplished at an initial flow rate of approximately 15 l/min. Compression and decompression (from 1 to 2 atmosphere oxygen/carbogen, and 2 to 1 atmosphere oxygen/carbogen) required approximately 2 min.

2.2 Steady-state diffuse reflectance spectroscopy (SSDRS) for measuring changes in tumor vascular oxygenation (ΔHbO_2)

The instrument used to acquire reflectance spectra from tumor tissue is a broadband diffuse reflectance spectrometer. Briefly, continuous wave (CW) light from a 20 W tungsten-halogen light source (HL-2000HP, ocean optics, FL) is coupled into a 2.6-mm core diameter fiber optic bundle, the distal end of which is placed in physical contact with the surface of the tumor. After being scattered in the tumor tissue, the transmitted light is collected by a 1-mm core

diameter detection fiber, the end of which is coupled to a hand-held spectrometer (USB2000, Ocean optics, FL). The broadband light diffuse spectrometer provides reflectance spectra from 400 to 900 nm.

According to the modified Beer-Lambert law, as given in Eqs. (1) and (2), changes of oxy- and deoxy-hemoglobin concentration, $\Delta[HbO_2]$ and $\Delta[Hb]$, can be derived from the measured amplitudes at two wavelengths (750nm and 830nm), by using extinction coefficients of oxy- and deoxy-hemoglobin published by Cope [9].

$$\log(\frac{A_b}{A_t})^{750} = (\varepsilon_{Hb}{}^{750}\Delta[Hb] + \varepsilon_{HbO_2}{}^{750}\Delta[HbO_2]) \cdot DPF \cdot d \quad (1)$$

$$\log(\frac{A_b}{A_t})^{830} = (\varepsilon_{Hb}{}^{830}\Delta[Hb] + \varepsilon_{HbO_2}{}^{830}\Delta[HbO_2]) \cdot DPF \cdot d \quad (2)$$

where A_b is the baseline amplitude, A_t is the transient amplitude during the intervention, and d is the direct source-detector separation. *DPF* (differential path-length factor) is a tissue-dependent parameter and defined as the ratio between the optical path length and the physical separation between the source and detector.

2.3 FOXY oxygen sensor for measuring oxygen tension of tumors (pO_2)

Simultaneously, regional pO_2 values in tumors were monitored by a multi-channel, fiber optic oxygen sensor (FOXY, Ocean Optics Inc, Dunedin, FL). Three fluorescence-quenched, optical fiber probes (AL300, tip diameter 410 μm) were inserted into different regions of the tumors. Light from a pulsed blue LED (475 nm) was coupled into one branch of a bifurcated optical fiber probe and propagated to the probe tip. The distal end of the probe is coated with a thin layer of a hydrophobic sol gel material, in which oxygen-sensing ruthenium complex is effectively trapped. Illumination of the ruthenium complex causes fluorescence at ~600 nm. If the excited ruthenium complex encounters oxygen molecule, the excess energy is transferred to the oxygen molecule, thus quenching the fluorescence signal. The degree of quenching correlates with the oxygen concentration, pO_2.

3. Results

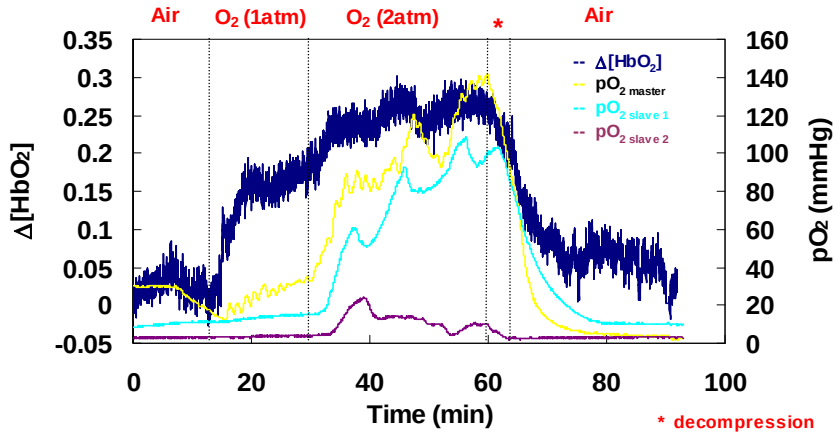

Fig.1 Time course of $\Delta[HbO_2]$ and pO_2 in response to respiratory challenge for a representative tumor, simultaneous measured by SSDRS (thicker curve) and FOXY (thinner curves). The symbol "*" represents the time needed for decompression.

Figure 1 shows simultaneous readings of changes in $[HbO_2]$ measured by SSDRS and three pO_2 traces in three regions of a breast tumor recorded by FOXY in response to respiratory challenge. This tumor showed a rapid response to oxygen intervention in normal pressure with a significant increase in $\Delta[HbO_2]$. The three readings in pO_2 displayed heterogeneous responses to normobaric oxygen inhalation. One region showed distinct improvement in pO_2, while the other two regions had little or no improvement in pO_2. When the oxygen was pressured to 2 atmospheres, $\Delta[HbO_2]$ had a further increase with an initial increasing rate less than that achieved with normobaric oxygen. However, pO_2 readings in the three respective regions showed significant improvement under the hyperbaric oxygen condition. Returning to air from hyperbaric oxygen produced a gradual decline for both $\Delta[HbO_2]$ and pO_2. A strong linear correlation was observed between maximal ΔpO_2 achieved with hyperbaric Oxygen/Carbogen intervention and that achieved at the same location with respect to normobaric oxygen/carbogen intervention in 11 tumors (Fig. 2).

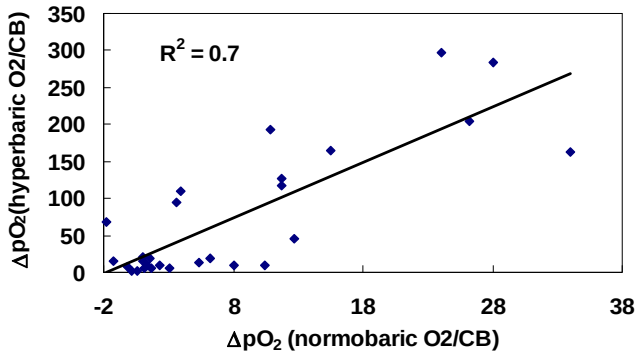

Fig. 2 The correlation between Maximal ΔpO_2 (unit: mmHg) during hyperbaric Oxygen/Carbogen intervention and that during normobaric oxygen/carbogen intervention in 11 tumors. CB: carbogen.

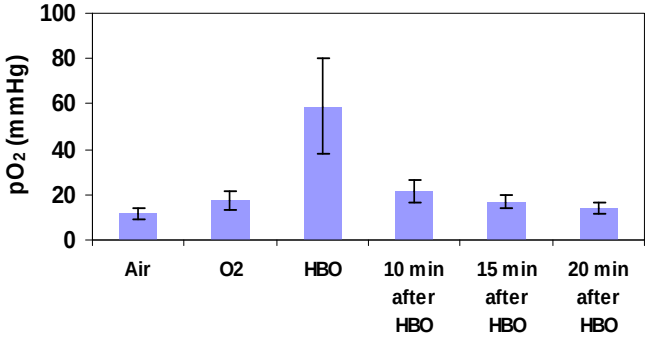

Fig. 3 Average pO_2 for a group of 6 tumors with hyperbaric oxygen intervention achieved with different gas. HBO: hyperbaric oxygen.

Tumor pO_2 (average value of a group of six tumors with HBO) in air was 11.7±2.6 mm Hg, and it increased significantly during normobaric oxygen to 17.5±4 mm Hg ($p < 0.01$). Hyperbaric oxygenation resulted in a more significant increase in pO_2 than normobaric oxygenation ($p < 0.005$), as shown in Figure 3. Following hyperbaric oxygen, the pO_2 decrease to 21.5±4.6 mmHg in 10 min, 16.9±3.1 mmHg in 15 min, and then 14.3±2.4 mmHg in 20 min. Tumor pO_2 values showed similar responses for a group of 5 tumors with hyperbaric carbogen intervention.

4. Discussion

This study shows that the two techniques, i.e., SSDRS and FOXY, are consistent and complementary with one another for tumor oximetry. Our data demonstrates that hyperbaric oxygenation improves the tumor oxygenation better than normobaric oxygen. It also suggests that an improvement in tumor tissue oxygenation achieved by hyperbaric oxygenation may be maintained over 10-20 minutes even after hyperbaric oxygenation.

5. Acknowledgements: This work was supported in part by the Department of Defense Breast Cancer Research grants of W81XWH-04-1-0411 (Mengna Xia) and NIH/NCI P20 CA086354 (RPM).

6. References

1. Hall EJ, "The oxygen effect and reoxygenation", in *Radiobiology for the Radiologist*, 4th ed., (J. B. Lippincott, Philadelphia, 1994).
2. Zhao D, Constantinescu A, Chang C-Hui, Hahn EW and Mason RP, "Correlation of Tumor Oxygen Dynamics with Radiation Response of the Dunning Prostate R3327-HI Tumor", Radiat Res., 159(5):621-31 (2003).
3. Bates T, "The treatment of stage 3 carcinoma of the cervix by external radiotherapy and high-pressure oxygen", Br. J. Radiol. 42, 266-9 (1969).
4. Berry GH, Dixon B, and Ward AJ, "The Leeds results for radiotherapy in HBO for carcinoma of the head and neck", Clin. Radiol. 30, 591-2 (1979).
5. Brady LW, Plenk HP, Hanley JA, Glassburn JR, Kramer S, and Parker RG, " hyperbaric oxygen therapy for carcinoma of the cervix stages IIB, IIIB, and IVA: results of a randomized study by the radiation therapy oncology group", Int. J. Radiat Oncol. Biol. Phys. 7, 991-8 (1981)
6. Becker A, Kuhnt T , Liedtke H, Krivokuca A, Bloching M , and Dunst J, " Oxygenation Measurements in head and neck cancer during hyperbaric oxygenation", Strahlenther Onkol. 2, 105-8 (2002).
7. Kinoshita T, Kohshi K, Kunugita N, Tosaki T, and Yokota A, " Preservation of tumor oxygen after hyperbaric oxygenation monitored by magnetic resonance imaging", Br. J. of Cancer 82, 88-92 (2000).
8. Hunugita N, Kkoshi K, Kinoshita Y, Katoh T , Abe H, Tosaki T , Kawamoto T , and Norimura T, " Radiotherapy after hyperbaric oxygenation improves radioresponse in experimental tumor models", Cancer Letter 164, 149-54 (2001).
9. Cope M, "the application of near infrared spectroscopy to non invasive monitoring of cerebral oxygenation in the newborn infant", Ph.D dissertation (1991).